

AD-753 651

STATIC, VIBRATION, AND THERMAL STRESS  
ANALYSES OF LAMINATED PLATES AND SHELLS  
BY THE HYBRID-STRESS FINITE-ELEMENT METHOD,  
WITH TRANSVERSE SHEAR DEFORMATION EFFECTS  
INCLUDED

Sheng-Taur Mau, et al

Massachusetts Institute of Technology

Prepared for:

Army Materials and Mechanics Research Center

October 1972

DISTRIBUTED BY:

**NTIS**

National Technical Information Service  
U. S. DEPARTMENT OF COMMERCE  
5285 Port Royal Road, Springfield Va. 22151

AD 753651



AD

AMMRC CTR 72-24

ASRL TR 169-2

**STATIC, VIBRATION, AND THERMAL STRESS  
ANALYSES OF LAMINATED PLATES AND SHELLS  
BY THE HYBRID-STRESS FINITE-ELEMENT  
METHOD, WITH TRANSVERSE SHEAR  
DEFORMATION EFFECTS INCLUDED**

October 1972

Sheng-Taur Mau  
Emmett A. Witmer

Aeroelastic and Structures Research Laboratory  
Department of Aeronautics and Astronautics  
Massachusetts Institute of Technology  
Cambridge, Massachusetts 02139

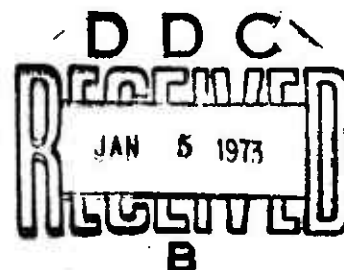
Final Report - Contract DAAG46-72-C-0029

Approved for public release; distribution unlimited.

Prepared for

**ARMY MATERIALS AND MECHANICS RESEARCH CENTER  
Watertown, Massachusetts 02172**

Reproduced by  
NATIONAL TECHNICAL  
INFORMATION SERVICE  
U.S. Department of Commerce  
Springfield, MA 01104



ACCESSION for	
NTIS	White Section <input checked="" type="checkbox"/>
DDC	Buff Section <input type="checkbox"/>
UNANNOUNCED	<input type="checkbox"/>
JUSTIFICATION	
ON	
DISPOSITION/AVAILABILITY CODES	
Doc.	Avail. code/SP. CHAR.
A	

The findings in this report are not to be construed as an official Department of the Army position, unless so designated by other authorized documents.

Mention of any trade names or manufacturers in this report shall not be construed as advertising nor as an official endorsement or approval of such products or companies by the United States Government.

#### DISPOSITION INSTRUCTIONS

Destroy this report when it is no longer needed.  
Do not return it to the originator.

AMMRC CTR 72-24

ASRL TR 169-2

STATIC, VIBRATION, AND THERMAL STRESS ANALYSES OF  
LAMINATED PLATES AND SHELLS BY THE HYBRID-STRESS  
FINITE-ELEMENT METHOD, WITH TRANSVERSE SHEAR  
DEFORMATION EFFECTS INCLUDED

Sheng-Taur Mau  
Emmett A. Witmer

Aeroelastic and Structures Research Laboratory  
Department of Aeronautics and Astronautics  
Massachusetts Institute of Technology  
Cambridge, Massachusetts 02139

October 1972

Final Report - - Contract DAAG46-72-C-0029

D/A Project 1W062113A661  
AMCMS Code 502N.11.070-X0-81132  
Reduction of Vulnerability ABM Systems  
Agency Accession Number DA OD4720

Approved for public release; distribution unlimited.

Prepared for

ARMY MATERIALS AND MECHANICS RESEARCH CENTER  
Watertown, Massachusetts 02172

I

## FOREWORD

This research was conducted by the Aeroelastic and Structures Research Laboratory, Department of Aeronautics and Astronautics, Massachusetts Institute of Technology, Cambridge, Massachusetts under Contract No. DAAG46-72-C-0029 with the Army Materials and Mechanics Research Center, Watertown, Massachusetts.

The authors would like to thank Professors P. Tong and T.H.H. Pian for their helpful technical advice and guidance throughout this effort.

The computations were performed at the Information Processing Center of the Massachusetts Institute of Technology.

## ABSTRACT

A method of analyzing laminated-composite, linear-elastic plate and shell structures has been developed based on the hybrid stress finite-element model. Flat-plate elements are used for both plate and shell structures. Three quadrilateral elements designated by ELEM1, ELEMZ, and ELEMZ, all with linear in-plane boundary displacement and linear in-plane stress assumptions, are chosen for use. Transverse shear deformation effects and rotary as well as in-plane inertia are included in all of these elements. The ELEM1 element can be applied to single-layer thin or moderately thick plates and shells. The ELEMZ element can be applied to multilayer thin plates and shells, and the ELEMZ element may be used to analyze single-layer or multilayer, thin or thick plates and shells.

The stiffness matrix, mass matrix, and equivalent thermal loading vector of these elements that are used in static, vibration, and thermal stress analyses, respectively, are developed and applied to analyze various plate and shell problems. Comparisons of results are made, whenever possible, with other existing solutions. This present method of analysis provides accurate, efficient predictions of (a) displacements and stresses under static or thermal loading and (b) natural frequencies under free vibration. The method developed in this study can be used as a reliable tool in structural analysis and design; it can also be applied to explore material property characterizations and selections for laminated composite materials.

## CONTENTS

<u>Section</u>	<u>Page</u>
1 INTRODUCTION	1
1.1 Purpose of the Study	1
1.2 Synopsis of the Investigation	4
2 STATIC ANALYSIS	
2.1 Formulation of Single-Layer Flat-Plate Elements	7
2.1.1 Derivation of Element Stiffness Matrices	7
2.1.2 Material, Stress, and Displacement Assumptions	9
2.2 Parametric Study and Selection of Single-Layer Elements	11
2.3 Formulation for Multilayer Flat-Plate Elements	16
2.3.1 Derivation of Element Stiffness Matrices	16
2.3.2 Stress and Displacement Assumptions	17
2.4 Flat-Plate Evaluation Examples	18
2.4.1 Single-Layer Isotropic Plates	18
2.4.2 Two-Layer Plates	20
2.4.3 Three-Layer Plates	21
2.5 Application to Shell Problems	22
2.5.1 Transformation for Single-Layer Elements	22
2.5.2 Transformation for Multilayer Elements	24
2.6 Shell Evaluation Examples	26
2.6.1 Thin Cylindrical Shells	26
2.6.2 Conical Shells	27
2.7 Summary and Comments	28
3 VIBRATION ANALYSIS	30
3.1 Vibration Analysis by the Hybrid Stress Model	30
3.2 Mass Matrices for an Element	33
3.3 Plate and Shell Evaluation Examples	36
3.3.1 Single-Layer Thin Plates	36

# CONTENTS CONTINUED

<u>Section</u>	<u>Page</u>
3.3.2 Two-Layer Thin and Thick Plates	38
3.3.3 A Simply-Supported Three-Layer Square Plate	39
3.3.4 A Simply-Supported Three-Layer Cross-Ply Cylindrical Shell	39
3.4 Summary	40
4 THERMAL STRESS ANALYSIS	41
4.1 Thermal Stress Analysis by the Hybrid Stress Model	41
4.2 Modeling of a Temperature Distribution	45
4.3 Stress Assumptions in an Element	48
4.4 Plate and Shell Evaluation Examples	50
4.4.1 In-Plane Expansion of a Free Single- Layer Thin Isotropic Rectangular Plate	50
4.4.2 Bending of a Clamped Thin Isotropic Rectangular Plate Subjected to Non- uniform Temperature	51
4.4.3 Simply-Supported, Infinitely-Long, Two- Layer, Cross-Ply ( $0^\circ/90^\circ$ ) Thin Strip Sub- jected to a Uniform Temperature Distribution	51
4.4.4 Simply-Supported, Three-Layer, Cross-Ply ( $0^\circ/90^\circ/0^\circ$ ), Thick, Cylindrical Shell Subjected to a Uniform Temperature Distribution	52
4.5 Summary	53
5 SUMMARY AND CONCLUSIONS	54
5.1 Summary	54
5.2 Conclusions	56
5.3 Suggestions for Future Research	58

## CONTENTS CONCLUDED

<u>Section</u>	<u>Page</u>
REFERENCES	59
TABLES	65
ILLUSTRATIONS	80
APPENDIX: COMPUTATIONAL SCHEMES FOR STATIC AND VIBRATION ANALYSIS	115

# LIST OF ILLUSTRATIONS

<u>Figure</u>		<u>Page</u>
1	Nomenclature for Composite Flat-Plate Finite Elements	80
2	Central Deflection of a Simply-Supported, Centrally-Loaded, Square, Isotropic, Thin, Single-Layer Plate	82
3	Central Deflection of a Simply-Supported, Uniformly-Loaded, Square, Isotropic, Thick, Single-Layer Plate	83
4	A Multilayer Element	84
5	Central Deflection of a Clamped, Square, Isotropic, Thin, Single-Layer Plate under Concentrated Central Load	84
6	Central Deflection of a Clamped, Isotropic, Rectangular, Thin, Single-Layer Plate under Uniform Load	85
7	Central Deflection of a Skewed, Single-Layer, Isotropic Thin Plate Under Uniform Load	86
8	Central Deflection of a Clamped, Two-Layer Rectangular, Cross-Ply Plate under Uniform Load	87
9	Central Deflection of a Clamped, Two-Layer, Square, Cross-Ply Plate under Uniform Load	87
10	Central Deflection of a Clamped, Two-Layer, Square Angle-Ply Plate under Uniform Load	88
11	Central Deflection for Simply-Supported Two-Layer ( $\pm \theta$ ) Square, Angle-Ply Plates	88
12	Displacement and Stress Solutions for an Infinite Three-Layer Cross-Ply Plate with Simply-Supported Edges, Subjected to Sinusoidal Loading	89
13	Displacement and Stress Solutions for a Simply-Supported Three-Layer Cross-Ply Square Plate Subjected to Sinusoidal Loading	90
14	Coordinate Transformation	91
15	Central Deflection of a Single-Layer, Isotropic, Pinched Cylindrical Thin Shell	91

# LIST OF ILLUSTRATIONS CONTINUED

<u>Figure</u>		<u>Page</u>
16	Predicted Central Radial Deflection of a Thin, Single-Layer, Isotropic Cylindrical Shell under Ring Load	92
17	Meridional Moment and Radial Deflections of a Thin, Single-Layer, Isotropic, Conical Shell under Ring Loads	93
18	Meridional Moment and Radial Displacement of a Thin, Isotropic, Single-Layer, Conical Shell under Ring Loads	95
19	Meridional Moment of Two Moderately Thick, Single-Layer, Isotropic, Conical Shells under Ring Loads	97
20	Radial Displacements of Two Single-Layer and One Two-Layer, Conical Shells under Ring Loads	98
21	Radial Displacement of a Sandwich Conical Shell under Ring Loads	99
22	Maximum Meridional and Circumferential Normal Stresses in the Cover and in the Base of a Two-Layer Conical Shell under Ring Loads	100
23	Coordinate Transformation for a Quadrilateral Element	102
24	The Lowest Frequency of a Simply-Supported, Single-Layer, Thin, Isotropic, Square Plate	102
25	The Lowest Frequency of a Clamped, Single-Layer, Isotropic, Thin, Rectangular Plate	103
26	The Lowest Frequency of a Clamped, Two-Layer, Cross-Ply Thin, Square Plate	104
27	The Lowest Frequencies of Infinite Two-Layer, Cross-Ply Plates with Simply-Supported Edges	104
28	Temperature Assumptions for One Layer of a Multilayer Quadrilateral Element	105

# LIST OF ILLUSTRATIONS CONCLUDED

<u>Figure</u>		<u>Page</u>
29	Dimension, Coordinate System, and Temperature Distribution of a Free, Single-Layer, Thin, Isotropic Rectangular Plate	106
30	Displacements of a Quarter of the Plate of Fig. 29	107
31	In-Plane Normal and Shear Stresses of the Plate of Fig. 29	108
32	Dimensions, Temperature, and Centerline Deflections of a Clamped Single-Layer, Thin, Isotropic Rectangular Plate	111
33	Dimensions, Coordinate System, Deflections, and Stresses of an Infinite Two-Layer Cross-Ply Thin Plate Simply Supported Along Edges and Subjected to Uniform Temperature	112
34	Radial and Axial Deflection of a Simply-Supported Three- Layer Cross-Ply Cylindrical Shell Subjected to Uniform Temperature	114

# LIST OF TABLES

<u>Table</u>		<u>Page</u>
1	Identification of the Various Types of Hybrid-Stress Flat-Plate Finite Elements Evaluated	65
2	Data for Single-Layer Isotropic Plates	66
3	Data for Two-Layer Plates	67
4	Data for Three-Layer Plates	68
5	Results of the 3-Layer Moderately-Thick Cross-Ply Plate under Transverse Loading	69
6	Data for Thin Cylindrical Shells	70
7	Data for Conical Shells	71
8	Percentage Error of the Lowest Frequency Predicted for a Simply-Supported Square Thin Plate Using ELEML	
9	Percentage Error of the Lowest Frequency Predicted for a Clamped Rectangular Thin Plate Using ELEML	72
10	Frequency Predictions for the First Seven Symmetric Modes of Vibration of a Simply-Supported Rectangular Thin Plate Using ELEML and the Hybrid-Rational Mass Matrix	73
11	Percentage Error of the Lowest Frequency Predicted for a Two-Layer Cross-Ply ( $0^\circ/90^\circ$ ) Square Thin Plate Using ELEMR and the HR Mass Matrix	74
12	Data for the Vibration Analysis of a Simply-Supported Two-Layer Cross-Ply ( $0^\circ/90^\circ$ ) Infinite Strip	74
13	Comparison of Predictions for the Lowest Frequencies of 3-Layer Simply-Supported Square Plates	75
14	Properties of a Three-Layer Cylindrical Shell	76
15	Comparison of Predictions for the Lowest Frequencies of 3-Layer Simply-Supported Cylindrical Shells in Axisymmetric Vibration	76

# LIST OF TABLES CONCLUDED

<u>Table</u>		<u>Page</u>
16	Data for a Free Single-Layer Isotropic Thin Rectangular Plate Subjected to Thermal Loading	77
17	Data for a Clamped Rectangular Single-Layer Isotropic Thin Plate Subjected to Thermal Loading	77
18	Data for a Simply-Supported Two-Layer Cross-Ply ( $0^\circ/90^\circ$ ) Infinitely-Long Thin Strip	78
19	Data for a Simply-Supported Three-Layer Cross-Ply ( $0^\circ/90^\circ/0^\circ$ ) Cylindrical Shell Subjected to Thermal Loading	79

## SECTION 1

### INTRODUCTION

#### 1.1 Purpose of the Study

In the design of structures consisting of layered-fiber reinforced composite materials, a designer is often faced with the problem of a complex structure subjected to complex loading conditions. The structure is usually in the form of combined shells and/or plates. The loadings may include static, vibratory, and/or transient mechanical loading as well as thermal loads. In order to assure that the structure can sustain various loading conditions without inducing failure of its normal functions, the designer must choose the most appropriate composite material, and determine the appropriate dimensions and configuration of the layered composite material. Therefore, reliable analytical tools are needed (1) to predict the behavior of a tentative design and (2) to improve, if necessary, a tentative design based on detailed analysis. More specifically, the designer should be able to predict (1) the stress and/or strain distribution at any point within the layered composite and (2) deflections of the structure, so that the failure or safety of the structure can be predicted (a) by comparing the stress or strain against an appropriate strength-failure criterion and/or (b) by comparing the calculated deflection against specified deflection limits. If the tentative design is not satisfactory, then the analysis will point out the weak points of the structure and suggest changes in the design, which could mean both a change in dimension and in orientation of the fiber directions of the composite.

The main objective of this project is to develop appropriate structural analysis tools to assist the designer in material selection and material characterization. In particular, it is intended that these analysis tools when adequately developed and validated be employed to make a realistic assessment of the types and values of composite materials/structures properties that will provide "optimum" resistance to the transient mechanical and/or thermal loads experienced by the structure. Because of the complex nature of the problem, the finite-element method is selected as an appropriate and versatile

mathematical model to cope with the complex structure and loading conditions. Because transverse shear deformation effects are known to be important in laminated composites [1,2,3,4]\*, the usual classical (Kirchhoff) thin plate and shell theory cannot be used directly; accordingly, the finite-element model developed and utilized in the present study includes transverse shear deformation effects. Since the conventional displacement finite-element method, when applied to relatively thick laminated plates, either has failed to predict accurately the local deformations and stresses of a plate under bending [5] or is too expensive to use because too many degrees-of-freedom are involved for even relatively simple problems [6], the hybrid stress finite-element model pioneered by Pian [7] provides a promising alternative.

The hybrid stress model of the finite-element analysis is characterized by an assumed stress field in the interior of the element as well as an assumed displacement field along the boundary of the element. Since a stress field is directly assumed, the prediction of stresses in a given problem is generally more accurate than that of the conventional assumed-displacement model where only the displacement field is assumed for both the interior and along the boundary of the element. Also great flexibility in terms of the formulation and the selection of element features is achieved because the assumed interior stress distribution and the assumed boundary displacement distribution functional can be selected independent of each other. The compatibility of the interelement displacements is easily satisfied, since only the boundary displacement is assumed, while in the conventional-displacement model the satisfaction of compatibility usually poses a difficult problem. More important is the fact that transverse shear deformation effects, which cannot be neglected in many laminated composite plate and shell problems, can be easily taken into account by the hybrid stress model without an increase in the number of element degrees-of-freedom, as indicated in Ref. 8. Because of transverse shear deformation effects, thick laminated plates may have different cross-sectional rotations for each layer. Thus, a severe warping of the original plane section of the whole laminate develops under certain loading

---

\*References are denoted by numbers in square [ ] brackets.

conditions. This phenomenon can be closely modeled by the hybrid stress model with ease as will be seen later in this report.

Structures of prime interest for future analysis and design include, among others, aerospace vehicles in the shape of a low-aspect-ratio lifting body, irregular shaped shells, and/or axisymmetric shapes. Cutouts, branches, stiffeners, etc. may be present. Layered anisotropic construction may comprise a significant portion of the structure.

For the analysis of curved shells, much recent finite-element work has been carried out using curved finite triangular and/or quadrilateral elements for cylindrical shells [9-11], conical shells [12], and shells of revolution [13,14]. These finite elements are convenient if the structure is smooth and regular since they can model the actual structure faithfully geometrically; however, these elements are not suitable or convenient for analyzing shells of irregular shape (irregular boundaries, arbitrarily-oriented cutouts, arbitrarily curved shape; ... ) Also, it should be noted that curved-shell elements are developed for some specific restricted geometry and hence when used for modeling irregular curved shells would entail significant geometric modeling errors unless the element size were very small compared with the main dimensions of the shell. Further, if the element size must necessarily be very small, it would be adequate to model the curved-shell structure by flat-plate elements. In this case the analyst enjoys the advantages of (a) simplicity in element stiffness derivation and computation and (b) great computer program versatility in being able to treat a wide variety of irregularly-shaped structures with relatively simple computer program logic and computations since the element compatibility conditions and the transformations from local element coordinates to a global coordinate system for the entire structure are handled in a uniform fashion.

Flat-plate elements based upon the assumed displacement approach have been used to analyze curved shells [15]. Recently, Wolf [16] used flat-plate hybrid stress finite elements to analyze the "pinched cylindrical shell"; his predictions compare favorably with an independent solution obtained with assumed displacement-type curved finite elements [13]. Further, the assumed stress hybrid model has been shown to be applicable readily to plates which

involve transverse shear deformation and/or thermal loading [8].

Based upon the above considerations and especially its relevance to the present objectives of this project, the hybrid-stress finite-element model has been selected for use in this study. In particular, flat-plate elements are developed for both plate and shell problems.

Before any problems involving complex transient loading conditions can be solved, it is essential to develop and establish the reliability of the pertinent finite elements under static loading conditions. Like conventional displacement finite-element models, the hybrid stress model for static analysis is also characterized by a stiffness matrix. Once the stiffness matrix of an element is proved to be suitable for use, then dynamic problems can be pursued by developing a mass matrix and by first applying it to vibration analyses to establish the reliability of the mass matrix.

As for thermal problems, the most important task is to develop an equivalent loading vector corresponding to a given temperature distribution.

Therefore, in the past twelve-month period, effort has been concentrated on the selection and verification of the behavior of selected finite elements under static loading conditions, on the development and verification of the mass matrix of each of several finite elements, and on an equivalent thermal loading vector.

## 1.2 Synopsis of the Investigation

A method of analyzing plate and shell structures built with layered-fiber-reinforced composite materials has been developed. The work done in the past twelve months is described in the following sections of this report.

In Section 2, the static analysis aspect is described. It begins with a derivation of the stiffness matrix for single-layer flat-plate elements. Then, several candidate elements are studied and compared against each other on two test examples. It is found that triangular-based quadrilateral elements are inferior to "basic" quadrilateral elements; therefore, a basic type of quadrilateral element is selected as the "best" element to be used in this study. This single-layer element is extended to a multilayer element in

Subsection 2.3 which also includes a general derivation of the stiffness matrix for a multilayer element. Both single-layer and multilayer elements are tested on plate problems in Subsection 2.4. Example problems include single-layer isotropic plate problems. Both thin plates and thick plates are included. In Subsection 2.5, the flat-plate elements are applied to shell problems, including shells of revolution. The necessary transformation for single-layer and multilayer flat-plate elements, when applied to shell geometries, are developed in Subsections 2.5.1 and 2.5.2, respectively. Example problems are discussed in Subsection 2.6, where problems of thin cylindrical shells and conical shells of different thicknesses are treated. In both the plate and shell examples, comparisons are made with exact elasticity solutions or other approximate solutions whenever possible. Excellent accuracy is observed. Predicted stresses are shown to be within 2% of the exact elasticity solution in one case. These examples are discussed in Subsection 2.7.

Section 3 begins with a discussion on the variational basis for selecting a mass matrix in the hybrid stress model. Then a hybrid-rational mass matrix as well as a lumped mass matrix is developed and compared. It is found that the hybrid-rational mass matrix is slightly better than the lumped mass matrix for thin plate vibrations. Since it is expected that the former will be much better than the latter for thicker plate vibration analyses, the hybrid-rational mass matrix is used thereafter throughout this study. Example problems of plate and shell vibration are given at the end of Section 3. The predictions for the lowest and next higher mode frequencies are compared with other solution method predictions and are found to be very accurate.

Thermal-stress analysis is described in Section 4. For given temperature distributions, an approximation of the temperature within an element is first established. Then an equivalent loading vector is calculated based on this approximate representation of the actual temperature distribution. Since numerical examples of thermal stress analysis do not appear frequently in the literature, in most of the examples given in this section, comparisons cannot be made. However, the equivalent loading vector is verified through simple examples.

A summary of the work for this period of study and concluding remarks are given in Section 5. This report ends with an appendix on the programming aspect of the present finite-element analysis.

## SECTION 2

### STATIC ANALYSIS

#### 2.1 Formulation of Single-Layer Flat-Plate Elements

##### 2.1.1 Derivation of Element Stiffness Matrices

The formulation of the element stiffness matrix by the hybrid stress model is based on the Principle of Minimum Complementary Energy (Ref. 7). Along each boundary of the element, an assumed displacement distribution is selected; these element-boundary displacements are then expressed in terms of the nodal displacements  $\underline{q}$ . Next, an assumed stress distribution in terms of undetermined stress parameters  $\underline{\beta}$  is chosen throughout the interior of the element; this same distribution function, if desired, may also be used to approximate the prescribed surface tractions. In terms of these distribution functions and associated unknowns  $\underline{q}$  and  $\underline{\beta}$ , one may write an expression for the complementary energy  $\pi_c$ . By setting  $\partial \pi_c / \partial \underline{\beta} = 0$  to minimize the complementary energy, one obtains an approximate solution for  $\underline{\beta}$  in terms of  $\underline{q}$ . This enables one to evaluate the internal strain energy  $U$  entirely in terms of the generalized nodal displacement unknowns  $\underline{q}$ . Then, by recognizing that the stiffness matrix  $\underline{k}$  appears in the following form for  $U$  as  $U = 1/2 \underline{q}^T \underline{k} \underline{q}$ , one thereby identifies  $\underline{k}$  in the hybrid stress model formulation. This procedure is presented in detail in the following.

The total complementary energy of one finite element is given by

$$\pi_c = \frac{1}{2} \int_V S_{ijkl} \sigma_{ij} \sigma_{kl} dV - \int_A T_i u_i dA \quad (2.1)$$

where

$S_{ijkl}$  = compliance constants of the material

$\sigma_{ij}$  = stresses

$V$  = volume

$A$  = boundary area

$T_i$  = surface traction

$u_i$  = prescribed boundary displacement

The functional  $\pi_c$  is a minimum when the stresses satisfy the equilibrium condition.

For convenience, consider a statically loaded continuum which is represented by a single finite element. In deriving the element stiffness matrix, the displacements along each boundary of the finite element are expressed in terms of the nodal displacements  $\underline{q}$  and certain interpolation functions  $\underline{L}$ , such that the displacement compatibility conditions with the neighboring elements (when one models the continuum with a number of finite elements) are satisfied,

$$\underline{u} = \underline{L} \underline{q} \quad (2.2)$$

The element stresses in the interior of the element are then expanded in terms of a finite number of stress parameters  $\underline{\beta}$

$$\underline{\sigma} = \underline{P} \underline{\beta} \quad (2.3)$$

where  $\underline{P}$  is chosen to satisfy the homogeneous equilibrium equations. The surface tractions can then be written in the form of

$$\underline{I} = \underline{R} \underline{\beta} \quad (2.4)$$

where  $\underline{R}$  is obtained by applying the element boundary conditions to  $\underline{P}$ . Substituting Eqs. 2.2 to 2.4 in Eq. 2.1, one obtains,

$$\pi_c = \frac{1}{2} \underline{\beta}^T \left( \int_V \underline{P}^T \underline{S} \underline{P} dV \right) \underline{\beta} - \underline{\beta}^T \left( \int_A \underline{R}^T \underline{L} dA \right) \underline{q} \quad (2.5)$$

By defining

$$\underline{H} = \int_V \underline{P}^T \underline{S} \underline{P} dV \quad (2.6)$$

and

$$\underline{G} = \int_A \underline{R}^T \underline{L} dA$$

Eq. 2.5 becomes

$$\pi_c = \frac{1}{2} \underline{\beta}^T \underline{H} \underline{\beta} - \underline{\beta}^T \underline{G} \underline{q} \quad (2.7)$$

The best approximate solution for  $\underline{\beta}$  for the problem is obtained by setting  $\partial \pi_c / \partial \underline{\beta}$  to zero. The result is

$$\underline{H}\underline{\beta} - \underline{G}\underline{\delta} = 0 \quad (2.8)$$

from which,

$$\underline{\beta} = \underline{H}^{-1}\underline{G}\underline{\delta} \quad (2.9)$$

The first term in Eq. 2.7 for  $\pi_c$  is the total strain energy  $U$  in the element. By substituting Eq. 2.9 into  $U$  one obtains

$$U = \frac{1}{2} \underline{\delta}^T \underline{G}^T \underline{H}^{-1} \underline{G} \underline{\delta} \quad (2.10)$$

By definition

$$U = \frac{1}{2} \underline{\delta}^T \underline{k} \underline{\delta} \quad (2.11)$$

where  $\underline{k}$  is the element stiffness matrix.

Thus, by the hybrid stress model, the element stiffness matrix is given by

$$\underline{k} = \underline{G}^T \underline{H}^{-1} \underline{G} \quad (2.12)$$

### 2.1.2 Material, Stress, and Displacement Assumptions

The matrix  $\underline{S}$  in Eq. 2.6 is the compliance matrix that relates stresses  $\underline{\sigma}$  to strains  $\underline{e}$ :

$$\underline{e} = \underline{S} \underline{\sigma} \quad (2.13)$$

In this study, the following square symmetric material properties are assumed for each layer of the composite material:

$$\begin{Bmatrix} e_x \\ e_y \\ e_z \\ e_{yz} \\ e_{xz} \\ e_{xy} \end{Bmatrix} = \begin{bmatrix} \frac{1}{E_1} & -\frac{\nu_{12}}{E_2} & -\frac{\nu_{13}}{E_3} & & & \\ -\frac{\nu_{21}}{E_1} & \frac{1}{E_2} & -\frac{\nu_{23}}{E_3} & & & \\ -\frac{\nu_{31}}{E_1} & -\frac{\nu_{32}}{E_2} & \frac{1}{E_3} & & & \\ & & & \frac{1}{G_{23}} & & \\ & & & & \frac{1}{G_{13}} & \\ & & & & & \frac{1}{G_{12}} \end{bmatrix} \begin{Bmatrix} \sigma_x \\ \sigma_y \\ \sigma_z \\ \sigma_{yz} \\ \sigma_{xz} \\ \sigma_{xy} \end{Bmatrix}$$

(2.14a)

with  $E_2 = E_3$ ,  $\nu_{12} = \nu_{13}$ ,  $\nu_{21} = \nu_{31}$ ,  $\nu_{23} = \nu_{32}$ ,  $G_{13} = G_{12}$ , and "1" being the longitudinal fiber direction.

In case the material axes do not coincide with the element coordinate axes (see Fig. 1a), the following transformed  $\bar{S}$  is used:

$$\bar{S} = \begin{bmatrix} S_{11}m^4 + S_{22}n^4 + (2S_{12} + S_{33})m^2n^2 & S_{11}n^4 + S_{22}m^4 + (2S_{12} + S_{33})m^2n^2 & 0 & 0 & 0 & 0 \\ S_{12}(m^4 + n^4) + (S_{11} + S_{22} - S_{33})m^2n^2 & S_{11}n^4 + S_{22}m^4 + (2S_{12} + S_{33})m^2n^2 & 0 & 0 & 0 & 0 \\ S_{12}m^2 + S_{23}n^2 & S_{12}n^2 + S_{23}m^2 & S_{22} & 0 & 0 & 0 \\ 0 & 0 & 0 & S_{44}m^2 + S_{55}n^2 & 0 & 0 \\ 0 & 0 & 0 & (S_{55} - S_{44})mn & S_{44}n^2 + S_{55}m^2 & 0 \\ (2S_{11} - 2S_{12} - S_{33})m^3n & (2S_{11} - 2S_{12} - S_{33})n^3m & 2(S_{12} - S_{23}) & 0 & 0 & 4(S_{11} - 2S_{12} + S_{22} - 2S_{33})m^2n^2 + (m^4 + n^4)S_{33} \\ (2S_{12} - 2S_{22} + S_{33})n^3m & (2S_{12} - 2S_{22} + S_{33})m^3n & 2(S_{12} - S_{23}) & 0 & 0 & 0 \end{bmatrix} \quad \text{sym.} \quad (2.14b)$$

where  $m = \cos \alpha$ ,  $n = \sin \alpha$ , and  $S_{ij}$  = the corresponding constants in Eq. 2.14b.

The in-plane interior (and boundary) stress field  $\underline{P}_1$  for  $\sigma_x, \sigma_y$ , and  $\sigma_{xy}$  consists of a stretching part  $\underline{P}_s$  and a bending part  $\underline{P}_b$ :

$$\underline{P}_1 = \underline{P}_s(x, y) + \underline{P}_b(x, y, z) \quad (2.15a)$$

In this study,  $\underline{P}_s$  is assumed to be linear in  $x$  and  $y$ , and  $\underline{P}_b$  is either linear in  $x$  and  $y$  or quadratic in  $x$  and  $y$ . The out-of-plane stress field  $\underline{P}_2$  for  $\sigma_{xz}, \sigma_{yz}$ , and  $\sigma_z$  is determined from the equilibrium equations of elasticity. The matrix  $\underline{P}$  in Eq. 2.3 consists of  $\underline{P}_1$  and  $\underline{P}_2$ . Different assumptions for different elements are summarized in Table 1 and a detailed description can be found in Subsection 2.2.

Along element boundaries (Fig. 1b), the following displacement field is assumed, for a typical side 1-2 of an element:

$$\begin{aligned} u &= u_1(1-s) + u_2 s + z [\theta_{y1}(1-s) + \theta_{y2} s] \\ v &= v_1(1-s) + v_2 s - z [\theta_{x1}(1-s) + \theta_{x2} s] \\ w &= w_1(1-s) + w_2 s \end{aligned} \quad (2.16)$$

where  $s$  is the coordinate measured along the side 1-2, and nodal displacements  $u$ ,  $v$ ,  $w$ ,  $\theta_x$ , and  $\theta_y$  are defined in Fig. 1b. In other words, the in-plane displacements  $u$  and  $v$  are linear in both  $z$  and  $s$ , while the transverse displacement  $w$  is linear in  $s$  but is independent of  $z$ . The number of degrees of freedom per node is 5. Both quadrilateral\* and triangular elements are considered in this study (Figs. 1c and 1d); therefore, the total degrees of freedom per element is, respectively, either 20 or 15.

Variations of Eq. 2.16 can be obtained by adding a mid-point node and changing the linear functions of  $s$  in Eq. 2.16 to quadratic functions.

Based on the assumed interior (and boundary) stress field  $\underline{P\beta}$  in Eq. 2.15 and the assumed element boundary displacement field  $\underline{Lq}$  in Eq. 2.16, the element stiffness matrix  $\underline{k}$  can be obtained by carrying out the appropriate integration of Eq. 2.6 and substituting into Eq. 2.12.

It should be noted that shear deformation effects are taken into account in Eq. 2.16, where  $\theta_x$  and  $\theta_y$  are the rotations of the normal element of a plate; these quantities are not to be identified with the slopes  $w_{,y}$  and  $w_{,x}$  of the middle surface. In other words, the normal to the undeformed middle surface does not remain normal to the deformed middle surface. Also, in the evaluation of  $\underline{H}$  by Eq. 2.6, the transverse shear energy terms are included.

Various elements with different assumed  $\underline{P\beta}$  and  $\underline{Lq}$  are studied and the results are described in the following subsection.

## 2.2 Parametric Study and Selection of Single-Layer Elements

Since the stress field of an element can be assumed independently of the boundary displacement field, it is possible to match different pairs of

\* Included are square, rectangular, and irregular quadrilateral geometries.

assumptions and to select those elements with the better convergence behavior.

The stresses in an individual lamina may be considered as the combination of the stretching and bending components as shown in Eq. 2.15. When the stretching component is represented by a complete linear expansion in  $x$  and  $y$ , while the bending component is represented by a complete quadratic expansion in  $x$  and  $y$ , the stress field can be represented by 34 independent stress parameters as follows:

[illegible]

In constructing the various models, one of the following three different stress fields is used in a given model:

- (a) Type  $(L, \bar{L})$ : This corresponds to columns 1-9, 10, 11, 12, 15, 18, 19, and 20 of the matrix in Eq. 2.17, with a total of 16  $\beta$ 's. The designation  $(L, \bar{L})$  stands for a complete linear expansion in  $x$  and  $y$  for the stretching component and an incomplete linear expansion in  $x$  and  $y$  for the bending component.
- (b) Type  $(L, L)$ : This corresponds to columns 1-20, with a total of 20  $\beta$ 's. The designation  $(L, L)$  stands for a complete linear expansion in  $x$  and  $y$  for both the stretching and the bending component.

- (c) Type (L,Q): This corresponds to columns 1-34, with a total of 34  $\beta$ 's. The designation (L,Q) stands for a complete linear expansion in the stretching components and a complete quadratic expansion in bending.

Three types of element-boundary displacement fields (along side 1-2, for example) are used:

- (a) Type (L): This corresponds to the following:

$$\begin{aligned}U &= U_1(1-s) + U_2s + z[\theta_{y1}(1-s) + \theta_{y2}s] \\V &= V_1(1-s) + V_2s - z[\theta_{x1}(1-s) + \theta_{x2}s] \\W &= W_1(1-s) + W_2s\end{aligned}\tag{2.18}$$

where  $s$  is the coordinate along one side of the element. The designation (L) stands for a complete linear expansion in  $s$ .

- (b) Type (Q): This corresponds to the following:

$$\begin{aligned}U &= U_1(1-s) + U_2s + 4U_m(1-s)s + z[\theta_{y1}(1-s) + \theta_{y2}s] \\V &= V_1(1-s) + V_2s + 4V_m(1-s)s - z[\theta_{x1}(1-s) + \theta_{x2}s] \\W &= W_1(1-s) + W_2s + 4W_m(1-s)s\end{aligned}\tag{2.19}$$

The subscript  $m$  stands for the mid-point side node. The designation (Q) stands for a complete quadratic expansion for the displacements.

- (c) Type (Q<sup>-</sup>): This corresponds to the following:

$$\begin{aligned}U &= U_1(1-s) + U_2s + z[\theta_{y1}(1-s) + \theta_{y2}s] \\V &= V_1(1-s) + V_2s - z[\theta_{x1}(1-s) + \theta_{x2}s] \\W &= W_1(1-s) + W_2s + (\theta_{n2} - \theta_{n1})(1-s)s\ell/2\end{aligned}\tag{2.20}$$

where  $\theta_n$  is the rotation along the element side and is a function of  $\theta_x$  and  $\theta_y$ . The designation (Q) stands for a quadratic expansion for  $w$  only. If type (Q) is used on certain sides and type (L) is used on the remainder, then the designation is (L,Q).

Because shear deformation effects are of major concern in this study, the selected elements should be able to converge rapidly both for thin and thick plates. Therefore, two extreme test problems are used to evaluate various elements in order to select the most suitable elements for future use. One is a simply-supported square thin plate with a thickness-to-side ratio of 1:100, and the other is a simply-supported square thick plate with a thickness-to-side ratio of 1:4. The former is centrally loaded and the latter is uniformly loaded.

A brief description of the elements studied and the associated example-problem solutions are summarized in Table 1 and in Figs. 2 and 3. Not every result is plotted in Figs. 2 and 3 because some are far below or above the range of the plots. A total of nine elements has been tried; these are described in the following, together with brief assessment-type comments:

- (a) ELEML: General quadrilateral element with stress type (L,L), displacement type (L).

This element is suitable for problems of plates or shells of revolution. Convergence is fast and computation of the  $k$  matrix is inexpensive. The total degrees-of-freedom per element is 20.

- (b) ELEMA: Triangular element with stress type (L,L) and displacement type (L)

This element does not converge to correct answers within reasonable mesh refinement limits. This element is too "stiff" and is rejected.

- (c) ELEMB: Triangular element with stress type (L,L) and displacement type (L,Q)

To improve ELEMA, a midpoint node is added to the interior boundary (see Table 1). The improvement is not enough. This element is still too stiff and is rejected.

- (d) ELEMC: Triangular element with stress type  $(L,L)$  and displacement type  $(Q)$   
 To make ELEMB more flexible, midpoint nodes are added to every boundary. Unfortunately, the stiffness matrix becomes singular even after the usual boundary constraining. This is due to the fact that the number of unwanted displacement modes which induce no stresses within the element (these modes are called kinematic modes) are too many (4 for bending only) to be completely suppressed by the imposed boundary conditions (Ref. 17). This element is rejected.
- (e) ELEMD: Triangular element with stress type  $(L,L)$  and displacement type  $(L,Q)$   
 Another way of making an element more flexible is to reduce the number of  $\beta$ 's. From ELEMB, the number of  $\beta$ 's is reduced to 16. This element converges rapidly as can be seen in Figs. 2 and 3. However, its application to future thermal analysis is limited because its stress field is too simple. Therefore, it is rejected.
- (f) ELEME: Triangular element with stress type  $(L,Q)$  and displacement type  $(L)$   
 To suppress the unwanted modes of ELEMC, a complete quadratic bending stress field is used. Due to the increase in the number of stress parameters  $\beta$ , it is too stiff and is rejected.
- (g) ELEMF: Triangular element with stress type  $(L,Q)$  and displacement type  $(Q)$   
 Midpoint nodes are added to ELEME to make it more flexible. It turns out that ELEMF is good for thin plates but is too flexible for thick plates as can be seen from Figs. 2 and 3.
- (h) ELEMG: Triangular element with stress type  $(L,Q)$  and displacement type  $(Q)$   
 This element has the advantage of increasing the order of  $w$  without increasing the number of degrees-of-freedom per node. The convergence is moderate. Since only  $w$  is quadratic, this element is not suitable for shell problems where  $u$ ,  $v$ , and  $w$  should be consistent. Therefore, it is rejected.
- (i) ELEM2: Four triangular elements with stress type  $(L,Q)$  and displacement type  $(L,Q)$   
 Four triangular elements assembled into one quadrilateral element. The convergence for a thick plate is very rapid and the convergence for a thin plate is fairly rapid. This element can be used for general shell problems.

Note that for solution, one quarter of the plate was modeled by uniform-sized finite elements. The number of degrees of freedom, DOF, indicated in Figs. 2 and 3 denotes the DOF's for the quarter plate.

Out of the nine elements tested (see Table 1), only two of them show fast convergence. The triangular-based quadrilateral element, ELEM2, is more sophisticated than the quadrilateral ELEM1. Consequently, more computing time is needed to calculate the stiffness matrix of ELEM2. Since ELEM2 shows no improvement over ELEM1, ELEM1 is used hereinafter throughout this study. In the following, ELEM1 is extended to represent a multilayer element.

## 2.3 Formulation for Multilayer Flat-Plate Elements

### 2.3.1 Derivation of Element Stiffness Matrices

In the present formulation of stiffness matrices for laminated plate finite elements, the self-equilibrating stresses for each lamina are initially assumed independently. The stress equilibrium conditions for the stresses at the interlamina boundaries are then introduced as a finite number of conditions of constraint

$$\underline{A}\underline{\beta} = 0 \quad (2.21)$$

Using the method of Lagrange Multipliers, the complementary energy functional of Eq. 2.7 is modified to

$$\pi_c' = \frac{1}{2} \underline{\beta}^T \underline{H} \underline{\beta} - \underline{\beta}^T \underline{G} \underline{\xi} + \underline{\lambda}^T \underline{A} \underline{\beta} \quad (2.22)$$

Again, by setting  $\partial \pi_c' / \partial \underline{\beta} = 0$  for each  $\underline{\beta}$ , one obtains

$$\underline{H} \underline{\beta} - \underline{G} \underline{\xi} + \underline{A}^T \underline{\lambda} = 0 \quad (2.23)$$

from which

$$\underline{\beta} = \underline{H}^{-1} \underline{G} \underline{\xi} - \underline{H}^{-1} \underline{A}^T \underline{\lambda} \quad (2.24)$$

Substituting into Eq. 2.21, results in

$$\underline{A} \underline{H}^{-1} \underline{G} \underline{\xi} - \underline{A} \underline{H}^{-1} \underline{A}^T \underline{\lambda} = 0 \quad (2.25)$$

or

$$\underline{\lambda} = (\underline{A}\underline{H}^T\underline{A}^T)^{-1}(\underline{A}\underline{H}^T\underline{G}\underline{\beta}) \quad (2.26)$$

Substituting  $\underline{\lambda}$  from Eq. 2.26 into Eq. 2.24 and then substituting the resulting  $\underline{\beta}$  into the strain energy  $U$ , one obtains

$$U = \frac{1}{2} \underline{\beta}^T [\underline{G}^T \underline{H}^T \underline{G} - \underline{G}^T \underline{H}^T \underline{A}^T (\underline{A}\underline{H}^T \underline{A}^T)^{-1} \underline{A}\underline{H}^T \underline{G}] \underline{\beta} \quad (2.27)$$

Thus, the stiffness matrix is given by

$$\underline{K} = \underline{G}^T \underline{H}^T \underline{G} - \underline{G}^T \underline{H}^T \underline{A}^T (\underline{A}\underline{H}^T \underline{A}^T)^{-1} \underline{A}\underline{H}^T \underline{G} \quad (2.28)$$

### 2.3.2 Stress and Displacement Assumptions

Multilayer laminated thick plates often exhibit a severe warping of the cross section as a result of the transverse shear deformation effects and the discontinuous material properties from layer to layer (Refs. 1, 2, 3, 4). To model this warping phenomenon closely, the rotational degrees-of-freedom  $\theta_x$  and  $\theta_y$  should be assumed to be different for each layer. Within each layer,  $\theta_x$  and  $\theta_y$  are still assumed to be a constant in the transverse direction; thus,  $\theta_x$  and  $\theta_y$  can be represented by the inplane displacements  $u$  and  $v$  at the upper and lower surface of that layer (Fig. 4). The transverse displacement  $w$  is still assumed to be a constant in the transverse direction for all layers. Therefore, the total degrees-of-freedom at a node consists of one  $w$  and  $(n+1)$  inplane displacements  $u$  and  $v$ , with  $n$  being the number of layers. The number of degrees-of-freedom per node is then  $2(n+1)+1$ .

For a typical layer  $i$ , the displacements along side 1-2 are:

$$\begin{aligned} u_{1-2}^{(i)} &= \frac{1}{2} (u_1^{(i+1)} + u_1^{(i)}) (1-S) + \frac{1}{2} (u_2^{(i+1)} + u_2^{(i)}) S + \frac{2}{h^{(i)}} [(u_1^{(i+1)} - u_1^{(i)}) (1-S) + (u_2^{(i+1)} - u_2^{(i)}) S] \\ v_{1-2}^{(i)} &= \frac{1}{2} (v_1^{(i+1)} + v_1^{(i)}) (1-S) + \frac{1}{2} (v_2^{(i+1)} + v_2^{(i)}) S + \frac{2}{h^{(i)}} [(v_1^{(i+1)} - v_1^{(i)}) (1-S) + (v_2^{(i+1)} - v_2^{(i)}) S] \\ w_{1-2}^{(i)} &= w_1 (1-S) + w_2 S \end{aligned} \quad (2.29)$$

For stress distributions, an independent set of  $\underline{p}_i \underline{\beta}_i$  (the same as that used for ELEM1) should also be assumed for each layer. The interface equilibrium is achieved by demanding that

$(\sigma_z, \sigma_{yz}, \sigma_{xz})$  at the top of the  $i$ th layer

$$\equiv (\sigma_z, \sigma_{yz}, \sigma_{xz}) \text{ at the bottom of the } (i+1)\text{th layer} \quad (2.30)$$

Equation 2.30 constitutes a constraint on the stress parameters  $\underline{\beta}$  and can be arranged in the form of Eq. 2.21. Then the stiffness matrix of a multilayer element can be computed using Eq. 2.28. This new element is designed as ELEMZ.

For relatively thin laminated plates and shells, the warping phenomenon is not severe and the usual assumption that a plane cross section remains plane is still applicable. The corresponding change in the element stiffness matrix can be easily achieved by demanding that the nodal displacements  $u$  and  $v$  be linear in the transverse direction and be replaced by, respectively,  $\theta_y$  and  $\theta_x$  just as in Eq. 2.16. Then the total number of degrees-of-freedom per node is back to 5 again and this reduced multilayer element will be designated as ELEMZ.

## 2.4 Flat-Plate Evaluation Examples

Several plate problems have been solved and a comparison of results is made with respect to exact solutions or other approximate solutions. In all but two examples, convergence studies are made to establish the reliability of the elements ELEM1, ELEMZ, and ELEMZ. Problem descriptions and the finite-element modelings used are given in Tables 2, 3, and 4 for, respectively, single-layer plates and three-layer plates.

### 2.4.1 Single-Layer Isotropic Plates

#### (a) Simply-Supported Square Thin Plate (Table 2, Fig. 2)

This is a problem used in the selection of elements. The errors of the predicted central transverse displacements  $w_c$  for elements 1, 2, A, D, and F are plotted for different meshes in a quarter of

the plate; advantage is taken of symmetry so that only one-quarter of the plate is modeled by equal-sized quadrilateral elements. The percentage errors are calculated by comparison with the exact solution of Ref. 18. From Fig. 2, it is seen that the error diminishes very rapidly and that ELEM1 provides somewhat superior results.

(b) Clamped Square Thin Plate (Table 2, Fig. 5)

To see whether or not boundary conditions affect the convergence of ELEM1 predictions, a clamped-plate problem is solved. A plot similar to that of Fig. 2 is presented as Fig. 5 and shows fast convergence. Comparison is based on the exact solution of Ref. 18.

(c) Clamped Rectangular Thin Plate (Table 2, Fig. 6)

Both a square element and a rectangular element (1:2 aspect ratio) for ELEM1 are used to see the effects of a large aspect ratio of the element. The results are compared with the exact solution of Ref. 18. From Fig. 6, it is observed that in both cases the convergence is fast although the pattern of convergence is reversed.

(d) Skewed Simply-Supported Thin Plate (Table 2, Fig. 7)

Since ELEM1 is a general quadrilateral element, it is not restricted to rectangular plate problems. Various solutions [19,20,21] of the skewed plate problem identified in Table 2 were collected in Ref. 18 and are reproduced here in Fig. 7 together with the present ELEM1 solutions. It is seen that the present simple element provides solution accuracy and efficiency comparable to other higher-order elements even though the free traction condition at the edge is not enforced in the present solutions (this enforcement would require a special element).

(e) Simply-Supported Square Thick Plate (Table 2, Fig. 3)

This is also a problem used in the selection of elements. Comparison of the predicted central displacement is made with the exact solution of Ref. 22. It is seen that ELEM1 converges even faster in this case. This is expected since ELEM1 is designed to

cope with shear deformation and in this problem the shear deformation is indeed important (about 25% of the total deformation).

The results of the above examples demonstrate the reliability of ELEM1 for isotropic plates. Since the present study is mainly intended for composite plates, the above results can only be regarded as a good start, and further evaluations have been carried out as discussed in the following.

#### 2.4.2 Two-Layer Plates

Four problems of two-layer plates are solved. The ELEM1 element is used for the first three, since they involve very thin plates with negligible warping. For the last one, which is a thick plate problem, ELEM2 is used.

(a) Clamped Cross-Ply Rectangular Thin Plate (Table 3, Fig. 8)

A clamped-edge rectangular plate consisting of two layers of fiber-reinforced composite materials with orientations of  $0^\circ/90^\circ$  with respect to the positive x-axis is uniformly loaded. The central deflection is calculated using ELEM1 for the same plate with or without the assumption of negligible shear deformation effects; since the plate is indeed very thin (with a side-to-thickness ratio of 1:100), the two present deflection predictions differ by only 1% and are both very close to but slightly larger than the CPT (classical laminated plate theory) approximate solutions of Ref. 23.

(b) Clamped Cross-Ply Square Thin Plate (Table 3, Fig. 9)

As indicated in Fig. 9, this problem is solved twice using ELEM1. In the first solution, the whole plate is oriented in the usual way, but in the second solution, it is rotated  $45^\circ$  so that the material axes are no longer parallel to the reference coordinate axes. The purpose is to make sure that the transformation of the compliance matrix has been correctly programmed, since both solutions should be the same if the transformation is correct. Indeed, these two solutions are identical and converge very rapidly in

comparison with the CPT solution of Ref. 23.

(c) Clamped Angle-Ply Square Thin Plate (Table 3, Fig. 10)

The problem considered is similar to the previous one but the fiber orientations are  $\pm 45^\circ$ . Again, the two solutions of ELEM2 are identical and converge rapidly; that is, to within 5% of the CPT solution of Ref. 23. It should be noted that the CPT solution tends to give less accurate predictions for angle-ply problems because the distortion of the plate is more severe than that of the cross-ply problems. Hence, the 5% difference here can be attributed largely to the error of the CPT solution.

(d) Simply-Supported Angle-Ply Square Thick Plate (Table 3, Fig. 11)

To investigate the shear deformation effects, a thick-plate problem is solved using ELEM2 for different orientations of the two-layer angle-ply. The present solutions differ from the approximate solutions of Ref. 24. Again, the difference can be attributed to the error of the approximate solution since other cases tested in Ref. 24 are also less accurate for thick laminated plates. Because of the shear deformation effects, the central deflections are approximately doubled compared with that for the case of zero transverse shear deformation. It should be pointed out that studies of this kind will assist the designer in the selection of the appropriate material orientations to fulfill certain specific design objectives.

### 2.4.3 Three-Layer Plates

(a) Infinite Cross-Ply Plate with Sinusoidal Loading  
(Table 4, Figs. 12a-12d)

The problem of an infinitely long thick plate loaded sinusoidally in the short direction and simply-supported along the two edges is a two-dimensional plane-strain problem and can be solved exactly according to elasticity theory as shown in Ref. 1. Using the

present finite-element method and ELEMZ, this problem is solved by putting a uniform mesh in one strip in the short direction since the solutions are independent of the long-direction coordinate. The displacement and stress predictions are very close to those of the exact solution as can be seen in Figs. 12a through 12d. It is observed that the other assumed displacement finite-element solution (Ref. 5), which also takes transverse shear deformation effects into account: (1) does not give accurate detailed predictions, but only average values of cross-section rotation and normal stresses, and (2) is very close to the CPT solution, which does not take shear effects into account at all.

(b) Simply-Supported Cross-Ply Plate (Tables 4 and 5, Fig. 13)

This finite-dimension problem is solved exactly in Ref. 2. Two examples with different aspect ratio and thickness ratio are given here (Table 4, cases b1 and b2; both are solved using ELEMZ. The first one is a moderately thick rectangular plate under bending; the maximum displacement and stress components predicted by the method are within 2% of the exact solution [2] as can be seen in Table 5. The second example is a thick square plate under bending; the stress and displacement distributions at crucial sections are plotted in Fig. 13. Also plotted are solutions obtained by using a 3-dimensional assumed-displacement finite element [6]; it is seen that the present method gives practically the same accuracy with many fewer degrees-of freedom (225 DOF vs. 990 DOF).

## 2.5 Application to Shell Problems

### 2.5.1 Transformation for Single-Layer Elements

In the application of flat-plate elements to shell problems, it is necessary to transform the element nodal degrees-of-freedom, which are in element coordinates, to a common or global nodal degree-of-freedom system. As discussed in Ref. 25, the transformation can be expressed in the following form:

$$\begin{Bmatrix} u \\ v \\ w \\ \theta_x \\ \theta_y \end{Bmatrix}_{\text{ELEMENT}} = \begin{bmatrix} \cos(X, \bar{X}) & \cos(X, \bar{Y}) & \cos(X, \bar{Z}) & & \\ & \cos(Y, \bar{X}) & \cos(Y, \bar{Y}) & \cos(Y, \bar{Z}) & 0 \\ & & \cos(Z, \bar{X}) & \cos(Z, \bar{Y}) & \cos(Z, \bar{Z}) \\ & & & 0 & \cos(X, \bar{X}) & \cos(X, \bar{Y}) & \cos(X, \bar{Z}) \\ & & & & \cos(Y, \bar{X}) & \cos(Y, \bar{Y}) & \cos(Y, \bar{Z}) \end{bmatrix} \begin{Bmatrix} u \\ v \\ w \\ \theta_x \\ \theta_y \\ \theta_z \end{Bmatrix}_{\text{NODE}} \quad (2.31a)$$

or

$$\underline{\underline{q}} = \underline{\underline{T}}_{5 \times 6} \underline{\underline{\bar{q}}} \quad (2.31b)$$

where the "barred" system is the common (global) nodal system.

If the z-axis of the common nodal coordinate system is chosen to be in the direction of the outer normal of the shell surface (Ref. 15), then the contributions of  $\cos(x, \bar{z})$  and  $\cos(y, \bar{z})$  in the last column are small compared with other terms and can be neglected. The resulting transformation is a 5x5 transformation and the nodal degrees-of-freedom consist of only  $u$ ,  $v$ ,  $w$ ,  $\theta_x$ , and  $\theta_y$ :

$$\begin{Bmatrix} u \\ v \\ w \\ \theta_x \\ \theta_y \end{Bmatrix}_{\text{ELEMENT}} = \begin{bmatrix} \cos(X, X) & \cos(X, Y) & \cos(X, Z) & & \\ & \cos(Y, X) & \cos(Y, Y) & \cos(Y, Z) & 0 \\ & & \cos(Z, X) & \cos(Z, Y) & \cos(Z, Z) \\ & & & 0 & \cos(X, X) & \cos(X, Y) \\ & & & & \cos(Y, X) & \cos(Y, Y) \end{bmatrix} \begin{Bmatrix} u \\ v \\ w \\ \theta_x \\ \theta_y \end{Bmatrix}_{\text{NODE}} \quad (2.32a)$$

or

$$\underline{\underline{q}} = \underline{\underline{T}}_{5 \times 5} \underline{\underline{\bar{q}}} \quad (2.32b)$$

The corresponding element stiffness matrix is

$$\underline{\underline{\bar{k}}} = \underline{\underline{T}}^T \underline{\underline{k}} \underline{\underline{T}} \quad (2.33)$$

Once  $\underline{\underline{\bar{k}}}$  is obtained from Eq. 2.33, this transformed element stiffness

matrix can be assembled into a system stiffness matrix  $\underline{K}$ , as usual, and the remaining procedure is the same as that for plate problems.

The above transformation is applicable to ELEMI and ELEM. R.

### 2.5.2 Transformation for Multilayer Elements

Since the nodal displacements of a multilayer element are completely represented by the interlayer displacements  $u$ ,  $v$ , and transverse displacement  $w$ , instead of  $u$ ,  $v$ ,  $w$ ,  $\theta_x$ , and  $\theta_y$ , the former should be expressed in terms of the latter before a transformation can be carried out. This is accomplished by defining an equivalent set of nodal degrees-of-freedom, which consists of the displacements  $u$ ,  $v$ , and  $w$  at the nodal mid-thickness station of an element and the rotations  $(\theta_x)_i$  and  $(\theta_y)_i$  of each layer of the element at a nodal station (see Fig. 14).

The relation between this new set of degrees-of-freedom and the old one can be put in matrix form as

$$\begin{Bmatrix} u_1 \\ v_1 \\ w_1 \\ u_2 \\ v_2 \\ \vdots \\ u_n \\ v_n \\ w \end{Bmatrix} = \underline{T}_{q\theta} \begin{Bmatrix} u \\ v \\ w \\ \theta_{x1} \\ \theta_{y1} \\ \vdots \\ \theta_{xn} \\ \theta_{yn} \end{Bmatrix} \quad (2.34a)$$

or

$$\underline{\xi} = \underline{T}_{q\theta} \underline{\theta} \quad (2.34b)$$

For a typical three-layer case as shown in Fig. 17, the matrix  $\underline{T}_{q\theta}$  is

$$T_{\theta\theta} = \begin{pmatrix} 1 & 0 & 0 & 0 & -d_1 & 0 & -d_2 & 0 & 0 \\ 0 & 1 & 0 & d_1 & 0 & d_2 & 0 & 0 & 0 \\ 1 & 0 & 0 & 0 & 0 & 0 & -d_2 & 0 & 0 \\ 0 & 1 & 0 & 0 & 0 & d_2 & 0 & 0 & 0 \\ 1 & 0 & 0 & 0 & 0 & 0 & d_3 & 0 & 0 \\ 0 & 1 & 0 & 0 & 0 & -d_3 & 0 & 0 & 0 \\ 1 & 0 & 0 & 0 & 0 & 0 & 0 & d_3 & d_4 \\ 0 & 1 & 0 & 0 & 0 & d_3 & 0 & -d_4 & 0 \\ 0 & 0 & 1 & 0 & 0 & 0 & 0 & 0 & 0 \end{pmatrix}$$

(2.35)

Then the transformation of this new local system to the common (global) system is

$$\begin{pmatrix} u \\ v \\ w \\ \theta_{x1} \\ \theta_{y1} \\ \vdots \\ \theta_{xn} \\ \theta_{yn} \end{pmatrix} = \begin{pmatrix} T_{3 \times 3} & & 0 \\ & T_{2 \times 3} & \\ 0 & & T_{2 \times 3} \end{pmatrix} \begin{pmatrix} u \\ v \\ w \\ \theta_{x1} \\ \theta_{y1} \\ \theta_{x2} \\ \theta_{y2} \\ \vdots \\ \theta_{xn} \\ \theta_{yn} \end{pmatrix}$$

(2.36a)

or

$$\tilde{\theta} = T_{\theta\theta} \tilde{\bar{\theta}}$$

(2.36b)

where the submatrices  $T_{3 \times 3}$  and  $T_{2 \times 3}$  are the submatrices of  $T_{5 \times 6}$  of Eq. 2.31.

The overall transformation matrix is found by combining Eq. 2.34 and Eq. 2.36:

$$\begin{aligned} \bar{u} &= T_{g0} u = T_{g0} T_{0g} \bar{u} \\ \text{or} \quad \bar{u} &= T_{gg} \bar{u} \\ T_{gg} &= T_{g0} T_{0g} \end{aligned} \tag{2.37}$$

The transformed element stiffness matrix  $\bar{k}$  is then

$$\bar{k} = T_{gg}^T k T_{gg} \tag{2.38}$$

The above transformation is applicable to ELEMZ.

## 2.6 Shell Evaluation Examples

Thin cylindrical shell problems are solved first. Then conical shells of various thickness are solved to demonstrate the effect of transverse shear deformation. The problem data and the finite-element modeling employed are given in Tables 6 and 7.

### 2.6.1 Thin Cylindrical Shells

#### (a) Pinched Cylindrical Shell (Table 6, case (a); Fig. 15)

Both analytical and finite-element solutions [16,20,26] are available for this problem and are collected by Wolf in Ref. 16. Although the present solution using ELEM1 does not enforce the free traction condition on the simply-supported edges, its accuracy is still comparable to other solutions as can be seen in Fig. 15.

#### (b) Cylindrical Shell under Ring Load (Table 6 case (b); Fig. 16)

An analytical solution for this problem is given in Ref. 27. Since the ring load is axisymmetric, this problem can be reduced to a one-dimensional problem and an extensive convergence study can be performed thriftily. It is seen in Fig. 16 that the deflection under the ring load as predicted with ELEM1 flat-plate elements converges rapidly to within 5% of that of the analytical

solution. An increase in the number of elements eventually further reduces the error to within 2%.

### 2.6.2 Conical Shells

To investigate the transverse shear deformation effects on a shell, several conical shell problems are solved with ELEML and ELEMUR flat-plate elements. They all have the same loading and geometry, except that they differ in the thickness and material constituents. The chosen loading is axisymmetric in order to minimize the computing cost.

#### (a) Isotropic Conical Shells (Table 7, Case (a); Figs. 17 to 20)

First, a shell with thickness = 0.025 in. is solved. Comparisons of displacement and moment distributions are made in Figs. 17a and 17b with those predicted by another higher-order finite-element solution (SABOR 4, Ref. 28). In using 45 elements along the meridian, the present solution is, within plotting accuracy, the same as that of SABOR 4. The latter does not take transverse shear deformation effects into account. Next, the thickness is increased to 0.1 in. (Figs. 18a and 18b) and then to 0.5 in. (Figs. 19 and 20). There are still no apparent transverse shear deformation effects. However, when the thickness is increased to 1 inch, which corresponds to a thickness-to-radius ratio = 1:15, pronounced transverse shear deformation effects, reflected by the difference between the present solutions of ELEML and those of the SABOR 4, are observed as is evident from Figs. 19 and 20. For a thicker shell, it can be concluded that transverse shear deformation effects must be taken into account in order to obtain any meaningful answer.

#### (b) Sandwich Conical Shell (Table 7, Case (b); Fig. 21)

Since no other solutions have been found for comparison, only a displacement distribution is presented for this example. The sandwich shell is treated as a three-layer shell, and ELEMUR is used. The displacement plot in Fig. 21 shows a rapid die-out of

the loading effect. A comparison with Fig. 17b shows that the edge deflection of the sandwich shell is smaller than that of an isotropic shell, which uses roughly the same amount of material as is used for the skin of the sandwich shell (0.025 in. thick vs. 0.02 in. thick). This clearly demonstrates the effectiveness of the sandwich structure in increasing the stiffness of the shell.

(c) Two-Layer Conical Shell (Table 7, Case (c); Figs. 20 and 22a-22b)

To simulate some missile-type structures, a glass-phenolic coating layer is placed on top of an aluminum base layer and this two-layer shell is analyzed using ELEM8. The normal displacement of this two-layer shell is plotted in Fig. 20 together with solutions for other similar conical shells. Since the coating layer is relatively soft, the deflection is larger than that of a similar but isotropic shell of 1-in. thickness. The maximum meridional normal stresses in both layers are plotted in Fig. 22a. As expected, the maximum stresses occur at the two outer surfaces of the shell. The maximum circumferential normal stresses are plotted in Fig. 22b. They occur at the interlayer surface and at the inner surface of the shell. The maximum stress in the base material is more than three times that of the coating material, due to the larger stiffness of the base.

It is clear that such a detailed description of the stress distributions will be of definite value to a designer who needs this basic information to determine whether or not the structure will withstand the given loading.

2.7 Summary and Comments

A method of analyzing fiber-reinforced laminated plate and shell structures under static loading has been developed. The hybrid stress finite-element method has been chosen as the mathematical model to analyze this complex problem. Because of the versatility of the hybrid stress method, problems like transverse shear deformation effects and multilayer laminates are dealt with easily.

The development of this basic analysis tool has been carried out step by step. First, several candidate single-layer-plate elements have been studied. Based on two test problems, a quadrilateral element (ELEM1) has been chosen for later use. Then, an extension to multilayer elements (ELEM2 and ELEM3) has been made, and various plate problems have been solved to establish the reliability of the present method.

Application to shell problems is achieved through a coordinate transformation. Then several shell problems have been solved to demonstrate the validity of this transformation and to study transverse shear deformation effects on shells.

In addition to the three elements selected for use as described in this section, another similar element designated as ELEM3 was developed in the research effort under this contract and is described in another report [29]\*. That element is designed for thin multilayer laminated plates. The only difference between ELEM3 and ELEM2 is that the former has a single set of stress assumptions for the whole flat plate element regardless of the number of layers, while the latter has an independent stress assumption for each layer of the flat-plate element. Studies reported in Ref. 29 show that for multilayer plates with thickness-to-side ratios ranging from 0.01 to 0.25, ELEM3 provides better results than does ELEM2. The errors of the results obtained by using ELEM3 are uniformly less than those of ELEM2. However, it should be stressed that for thick laminates with a typical thickness-to-side ratio equal to or greater than about 0.1, the multilayer element ELEM3 should be used to avoid excessive error; for such thickness ratios, ELEM3 and ELEM2 are both deficient.

---

\* In Ref. 29, both ELEM1 and ELEM2 of this report are referred to as ELEM1, since they have the same number of degrees-of-freedom per element.

## SECTION 3

### VIBRATION ANALYSIS

#### 3.1 Vibration Analysis by the Hybrid Stress Model

As is seen in the previous section, the static hybrid stress finite-element analysis takes the same form as does the displacement finite-element analysis; that is, each element is represented by an element stiffness matrix and the final unknown parameters are the element nodal generalized displacements. In other words, the hybrid stress model can be viewed as just an alternative way of deriving a stiffness matrix. Along this line of thinking, it seems that analogous with, but somewhat different from the consistent mass matrix approach used in the displacement finite element dynamic analysis, a mass matrix for the hybrid stress model can be constructed by using a displacement field for the interior of an element based on a suitable interpolation of the assumed boundary displacements of the hybrid stress element, and by evaluating the corresponding kinetic energy of the element in terms of the generalized nodal velocities, thereby identifying the associated mass matrix. This was done by Dungar, Severn, and Taylor [30] for a general triangular flat-plate element and a right-angled triangular flat-plate element, and later by Dungar and Severn [31] for a triangular plate element with variable thickness. Numerical examples in both Ref. 30 and Ref. 31 showed convergence of the predicted natural frequencies. This approach was extended to treat a cylindrical shell element by Henshell, Neale, and Warbuton [32], and to accommodate a triangular flat-plate element and a rectangular flat-plate element by Neale, Henshell and Edwards [33].

An alternative approach is provided by Tabarrok [34,35] who formulates the vibration problem according to Toupin's Principle [36] with the impulse tensor and velocities as field variables. This formulation is consistent with the hybrid stress model; accurate frequency predictions are obtained by Sakaguchi for plate vibration problems [37]. Unfortunately, this approach produces neither a mass matrix nor a stiffness matrix, but rather a frequency matrix; the zeros of its determinant are the frequencies of a system. As a

result, this approach is not applicable to transient dynamic problems.

Recently, efforts have been made to develop a variational principle to justify the approach of interpolating boundary displacements of an element as a legitimate way of obtaining a mass matrix [38,39] so that the conventional formulation for stiffness and mass matrices can be safely adopted in a hybrid stress finite-element dynamic analysis. In the following, a brief description of the derivation of a mass matrix from a variational principle for the hybrid stress model is given.

Consider a functional in the form of a modified Reissner principle [39,40] for the free vibration of a continuum,

$$\begin{aligned} \pi_{mR} = \sum_n \left\{ \int_{V_n} \left[ -\frac{1}{2} S_{ijkl} \sigma_{ij} \sigma_{kl} + \frac{1}{2} \sigma_{ij} (u_{i,j} + u_{j,i}) - \frac{1}{2} \rho \dot{u}_i \dot{u}_i \right] dV \right. \\ \left. - \int_{\partial V_n} T_i (u_i - \bar{u}_i) dA \right\} \end{aligned} \quad (3.1)$$

where  $\partial V_n$  refers to the boundary of the region  $V_n$ ,  $\sigma_{ij}$  and  $u_i$  are defined within the interior volume  $V_n$  of the element and on  $\partial V_n$ , and  $T_i$  and  $\bar{u}_i$  are the boundary traction and boundary displacements, respectively. One can recognize that one of the equations obtained by setting  $\delta \pi_{mR} = 0$  is that

$$T_i = \sigma_{ij} \nu_j \quad (3.2)$$

along the element boundary  $\partial V_n$ , where  $\nu_j$  is the direction cosine on  $\partial V_n$ . Thus, if  $T_i$  in Eq. 3.1 is replaced by  $\sigma_{ij} \nu_j$  and integration by parts is carried out for the term  $1/2 \sigma_{ij} (u_{i,j} + u_{j,i})$ , the following functional is obtained:

$$\pi_{mR} = \sum_n \left\{ \int_{V_n} \left[ -\frac{1}{2} S_{ijkl} \sigma_{ij} \sigma_{kl} - \sigma_{ij,j} u_i - \frac{1}{2} \rho \dot{u}_i \dot{u}_i \right] dV + \int_{\partial V_n} \sigma_{ij} \nu_j \bar{u}_i dA \right\} \quad (3.3)$$

Note that only three field variables are involved:  $\sigma_{ij}$  and  $u_i$  in  $V_n$ , and  $\bar{u}_i$  on  $\partial V_n$ .

Assume that the stress distribution in the interior of the element may be written as

$$\underline{\sigma} = \underline{P} \underline{\beta} \quad (3.4a)$$

and that the displacements along the boundaries of the element are assumed to be expressed as

$$\underline{\bar{u}} = \underline{L} \underline{q} \quad (3.4b)$$

as before, and represent the displacement field u in the interior of the element by

$$\underline{u} = \underline{N} \underline{q} \quad (3.5)$$

where N is a "suitable" interpolation function which relates u to the nodal generalized displacements q. Substituting Eqs. 3.4 and 3.5 into Eq. 3.3 results in

$$\pi_{mR} = \sum_n \left[ -\frac{1}{2} \underline{\beta}^T \underline{H} \underline{\beta} - \underline{\beta}^T \underline{D} \underline{\delta} - \frac{1}{2} \dot{\underline{\delta}}^T \underline{m} \dot{\underline{\delta}} + \underline{\beta}^T \underline{G} \underline{\delta} \right] \quad (3.6)$$

where H and G are the same as defined in Eq. 2.6, and

$$\begin{aligned} \underline{D} &= \int_{V_n} (\underline{P}')^T \underline{N} dV \\ \underline{m} &= \int_{V_n} \rho \underline{N}^T \underline{N} dV \end{aligned} \quad (3.7)$$

with P' representing the derivatives of P ( $c_{ij,j}$ ).

The stationary conditions of  $\pi_{mR}$  with respect to variations of β then yield

$$-\underline{H} \underline{\beta} + (\underline{G} - \underline{D}) \underline{\delta} = 0 \quad (3.8)$$

By solving for β from Eq. 3.8 and substituting into Eq. 3.6, one obtains

$$\pi_{mR} = \sum_n \left( \frac{1}{2} \underline{\delta}^T \underline{K} \underline{\delta} - \frac{1}{2} \dot{\underline{\delta}}^T \underline{m} \dot{\underline{\delta}} \right) \quad (3.9)$$

where

$$\underline{K} = (\underline{G} - \underline{D})^T \underline{H}^{-1} (\underline{G} - \underline{D}) = \text{element stiffness matrix} \quad (3.10)$$

and  $\underline{m} = \int_{V_n} \rho \underline{N}^T \underline{N} dV = \text{"hybrid-rational" mass matrix}$

If the stress function P is chosen such that

$$\sigma_{ij,j} = 0 \quad (3.11)$$

then D is zero and the element stiffness matrix K in Eq. 3.10 reduces to

$$\underline{K} = \underline{G}^T \underline{H}^{-1} \underline{G} \quad (3.12)$$

which is the stiffness matrix of the hybrid stress model. From Eq. 3.9, the following equation is obtained by taking  $\delta\pi_{mR} = 0$  since  $\delta q$  is arbitrary:

$$\sum_n (\underline{K} \underline{\xi} + \underline{m} \ddot{\underline{\xi}}) = 0 \quad (3.13)$$

The element nodal generalized displacements  $\underline{q}$  can be connected to the global generalized displacements  $\underline{q}^*$  by

$$\underline{\xi} = \underline{T}_{q q^*} \underline{q}^* \quad (3.14a)$$

Note also that

$$\ddot{\underline{\xi}} = \underline{T}_{q q^*} \ddot{\underline{q}}^* \quad (3.14b)$$

where  $\underline{T}_{q q^*}$  is a transformation matrix relating  $\underline{q}$  to  $\underline{q}^*$ .

Applying Eqs. 3.14a and 3.14b to Eq. 3.13, the following equations of dynamic equilibrium of the non-forced complete assembled discretized structure is obtained:

$$\underline{M} \ddot{\underline{q}}^* + \underline{K} \underline{q}^* = 0 \quad (3.15)$$

where  $\underline{M}$  and  $\underline{K}$  represent, respectively, the mass matrix and the stiffness matrix for the complete assembled discretized structure referred to the global system.

It is seen that the final governing equations of free vibration analysis are of the same form for both the displacement and the hybrid stress finite-element model. For free vibration analysis, one may assume that

$$\ddot{\underline{q}}^* = -\omega^2 \underline{q}^* \quad (3.16)$$

where  $\omega$  is the natural frequency of the system. Thus, the following familiar eigenvalue problem results from Eq. 3.15:

$$(\underline{K} - \omega^2 \underline{M}) \underline{q}^* = 0 \quad (3.17)$$

### 3.2 Mass Matrices for an Element

By resorting to the modified Reissner principle expressed by Eq. 3.1, the procedure explained in Subsection 3.1 shows how one may obtain both the hybrid-stress stiffness matrix and a "hybrid rational" element mass matrix. Although this mass matrix is "rational", it is not consistent in the sense widely understood in connection with the finite element assumed displacement method. In the latter, the assumed displacement field is used to obtain the

element stiffness matrix, and a velocity field consistent with the assumed displacement field is used to represent the kinetic energy of the system thereby identifying a consistent mass matrix. In the hybrid stress model on the other hand, the displacement field utilized for constructing the kinetic energy to identify a rational mass matrix is not employed in any sense in the determination of the element stiffness matrix given by Eq. 3.12.

In addition to the "rational element mass matrix procedure" explained in Subsection 3.1, one may also construct a lumped mass matrix by commonly used procedures, or from a special case of the present procedure. For example, if the displacement field interpolation function  $\underline{N}$  of Eq. 3.5 were assumed to be such that the displacements within the tributary region of a particular node are identical to the displacements of that node, then the so-called lumped mass matrix [41] results. For the quadrilateral element considered in this study, the tributary region may be defined, for simplicity, as one-fourth of the total plane-area of the element regardless of the shape of the quadrilateral element. Then, for the single-layer element ELEM1, the following diagonal-lumped mass matrix  $\underline{m}_{1-L}$  is obtained:

$$\underline{m}_{1-L} \underline{q} = \frac{\rho A}{4} \begin{bmatrix} d & & & 0 \\ & d & & \\ & & d & \\ 0 & & & d \end{bmatrix} \begin{Bmatrix} q_1 \\ q_2 \\ q_3 \\ q_4 \end{Bmatrix} \quad (3.18)$$

where  $A$  = plane area,  $\rho$  = density,  $(q_i)^T = (u_i, v_i, w_i, \theta_{xi}, \theta_{yi})^T$ ,  $i = 1, 2, \dots, 4$ , and the diagonal terms in  $d$  are  $(H_1, H_1, H_1, H_3, H_3)$  with  $H_1 = \int_{-h/2}^{h/2} dz$  and  $H_3 = \int_{-h/2}^{h/2} z^2 dz$ .

Next, consider the development of a hybrid-rational mass matrix for ELEM1. Since the element boundary displacements are assumed to be linear for ELEM1, a convenient and suitable interpolation for  $\underline{N}$  would be a bilinear expansion in terms of a pair of transformed coordinates  $(\xi, \eta)$ :

$$\begin{aligned}
u &= \sum_{i=1}^4 [(u_i + z \theta_{yi}) N_i] \\
v &= \sum_{i=1}^4 [(v_i - z \theta_{xi}) N_i] \\
w &= \sum_{i=1}^4 (w_i N_i)
\end{aligned} \tag{3.19}$$

where

$$\begin{aligned}
N_1 &= (1-\xi)(1-\eta) \\
N_2 &= (1-\eta)\xi \\
N_3 &= \xi\eta \\
N_4 &= (1-\xi)\eta
\end{aligned} \tag{3.20}$$

The relations between the original coordinates  $(x,y)$  and the transformed coordinates  $(\xi,\eta)$  are (see Fig. 23):

$$\begin{aligned}
x &= \sum_{i=1}^4 x_i N_i \\
y &= \sum_{i=1}^4 y_i N_i
\end{aligned} \tag{3.21}$$

Having Eq. 3.19 (which is the equivalent of Eq. 3.5), the mass matrix of ELEM1 can be obtained by substituting Eq. 3.19 into Eq. 3.7 and performing the necessary integrations. The resulting mass matrix will be designated as  $m_{1-HR}$  and will be called a hybrid-rational (HR) mass matrix in the sense that the interpolated displacements within the element conform with the element boundary displacements and is derived from an established variational principle.

To derive lumped and HR mass matrices for the multilayer element ELEM2, it is only necessary to note that for each layer the above-derived mass matrices  $m_{1-L}$  and  $m_{1-HR}$  are applicable. However, the following transformation

$$\begin{Bmatrix} u_i \\ v_i \\ w \\ \theta_{xi} \\ \theta_{yi} \end{Bmatrix} = \begin{bmatrix} 0.5 & 0 & 0.5 & 0 & 0 \\ 0 & 0.5 & 0 & 0.5 & 0 \\ 0 & 0 & 0 & 0 & 1 \\ 0 & 1/h_i & 0 & -1/h_i & 0 \\ -1/h_i & 0 & 1/h_i & 0 & 0 \end{bmatrix} \begin{Bmatrix} u_i \\ v_i \\ u_{i+1} \\ v_{i+1} \\ w \end{Bmatrix}$$

$i = 1, 2, \dots, n \tag{3.22}$

$$\tilde{\delta}_\theta = \tilde{T}_{\theta 2} \tilde{\delta}_2 \quad (3.23)$$

is needed to transform the nodal displacements of ELEM1 to that of ELEMZ. Then the complete mass matrix of ELEMZ can be obtained by summing the transformed lumped or HR mass matrix  $\tilde{T}_{\theta 2}^T \tilde{m}_1 \tilde{T}_{\theta 2}$  for each layer through the thickness in the same way as individual element stiffness matrices are assembled into a system matrix. The corresponding mass matrices for ELEMZ will be designated as  $\tilde{m}_{Z-L}$  and  $\tilde{m}_{Z-HR}$ , respectively.

As for the reduced multilayer element ELEMZ, the corresponding mass matrices  $\tilde{m}_{R-L}$  and  $\tilde{m}_{R-HR}$  can be obtained by reducing  $\tilde{m}_{Z-L}$  or  $\tilde{m}_{Z-HR}$  in the same way as its stiffness matrix is reduced from that of ELEMZ (see Subsection 2.3.1).

### 3.3 Plate and Shell Evaluation Examples

To test the reliability of the above-developed mass matrices, several examples have been solved and the results compared with other known solutions. A computational scheme making use of the Sturm sequence property [42,43,44] has been adopted to solve the eigenvalue problem of Eq. 3.17. The computer program developed is capable of finding vibration frequencies and mode shapes for any number of vibration modes. A brief description of the solution scheme is contained in the Appendix at the end of this report.

#### 3.3.1 Single-Layer Thin Plates

Both the lumped mass matrix  $\tilde{m}_{1-L}$  and the hybrid-rational mass matrix  $\tilde{m}_{1-HR}$  of the single-layer element ELEM1 are used in solving the following two problems of classical thin plate vibrations:

##### (a) Simply-Supported Square Thin Isotropic Plate (Table 8, Fig. 24)

The dimensions and material properties of the plate can be found in Table 8, together with the numerical results. The single-layer element ELEM1 is used and the lowest frequency found by using  $\tilde{m}_{1-L}$  and  $\tilde{m}_{1-HR}$  is plotted in Fig. 24 for various finite-element modelings with uniform meshes up to 8x8 in a quarter of the plate; shown is the percentage error for each of the present predictions of the lowest

frequency in comparison with the exact values reported in Ref. 45. For this problem, the lumped and the hybrid-rational mass matrices give almost the same degree of accuracy, except that the errors are opposite in sign.

(b) Clamped Rectangular Thin Isotropic Plate (Table 9, Fig. 25)

A clamped rectangular plate of aspect ratio 1:2 with the material properties the same as that of the previous example has been analyzed. Again, both lumped and HR mass matrices have been tested; the results for the lowest predicted frequency are plotted in Fig. 25 and also are contained in Table 9. Comparisons are made with the exact solution of Ref. 45. It is shown in Fig. 25 that for a given number of degrees of freedom (DOF), the HR mass prediction is superior to that obtained by using the lumped mass matrix.

Since by using the present solution scheme, the computing effort for a system with a diagonal mass matrix is not very much reduced when compared with one which uses a mass matrix which has non-diagonal terms, in subsequent calculations only the HR mass matrices will be used so that better accuracy can be obtained.

In the examples presented thus far, only the lowest frequency has been computed. To test the ability of the solution scheme for higher modes, the following problem has been solved:

(c) Simply-Supported Rectangular Thin Isotropic Plate (Table 10)

A simply-supported rectangular plate of the same dimensions and material properties as that of example (b) has been analyzed for symmetrical modes of vibration. A quarter of the plate was analyzed by applying ELEMI (with the HR mass matrix' to two different uniform meshes 6x12 and 8x8. The first seven frequencies of symmetric nodes of vibration computed and the errors calculated by comparing with the exact solution [45] are shown in Table 10. As can be seen in Table 10, better predictions are obtained for the lower frequencies. This is expected since the accuracy depends on the ability of the elements to model the proper deformed

shape of the structure, and higher nodes involve higher wave numbers of deformation; i.e., more complicated mode shapes. Thus, better modeling is provided by the 6x12 mesh than by the 8x8 mesh for the mode designated by 5-1 in Table 10, for example, because more elements are put in the direction which has a wave number equal to 5 (that is, along the long side). The opposite is true for mode 1-3 in Table 10 since higher wave numbers now appear in the other (short side) direction.

In summary, the better solutions of the two meshes for the first five symmetric modes produce no error in predicted frequency larger than 4%. For higher modes, apparently, more elements are needed.

### 3.3.2 Two-Layer Thin and Thick Plates

Since two-layer laminates are usually "unbalanced", the extensional mode and bending mode of vibration are coupled. The following two problems are chosen to demonstrate the ability of the present finite-element method to predict the lowest frequency of vibration of unbalanced plates.

#### (a) Clamped Cross-Ply Square Thin Plate (Table 11, Fig. 26)

For thin multilayer plate problems, ELENR can be used. The present problem is described in Table 11, together with the results of the lowest predicted frequency for each of various modeling meshes. Comparisons are made with the CPT solution of Ref. 22 which does not include transverse shear deformation effects. The present finite-element solution converges very rapidly and the small discrepancy between the two solutions may be attributed to the transverse shear deformation effects.

#### (b) Simply-Supported Infinite Strip (Table 12, Fig. 27)

In Ref. 46, exact elasticity solutions are obtained for two-layer cross-ply infinite strips of various thickness-to-span ratios. For the finite-element analysis, only one row of elements arranged in the short-span direction is needed. In fact, only eight ELENR elements are used along the half span because of symmetry. Since a

considerable amount of local deformation of the plate cross section is expected, the two-layer thickness is divided into four sublayers. Even so, the finite element predictions of the lowest frequency for the higher thickness-to-span ratio still are about 20% higher than the exact values. However, as can be seen in Fig. 27, great improvement is obtained by the present (ELEMZ, HR-mass) finite-element solution over (1) the classical solutions and (2) solutions which include rotary inertia and in-plane mass inertia but neglect the local deformation caused by transverse shear deformation.

### 3.3.3 A Simply-Supported Three-Layer Square Plate

The exact vibration analysis of a three-layer square plate, with each layer being isotropic has been done in Ref. 47. The present finite-element solution uses, ELEMZ the HR mass matrix, and a 4x4 mesh in a quarter of the plate. No subdivision of each layer is needed. The predicted lowest frequencies show excellent accuracy, as can be seen in Table 13 for various combinations of density ratios and shear modulus ratios. Also included in Table 13 are predictions by the classical plate theory which neglects transverse shear deformation; the latter, obviously does not yield accurate results even for only moderately thick plates (total thickness = 0.1 side length).

### 3.3.4 A Simply-Supported Three-Layer Cross-Ply Cylindrical Shell

Numerical solutions for both exact and approximate vibration analyses of a three-layer cylindrical shell simply supported at both ends have been obtained by other authors [47,48]. The material properties are given in Table 14. In the present investigation, only the lowest frequency of the axisymmetric mode is explored in order to restrict the present computational effort. As in the previous example, only eight elements in a half span are used. Both ELEMZ and ELEMR are used and the transformations described in Subsections 2.5.1 and 2.5.2 are utilized to transform the flat-plate nodal displacements of ELEMZ and ELEMR into common shell nodal displacements. The results for various thickness-to-length ratios, together with classical (CST, Ref. 49), exact (ET, Ref. 47), and approximate (RST, Ref. 48) solutions are listed in Table 15. Excellent accuracy is observed for ELEMZ compared with the Ref. 47 solution.

Even ELEMZ, which neglects the local warping of the shell cross section, yields fair results -- comparable to those of the so-called refined shell theory.

### 3.4 Summary

Both lumped and hybrid-rational mass matrices for elements ELEM1, ELEMZ, and ELEMZ have been developed. Because of their better accuracy as evidenced by the present studies of natural frequencies of vibration for various plates, the hybrid-rational mass matrices are chosen for future use.

Frequency analysis of thin plates shows that FE predictions for lower modes of vibration are better than those for higher modes, mainly because the finite-element discretization employed models the lower modes more closely; finer meshing is needed to improve frequency predictions for the higher modes -- a commonly noted fact. The same phenomenon exists for Rayleigh-Ritz approximate analysis.

For very thick plates (whose thickness-to-side ratio is in the order of one) subdivision of each layer is needed to model the local deformation closely.

Analyses of a three-layer plate and of a three-layer cylindrical shell in the present study show excellent accuracy of the multilayer element ELEMZ.

The present formulation provides a dependable HR mass matrix which can be confidently applied to transient dynamic analysis.

## SECTION 4

### THERMAL STRESS ANALYSIS

Since aerodynamic heating and/or other sources of heating may produce elevated nonuniform temperatures in aerospace structures, the analysis of the attendant effects such as thermally-induced distortions and stresses is of interest. Accordingly the present section pertains to the analysis of thermal stresses and deformations in the context of applying the hybrid-stress finite-element model and method. This analysis is developed and applied to several simple thermal/structural problems involving either isotropic or anisotropic materials in single-layer or multilayer configurations.

It is assumed that a steady-state type of nonuniform temperature distribution is known; the attendant static thermal stresses and distortions are then analyzed. In other words, the temperature problem and the elasticity problem are considered to be uncoupled.

#### 4.1 Thermal Stress Analysis by the Hybrid Stress-Model

For a given temperature distribution, the thermal stress analysis of an elastic body by the displacement finite-element model is quite straightforward. The thermal loading can be transformed into a set of equivalent nodal forces by an initial-strain approach [51,52]. For a hybrid-stress model, equivalent nodal forces can also be obtained by an initial-strain approach [8].

Consider a single element. The complementary energy functional to be minimized in the presence of a temperature distribution over the entire element is shown in Ref. 8 to be

$$\pi_c = \int \left( \frac{1}{2} S_{ijkl} \sigma_{ij} \sigma_{kl} + \epsilon_{oij} \sigma_{ij} \right) dV - \int T_i u_i dA \quad (4.1)$$

where  $\epsilon_{oij}$  is the initial strain obtainable by the following formula:

$$\begin{Bmatrix} \epsilon_{0x} \\ \epsilon_{0y} \\ \epsilon_{0z} \\ \epsilon_{0yz} \\ \epsilon_{0xz} \\ \epsilon_{0xy} \end{Bmatrix} = \begin{bmatrix} l^2 & m^2 & 0 & 0 & 0 & lm \\ m^2 & l^2 & 0 & 0 & 0 & -lm \\ 0 & 0 & 1 & 0 & 0 & 0 \\ 0 & 0 & 0 & l & -m & 0 \\ 0 & 0 & 0 & m & l & 0 \\ -2lm & 2lm & 0 & 0 & 0 & l^2 - m^2 \end{bmatrix} \begin{Bmatrix} \alpha_1 \\ \alpha_2 \\ \alpha_3 \\ 0 \\ 0 \\ 0 \end{Bmatrix} \cdot \Delta T$$

(4.2)

In Eq. 4.2,  $\alpha_1$ ,  $\alpha_2$ , and  $\alpha_3$  are the coefficients of linear thermal expansion in the respective three principal directions of the material.  $\Delta T$  is the temperature rise from a stress-free temperature state, and  $l$  and  $m$  are the plane direction cosines between the material axes and the element axes. In short, Eq. 4.2 is nothing but a strain transformation formula that relates the initial strains in the material axes to those with respect to the element axes.

The stress-strain relation in the presence of thermal initial strain is

$$\epsilon_{ij} = \sigma_{kl} S_{ijkl} + \epsilon_{0ij} \quad (4.3)$$

The inversion of Eq. 4.3 leads to the following expression for the stress  $\sigma'_{ij}$  which corresponds to the total strain  $\epsilon_{ij}$ :

$$\sigma'_{ij} = \sigma_{ij} + \sigma_{0ij} \quad (4.4)$$

where

$$\sigma_{0ij} = C_{ijkl} \epsilon_{0kl} \quad (4.5)$$

Here  $\sigma_{0ij}$  is the stress corresponding to the initial strain and  $\sigma_{ij}$  is the actual stress. Since usually a linear distribution of  $\sigma_{ij}$  in the transverse direction can be assumed for plate or shell structures, it follows that  $\sigma'_{ij}$  is linear in the transverse direction. The actual stress  $\sigma_{ij}$ , however, may not be linear in the transverse direction, since  $\sigma_{0ij}$  may not be linear:

$$\sigma_{ij} = \sigma'_{ij} - \sigma_{0ij} \quad (4.6)$$

In the following, equivalent nodal forces will be derived for the multi-layer element ELEMZ. The equivalent nodal forces for ELEMZ and ELEM1 can be obtained directly from those of ELEMZ by appropriate reductions of the nodal degrees of freedom.

For the stress field, one may assume that

$$\underline{\sigma} = \underline{P}\underline{\beta} + \underline{P}_t\underline{\beta}_t - \underline{P}_0\underline{\beta}_0 \quad (4.7)$$

for each layer, where  $\underline{P}\underline{\beta}$  is the part of  $\sigma'_{ij}$  that has unknown parameters  $\underline{\beta}$ ,  $\underline{P}_t\underline{\beta}_t$  is the part of  $\sigma'_{ij}$  that is necessary to balance the initial stress  $\underline{P}_0\underline{\beta}_0$ , so that all together the actual stress  $\underline{\sigma}$  satisfies the equilibrium equations of elasticity.

Note that one could make  $\underline{P}_t\underline{\beta}_t$  identical to  $\underline{P}_0\underline{\beta}_0$ . Then the resulting stresses  $\sigma_{ij}$  would be represented only by  $\underline{P}\underline{\beta}$ , whose in-plane stresses are linear in  $z$ . Since, in general, the actual in-plane stresses may not be linear in  $z$ , this would be too restrictive. Thus  $\underline{P}_t\underline{\beta}_t$  is not made equal to  $\underline{P}_0\underline{\beta}_0$ , as will be seen later.

For the boundary displacements, one may assume that

$$\underline{u} = \underline{L}\underline{q} \quad (4.8)$$

as before. The functional of Eq. 4.1 becomes, in matrix notation,

$$\begin{aligned} \Pi_c &= \int \left( \frac{1}{2} S_{ijkl} \sigma_{ij} \sigma_{kl} + S_{ijkl} \sigma_{ij} \sigma_{0kl} \right) dV - \int T_i u_i dA \\ &= \int \frac{1}{2} (\underline{P}\underline{\beta} + \underline{P}_t\underline{\beta}_t - \underline{P}_0\underline{\beta}_0)^T \underline{S} (\underline{P}\underline{\beta} + \underline{P}_t\underline{\beta}_t - \underline{P}_0\underline{\beta}_0) + 2\underline{P}_0\underline{\beta}_0^T dV \\ &\quad - \int (\underline{R}\underline{\beta} + \underline{R}_t\underline{\beta}_t - \underline{R}_0\underline{\beta}_0)^T \underline{L}\underline{q} dA \\ &= \int \left[ \frac{1}{2} \underline{\beta}^T \underline{P}^T \underline{S} \underline{P} \underline{\beta} + \underline{\beta}^T \underline{P}^T \underline{S} \underline{P}_t \underline{\beta}_t + \frac{1}{2} \underline{\beta}_t^T \underline{P}_t^T \underline{S} \underline{P}_t \underline{\beta}_t - \frac{1}{2} \underline{\beta}_0^T \underline{P}_0^T \underline{S} \underline{P}_0 \underline{\beta}_0 \right] dV \\ &\quad - \int (\underline{\beta}^T \underline{R}^T \underline{L} \underline{q} + \underline{\beta}_t^T \underline{R}_t^T \underline{L} \underline{q} - \underline{\beta}_0^T \underline{R}_0^T \underline{L} \underline{q}) dA \end{aligned}$$

(4.9)

In Eq. 4.9, the matrices  $\underline{R}$ ,  $\underline{R}_t$ , and  $\underline{R}_o$  are obtained by specifying boundary coordinates in the function  $\underline{P}$ ,  $\underline{P}_t$ , and  $\underline{P}_o$ , respectively, of Eq. 4.7.

By expressing

$$\begin{aligned}\underline{H} &= \int \underline{P}^T \underline{S} \underline{P} \, dV \\ \underline{G} &= \int \underline{R}^T \underline{L} \, dA\end{aligned}\tag{4.10a}$$

as before, and defining

$$\begin{aligned}\underline{H}_t &= \int \underline{P}_t^T \underline{S} \underline{P}_t \, dV \\ \underline{G}_t &= \int \underline{R}_t^T \underline{L} \, dA \\ \underline{G}_o &= \int \underline{R}_o^T \underline{L} \, dA\end{aligned}\tag{4.10b}$$

the functional in Eq. 4.9 becomes

$$\pi_c = \frac{1}{2} \underline{\beta}^T \underline{H} \underline{\beta} - \underline{\beta}^T \underline{G} \underline{\xi} + \underline{\beta}_t^T \underline{H}_t \underline{\beta}_t - \underline{\beta}_t^T \underline{G}_t \underline{\xi} + \underline{\beta}_o^T \underline{G}_o \underline{\xi}\tag{4.11}$$

In Eq. 4.11, the constant terms  $\int \underline{\beta}_t^T \underline{P}_t^T \underline{S} \underline{P}_t \underline{\beta}_t \, dV$  and  $\int \underline{\beta}_o^T \underline{P}_o^T \underline{S} \underline{P}_o \underline{\beta}_o \, dV$  are dropped, since they have no contribution upon taking variations of  $\pi_c$ .

Since a multilayer element is being considered, the interlayer equilibrium of stresses will lead to a set of constraint on  $\underline{\beta}$  (see Subsection 2.3.1):

$$\underline{A} \underline{\beta} = \underline{B}\tag{4.12}$$

Upon introducing the Lagrange multiplier  $\underline{\lambda}$ , a new functional is formed by combining Eq. 4.11 and Eq. 4.12:

$$\pi'_c = \pi_c + \underline{\lambda}^T (\underline{A} \underline{\beta} - \underline{B})\tag{4.13}$$

Taking the variation of  $\pi'_c$  with respect to  $\underline{\beta}$ , one obtains

$$\underline{H} \underline{\beta} - \underline{G} \underline{\xi} + \underline{H}_t \underline{\beta}_t + \underline{A}^T \underline{\lambda} = 0$$

or

$$\underline{\beta} = \underline{H}^{-1} (\underline{G} \underline{\xi} - \underline{H}_t \underline{\beta}_t - \underline{A}^T \underline{\lambda})\tag{4.14}$$

Substituting  $\underline{\beta}$  of Eq. 4.14 into Eq. 4.12, one obtains

$$\underline{A} \underline{H}^{-1} (\underline{G} \underline{\xi} - \underline{H}_t \underline{\beta}_t - \underline{A}^T \underline{\lambda}) = \underline{B}$$

or

$$\underline{\lambda} = (\underline{A} \underline{H}^{-1} \underline{A}^T)^{-1} (\underline{A} \underline{H}^{-1} \underline{G} \underline{\xi} - \underline{A} \underline{H}^{-1} \underline{H}_t \underline{\beta}_t - \underline{B}) \quad (4.15)$$

Substituting  $\underline{\beta}$  and  $\underline{\lambda}$  back into Eq. 4.13, the new functional  $\pi'_c$  now contains only  $\underline{q}$ :

$$\begin{aligned} \pi'_c = & -\frac{1}{2} \underline{\xi}^T [\underline{G}^T \underline{H}^{-1} \underline{G} - \underline{G}^T \underline{H}^{-1} \underline{A}^T (\underline{A} \underline{H}^{-1} \underline{A}^T)^{-1} \underline{A} \underline{H}^{-1} \underline{G}] \underline{\xi} \\ & - \underline{\xi}^T \underline{G}^T \underline{H}^{-1} \underline{A}^T (\underline{A} \underline{H}^{-1} \underline{A}^T)^{-1} (\underline{B} + \underline{A} \underline{H}^{-1} \underline{H}_t \underline{\beta}_t) - \underline{\xi}^T (\underline{G}_t^T \underline{\beta}_t - \underline{G}^T \underline{H}^{-1} \underline{H}_t \underline{\beta}_t) \\ & + \underline{\xi}^T \underline{G}_o^T \underline{\beta}_o \end{aligned} \quad (4.16)$$

Again, a constant term in  $\pi'_c$  has been dropped. Finally, by taking the variation of  $\pi'_c$  with respect to  $\underline{q}$ , one obtains

$$\begin{aligned} & [\underline{G}^T \underline{H}^{-1} \underline{G} - \underline{G}^T \underline{H}^{-1} \underline{A}^T (\underline{A} \underline{H}^{-1} \underline{A}^T)^{-1} \underline{A} \underline{H}^{-1} \underline{G}] \underline{\xi} \\ & = -\underline{G}^T \underline{H}^{-1} \underline{A}^T (\underline{A} \underline{H}^{-1} \underline{A}^T)^{-1} (\underline{B} + \underline{A} \underline{H}^{-1} \underline{H}_t \underline{\beta}_t) - (\underline{G}_t^T \underline{\beta}_t - \underline{G}^T \underline{H}^{-1} \underline{H}_t \underline{\beta}_t) + \underline{G}_o^T \underline{\beta}_o \end{aligned} \quad (4.17)$$

Thus, the element stiffness matrix  $\underline{k}$  of Eq. 2.28 remains valid and an equivalent element nodal thermal force vector:

$$\underline{f} = \underline{G}^T \underline{H}^{-1} \underline{H}_t \underline{\beta}_t - \underline{G}^T \underline{H}^{-1} \underline{A}^T (\underline{A} \underline{H}^{-1} \underline{A}^T)^{-1} (\underline{B} + \underline{A} \underline{H}^{-1} \underline{H}_t \underline{\beta}_t) + \underline{G}_o^T \underline{\beta}_o - \underline{G}_t^T \underline{\beta}_t \quad (4.18)$$

is obtained.

## 4.2 Modeling of a Temperature Distribution

The equivalent thermal loading vector derived in Subsection 4.1 depends on the temperature distribution of an element. In theory, any given function of temperature distribution can be used in Eq. 4.2 to yield a vector of initial strain and eventually the vector  $\underline{P}_o \underline{\beta}_o$  in Eq. 4.7. That, however, would introduce difficulties in evaluating Eq. 4.10b. Since the basic stress distribution

represented by  $\underline{P\beta}$  in Eq. 4.7 is only linear in  $x$  and  $y$  (see Subsection 2.3.2), higher-order descriptions of temperature for the equivalent nodal force calculation may be essentially futile unless higher-order stress-distribution functions are used in developing the hybrid stress finite-element properties. Therefore, the following simplification in temperature-distribution representation is adopted in this study. A given arbitrary temperature distribution  $\Delta T_o(x,y,z)$  for any one layer of an element is modeled by a simple distribution  $\Delta T(x,y,z)$ :

$$\begin{aligned}\Delta T(x,y,z) = & T_1 + T_2 x + T_3 y + z(T_4 + T_5 x + T_6 y) \\ & + z^2(T_7 + T_8 x + T_9 y)\end{aligned}\quad (4.19)$$

which is parabolic in  $z$  and linear in  $x$  and  $y$ . The coefficients  $T_1, T_2, \dots, T_9$  are determined by minimizing the square errors of surface-fitting  $\Delta T$  at the 12 corner points of that layer of an element (Fig. 28a).

Equation 4.19 can also be expressed in terms of temperatures in the bottom ( $T_b$ ), middle ( $T_m$ ), and top ( $T_t$ ) surface of that layer (see Fig. 28b):

$$\begin{aligned}T_1 + T_2 x + T_3 y &\equiv T_{m1} + T_{m2} x + T_{m3} y \\ T_4 + T_5 x + T_6 y &\equiv \frac{1}{h} [(T_{t1} - T_{b1}) + (T_{t2} - T_{b2})x + (T_{t3} - T_{b3})y] \\ T_7 + T_8 x + T_9 y &\equiv \frac{2}{h^2} [(T_{t1} - T_{b1} - 2T_{m1}) + (T_{t2} - T_{b2} - 2T_{m2})x \\ &\quad + (T_{t3} - T_{b3} - 2T_{m3})y]\end{aligned}\quad (4.20)$$

where  $h$  is the thickness of that particular layer.

Thus, the minimization of errors in  $\Delta T(x,y,z)$  can be carried out for the three surfaces separately. Denote by  $T_{oi}$  the actual temperatures at the four corner points for any one of the three surfaces calculated from the original  $\Delta T_o(x,y,z)$ , and denote by  $\bar{T}_i$  the approximate values calculated from Eq. 4.19 and Eq. 4.20. Then the square error  $E_x$  of the temperature description for that

surface is

$$E_r = \sum_{i=1}^4 (T_{oi} - \bar{T}_i)^2 \quad (4.21)$$

and

$$\bar{T}_i = T_{s1} + T_{s2} x_i + T_{s3} y_i \quad s = b, \text{ or } m, \text{ or } t \quad (4.22)$$

where  $x_i$  and  $y_i$  are the corner coordinates of the element.

To minimize  $E_r$ :

$$\frac{\partial E_r}{\partial T_{s1}} = \sum_{i=1}^4 (-2) (T_{oi} - \bar{T}_i) = 0$$

$$\frac{\partial E_r}{\partial T_{s2}} = \sum_{i=1}^4 (-2x_i) (T_{oi} - \bar{T}_i) = 0$$

$$\frac{\partial E_r}{\partial T_{s3}} = \sum_{i=1}^4 (-2y_i) (T_{oi} - \bar{T}_i) = 0$$

(4.23)

After rearranging the terms in Eq. 4.23, and using Eq. 4.22, the following equations are obtained:

$$\begin{bmatrix} 4 & \sum_{i=1}^4 x_i & \sum_{i=1}^4 y_i \\ & \sum_{i=1}^4 x_i^2 & \sum_{i=1}^4 x_i y_i \\ \text{sym.} & & \sum_{i=1}^4 y_i^2 \end{bmatrix} \begin{bmatrix} T_{s1} \\ T_{s2} \\ T_{s3} \end{bmatrix} = \begin{bmatrix} \sum_{i=1}^4 T_{oi} \\ \sum_{i=1}^4 T_{oi} x_i \\ \sum_{i=1}^4 T_{oi} y_i \end{bmatrix}$$

(4.24)

Then  $T_{s1}$ ,  $T_{s2}$ ,  $T_{s3}$  can be solved easily in terms of temperatures at corner points  $T_{oi}$ , and the modeling of the temperature distribution  $\Delta T_O(x,y,z)$  by  $\Delta T(x,y,z)$  is completed upon substituting the expressions in Eq. 4.20 into Eq. 4.19.

### 4.3 Stress Assumptions in an Element

The actual stress  $\underline{\sigma}$  consists of three parts:  $\underline{P}\underline{\beta}$ ,  $\underline{P}_t\underline{\beta}_t$ , and  $\underline{P}_{o-o}\underline{\beta}_o$  as can be seen in Eq. 4.7. For each layer of a multilayer element,  $\underline{P}\underline{\beta}$  is the same as that of ELEMI, and  $\underline{P}_{o-o}\underline{\beta}_o$  can be calculated from

$$\underline{P}_{o-o}\underline{\beta}_o \equiv \begin{Bmatrix} \sigma_{ox} \\ \sigma_{oy} \\ \sigma_{oz} \\ \sigma_{oyz} \\ \sigma_{oxz} \\ \sigma_{oxy} \end{Bmatrix} = \begin{Bmatrix} C_{11} & C_{12} & C_{13} & 0 & 0 & C_{16} \\ & C_{22} & C_{23} & 0 & 0 & C_{26} \\ & & C_{33} & 0 & 0 & C_{36} \\ & & & C_{44} & C_{45} & 0 \\ & \text{sym.} & & & C_{55} & 0 \\ & & & & & C_{66} \end{Bmatrix} \begin{Bmatrix} \epsilon_{ox} \\ \epsilon_{oy} \\ \epsilon_{oz} \\ \epsilon_{oyz} \\ \epsilon_{oxz} \\ \epsilon_{oxy} \end{Bmatrix} = \begin{Bmatrix} \bar{\sigma}_{ox} \\ \bar{\sigma}_{oy} \\ \bar{\sigma}_{oz} \\ 0 \\ 0 \\ \bar{\sigma}_{oxy} \end{Bmatrix} \Delta T(x,y,z) \quad (4.25)$$

where the matrix  $\underline{C}$  is the elastic matrix and can be obtained by inverting the compliance matrix  $\underline{S}$  of Eq. 2.14; the initial strain vector is obtained from Eq. 4.2. Since  $\underline{P}\underline{\beta}$  satisfies the three equilibrium equations of elasticity identically, it is now necessary to derive  $\underline{P}_t\underline{\beta}_t$  such that  $(\underline{P}_t\underline{\beta}_t - \underline{P}_{o-o}\underline{\beta}_o)$  will satisfy the equilibrium equations identically. Substituting  $\underline{P}_{o-o}\underline{\beta}_o$  of Eq. 4.25 into the following equilibrium equations

$$(\sigma_{ox} - \sigma_{tx}),_x + (\sigma_{oxy} - \sigma_{txy}),_y + (-\sigma_{txz}),_z = 0$$

$$(\sigma_{oxy} - \sigma_{txy}),_x + (\sigma_{oy} - \sigma_{ty}),_y + (-\sigma_{tyz}),_z = 0$$

$$(-\sigma_{txz}),_x + (-\sigma_{tyz}),_y + (-\sigma_{tz}),_z = 0$$

(4.26)

and integrating, one finds the following for  $\underline{P}_t\underline{\beta}_t$ :

$$\underline{P}_t \underline{\beta}_t \equiv \begin{Bmatrix} \sigma_{tx} \\ \sigma_{ty} \\ \sigma_{tz} \\ \sigma_{tzy} \\ \sigma_{txz} \\ \sigma_{txy} \end{Bmatrix} = \begin{Bmatrix} 0 \\ 0 \\ \bar{\sigma}_{oz} \\ \bar{\sigma}_{oxy}(ZT_2 + \frac{Z^2}{2}T_5 + \frac{Z^3}{3}T_8) + \bar{\sigma}_{oy}(ZT_3 + \frac{Z^2}{2}T_6 + \frac{Z^3}{3}T_9) \\ \bar{\sigma}_{ox}(ZT_2 + \frac{Z^2}{2}T_5 + \frac{Z^3}{3}T_8) + \bar{\sigma}_{oxy}(ZT_3 + \frac{Z^2}{2}T_6 + \frac{Z^3}{3}T_9) \\ 0 \end{Bmatrix} \cdot \Delta T(x,y,z) \quad (4.27)$$

Thus, the stresses of any layer of an element consist of  $\underline{P}\underline{\beta}$  of ELEM1,  $\underline{P}_o\underline{\beta}_o$  of Eq. 4.25, and  $\underline{P}_t\underline{\beta}_t$  of Eq. 4.27.

The interlayer equilibrium conditions impose constraints on  $\sigma_z$ ,  $\sigma_{yz}$ , and  $\sigma_{xz}$  (see Eq. 2.30). The equilibrium of  $\sigma_z$  is automatically satisfied, since  $\sigma_z$  of  $\underline{P}\underline{\beta}$  is zero and  $\sigma_z = 0 + \sigma_{tz} - \sigma_{oz} = 0$  by Eq. 4.27. The equilibrium of  $\sigma_{xz}$  and  $\sigma_{yz}$  leads to

$$\begin{aligned} & [(\sigma_{xz}, \sigma_{yz}) \text{ of } \underline{P}\underline{\beta} + (\sigma_{xz}, \sigma_{yz}) \text{ of } \underline{P}_t\underline{\beta}_t] \text{ at the top of the } i\text{th layer} \\ & \equiv [(\sigma_{xz}, \sigma_{yz}) \text{ of } \underline{P}\underline{\beta} + (\sigma_{xz}, \sigma_{yz}) \text{ of } \underline{P}_t\underline{\beta}_t] \text{ at the bottom of the } (i+1)^{\text{th}} \text{ layer} \end{aligned} \quad (4.28)$$

since  $\underline{P}_o\underline{\beta}_o$  does not contain nonzero transverse shear stresses. In Eq. 4.28, the part of  $\underline{P}\underline{\beta}$  yields the (same) coefficient matrix  $\underline{A}$  of  $\underline{\beta}$  in Eq. 21 of ELEM2, and the part of  $\underline{P}_t\underline{\beta}_t$  yields constant terms which constitute the vector  $\underline{B}$  in the constraint equation

$$\underline{A}\underline{\beta} = \underline{B} \quad (4.29)$$

Thus, all of the ingredients needed to calculate the equivalent nodal forces

are now available. In summary, the equivalent nodal forces can be obtained from Eq. 4.18, in which the matrices  $G$ ,  $H$ , and  $A$  are the same as defined for ELEMZ before, the vectors  $H_t \beta_t$  and  $G_t \beta_t$  are obtained by using Eq. 4.10 and Eq. 4.27, the vector  $G_o^T \beta_o$  is obtained from Eq. 4.10 and Eq. 4.25, and the vector  $\beta$  is obtained from Eqs. 4.27 and 4.28.

#### 4.4 Plate and Shell Evaluation Examples

##### 4.4.1 In-Plane Expansion of a Free Single-Layer Thin Isotropic Rectangular Plate

To test the accuracy of the equivalent thermal loading representation, a problem for which both experimental and approximate-theoretical [53] thermal stress data are available is chosen as a test problem. It is a free single-layer thin rectangular isotropic plate heated linearly in the plate plane and uniformly across the plate thickness direction as illustrated in Fig. 29; other pertinent data for this problem are given in Table 16. Because of the symmetry of the plate and the temperature distribution, only a quarter of the plate is used in the analysis and only the in-plane displacements and stresses need to be considered.

The in-plane displacement pattern calculated by the present finite-element method using a 5x4 mesh is plotted in Fig. 30. In Figs. 31a, 31b, and 31c, the in-plane stresses  $\sigma_x$ ,  $\sigma_y$ , and  $\sigma_{xy}$ , respectively, are plotted against both experimental and theoretical results of Ref. 53. It is seen that the direct stresses ( $\sigma_x$  and  $\sigma_y$ ) calculated by using the present finite-element method agree very well with both results; the shear stress ( $\sigma_{xy}$ ) prediction is also very good, except near the edges, because the free traction edge condition is satisfied only in an average sense in the present finite element modeling. It should be mentioned that the theoretical results of Ref. 53 are only approximate; the direct stress  $\sigma_x$  is first assumed according to a distribution which is exact for an infinite strip under thermal loading and the other stresses are then determined according to the Principle of Complementary Energy. Also, as mentioned in Ref. 53, the temperature control to give the temperature distribution of Fig. 29 for the experiment is not perfect. Therefore, some slight discrepancies between the theoretical and experimental

results are expected. However, the present prediction agrees very well with both of the comparison results. This demonstrates the accuracy of the present equivalent thermal loading calculation and the associated FE analysis.

#### 4.4.2 Bending of a Clamped Thin Isotropic Rectangular Plate Subjected to Nonuniform Temperature

The dimensions and properties of the plate under consideration are listed in Table 17. For a thin rectangular isotropic plate under thermal loading and having all four sides ideally clamped, the thermal stress problems can be solved by recognizing that the governing equations on the transverse displacements are identical to those of the same plate under distributed static lateral loading. In Ref. 54, it is shown that this equivalent static load, denoted by  $p^*$  is

$$p^* = - \frac{1}{1-\nu} (\nabla^2 M_t) \quad (4.30)$$

where

$$M_t = \alpha E \int_{-h/2}^{h/2} T z dz \quad (4.31)$$

where  $\nu$  is the Poisson ratio,  $E$  is Young's modulus,  $\alpha$  is the linear thermal expansion coefficient, and  $T$  is the temperature distribution. In the present example, a temperature distribution constant in  $x$ , parabolic in  $y$ , and linear in  $z$  is assumed (see Fig. 32a). Thus, the results calculated by the present hybrid-stress FE approach can be compared with that of the classical solution [18] for a clamped rectangular plate under uniform loading. The displacements along the central lines of the plate, obtained by the present method with an  $8 \times 8$  uniform mesh in a quarter of the plate are plotted in Figs. 32b and 32c, together with the central deflection predicted by the classical solution for static bending [18]. The present prediction for the central deflection is almost identical to the classical exact solution of Ref. 18.

#### 4.4.3 Simply-Supported, Infinitely-Long, Two-Layer, Cross-Ply (0°/90°) Thin Strip Subjected to a Uniform Temperature Distribution

The material properties and dimensions of the thin flat strip are described in Table 18; the pertinent coordinates and geometry are depicted in

Fig. 33a. Since this laminated plate is not balanced in the sense that the expansion properties are not symmetric in  $z$ , even a uniform temperature will cause a transverse displacement as can be seen in Fig. 33b. Also, thermal stresses are induced. Plotted in Figs. 33c through 33f are the in-plane stresses and interlaminar shear stresses. No other solutions are available at present for this problem; therefore, no comparisons can be made. From Figs. 33c and 33d it is seen that the maximum  $\sigma_x$  occurs near the simply-supported edges ( $x = \pm 8$  in.) in the lower layer because the lower layer has a larger elastic constant  $E_1$  in the  $x$ -direction. The maximum interlaminar shear stress  $\sigma_{xz}$  (Fig. 33e) occurs at the supported edge and the  $\sigma_y$  stress is almost constant along the  $x$ -direction.

#### 4.4.4 Simply-Supported, Three-Layer, Cross-Ply ( $0^\circ/90^\circ/0^\circ$ ), Thick, Cylindrical Shell Subjected to a Uniform Temperature Distribution

A uniform temperature is applied to a three-layer cylindrical shell of finite length, simply supported at each end. The material properties and the dimensions of the shell are described in Table 19. Since this is an axisymmetric problem, only one strip of the shell is needed in the finite-element modeling. In fact, only half a strip is used because of symmetry in the axial direction also. The calculated radial displacements resulting from the applied temperature are plotted in Fig. 34a. It is interesting to note that the maximum radial deflection does not occur at the central section but at a place near the center section. However, this phenomenon is a result of the particular combination of the length, thickness, and radius ratios used in this example and should not be regarded as a general result. In Fig. 34b, the axial displacements of six representative sections are plotted. The distortion from the original plane section is most severe at the supported edge but dies out gradually toward the central section. A reverse of the direction of rotation of the cross section occurs near the central section ( $x=7$ ). This is consistent with the small decrease of radial displacement near the central section (Fig. 34a).

#### 4.5 Summary

The thermal-stress analysis by the present hybrid-stress finite-element method is shown to be equivalent to a static analysis (as is well known to be true also for other types of thermal analyses). The equivalent thermal loading vector for a hybrid stress model is derived using an initial-strain approach. Arbitrary temperature distributions on any element are approximated by simple functions: linear in  $x$  and  $y$ , and parabolic in  $z$ . The accuracy of the present method is demonstrated in two simple problems: (1) in-plane plate expansion and (2) thermal-induced bending of a plate; good agreement is observed for both displacement and stress predictions. Two other problems, a two-layer plate and a three-layer cylindrical shell, each under a uniform temperature distribution, are also solved and the results are discussed.

## SECTION 5

### SUMMARY AND CONCLUSIONS

#### 5.1 Summary

This study has been devoted to the development and evaluation of hybrid stress flat-plate finite elements for use in analyzing laminated plate and shell structures. Transverse shear deformation effects as well as in-plane and rotary inertia for vibration analysis are included. The plate and shell structures under consideration range from very thin to very thick. According to the loading conditions applied to the structure, this study can be divided into three categories: static analysis, vibration analysis, and thermal stress analysis.

These three types of loading conditions are discussed since they represent the basic loading environment that many structures, particularly aeronautical and aerospace structures, may encounter. These basic analyses serve as the foundation for future studies on transient dynamic and other complicated loading conditions. Also, they are necessary aspects in the evaluation of the properties of certain finite elements developed so that the reliability and limitations of these finite elements can be assessed before these finite elements are applied to practical structural analysis and design.

In static finite-element analysis, the basic task is to develop reliable stiffness matrices that converge rapidly to correct solutions, with a "minimum" number of degrees of freedom. To achieve this goal, studies were made first on single-layer elements. An outline of the derivation of single-layer flat-plate elements by the hybrid stress model is given and a total of nine elements with different stress and boundary displacement assumptions were tested on a very thin flat plate as well as on a very thick flat plate. Among these nine finite elements, a quadrilateral element designated as ELEML (with linear boundary displacements and linear in-plane stress assumptions) is chosen for use because of its fast convergence, excellent accuracy, and simplicity.

Then the derivation of the stiffness matrix for a multilayer element

was carried out by extending the basic single-layer flat-plate element ELEM1 to a multilayer element (designated by ELEMZ) which has independent boundary displacements that can model the local deformation of each layer of a plate or shell closely. For relatively thin multilayer plates or shells, an element designated by ELEM2 is obtained by reducing the nodal degrees-of-freedom of ELEMZ.

Two transformation formulas are given for single-layer and multilayer flat-plate elements so that their application can be broadened to include curved-shell problems.

Various static-plate and curved-shell problems, including both thin and thick, single-layer, two-layer, and three-layer problems, have been solved using the three elements developed in this study, and comparisons have been made with other existing solutions. It is found that these elements are indeed very effective in predicting both displacements and stresses of plate and shell structures under static loading.

For vibration analyses using the hybrid-stress model, a brief discussion of the variational basis of the derivation of a mass matrix is given, followed by the development of lumped and hybrid-rational mass matrices for the three elements mentioned earlier. Based on the results of test problems, the less accurate lumped-mass approach was discarded, and the superior hybrid-rational mass approach was adopted for subsequent use. Several example problems were solved. Frequency predictions were compared with other existing solutions, and good accuracy of the present predictions is observed in general.

The steady-state thermal stress analysis carried out by the hybrid-stress finite-element model is characterized by the development of an equivalent thermal loading vector; the analysis is otherwise similar to a static analysis. The temperature distribution within an element is modeled for convenience in the present study by a linear approximation in the plane surface and by a parabolic fit in the transverse direction. Then initial strains and their corresponding stresses are computed based on these temperature distributions; the total stress assumptions are such that they satisfy the equilibrium conditions of elasticity. The equivalent thermal loading vector is obtained through the application of a

variational principle that includes the temperature effects as initial strains.

Problems involving in-plane expansion and transverse bending induced by temperature were solved. Because of the limited number of existing numerical solutions on thermal stress problems, only two of the example problems were compared to other solutions; they show very good accuracy for displacement and stress predictions.

In summary, three quadrilateral flat-plate elements: ELEM1, ELEM2, and ELEM3 were developed and verified to provide reasonably accurate and reliable predictions for static, vibration, and thermal stress problems. They all have similar assumptions on stresses and boundary displacements but differ in their applicability to (1) thin or thick and (2) single-layer or multilayer plate and/or shell problems.

## 5.2 Conclusions

Based upon the results of various numerical verifications included in this study, the following conclusions may be stated:

- (a) The present finite-element method is reasonably efficient and accurate for predicting stress and displacement responses to static or thermal loadings and natural frequencies for free vibrations of plate and shell structures.
- (b) For single-layer problems, ELEM1 is recommended for use. However, if the thickness becomes large (for thickness-to-side ratio  $h/l$  greater than about 0.1), it is advisable to subdivide the single-layer into sublayers and use ELEM3 to model the local deformation more closely.
- (c) For relatively thin multilayer plates or shells with  $h/l$  or  $h/R$  ( $R$  = radius) smaller than 0.1, the ELEM2 element can be used. It has been pointed out in Subsection 2.7 that the element reported in Ref. 29 is a better choice for this range of application.

- (d) For (1) relatively thick plates or shells or (2) laminates that have relatively low shear moduli and/or a high ratio of elastic constants in different directions, the ELEMZ multilayer element should be used so that local deformations and stresses are predicted accurately.
- (e) Predictions of the lowest natural frequency are usually accurate even when a small number of elements is used, but more elements are needed for suitably accurate predictions of the higher frequencies.
- (f) Comparisons of predictions from using two assumed-displacement finite elements for thick laminated plates on static problems showed that the present hybrid-stress element ELEMZ provides more accurate predictions for a given number of unknowns (and hence is less expensive).
- (g) Thermal effects are accurately accounted for through the computation of an equivalent thermal loading vector in the present hybrid-stress formulation. The limitations on the present finite-element methods lie in the fact that the normal stress  $\sigma_z$  is assumed to be zero and the transverse displacement  $w$  is assumed to be constant throughout the whole thickness of an element. While errors in the  $\sigma_z$  or the  $w$  prediction are usually negligible, these restrictive assumptions do have some effect on the other stress predictions. The present approach always yields symmetric results with respect to the middle surface of an element if the laminate is symmetric; however, the actual results may involve some deviation from symmetry because the load may act on only one surface of the laminate. Fortunately, such deviation is usually negligible except for very thick plates, for example, for  $h/l$  greater than about 0.25 [2].

In general, the stiffness matrices, mass matrices, and the equivalent thermal loading vectors developed in this study are very effective. They can be used for detailed displacement and stress analysis. Also they constitute a

sound foundation for transient dynamic analysis.

### 5.3 Suggestions for Future Research

A direct and useful extension of the present work would be the study of the response of layered structures under transient dynamic loadings. Since the basic stiffness matrix and the mass matrix are already developed, in theory it is necessary only to select an efficient timewise numerical integration scheme [55] to solve the transient equations of motion if damping can be neglected. Otherwise, a damping matrix will have to be developed.

The geometric stiffness matrix needed in a buckling analysis could be developed in a manner similar to the treatment used in the derivation of a mass matrix by the hybrid stress model. In fact, the derivation of a geometric stiffness matrix based on a mixed variational principle has already been reported by Allman [56]; even earlier Lundgren [57] obtained a geometric stiffness matrix for laminated plates by independently-assumed displacement functions. Thus, the extension of the present work to a linear buckling analysis including thermal buckling seems to be quite feasible.

Another area of interest is the nonlinear analysis of plates and shells. Both geometric and material nonlinearities could be considered. For geometrically nonlinear problems, the incremental approach [58] seems to be the most direct solution. However, some modifications of the present finite-element models would be needed since the present quadrilateral flat-plate element will not fit the deformed shape of a plate or a shell. For elastic-plastic-type material properties, some progress has been made recently [59] for hybrid stress finite-element models. The inclusion of elastic-plastic behavior in this hybrid-stress finite-element context may turn out not to be as difficult as the treatment of geometrically nonlinear problems. These nonlinear effects, of course, have been accommodated in assumed-displacement finite-element, finite-difference, and other methods for isotropic single-layer and/or multilayer structures.

## REFERENCES

1. Pagano, N.J. "Exact Solutions for Composite Laminates in Cylindrical Bending." *J. Composite Materials*, Vol. 3, 1969, pp. 398-411.
2. Pagano, N.J. "Exact Solutions for Rectangular Bidirectional Composites and Sandwich Plates." *J. Composite Materials*, Vol. 4, 1970, pp. 20-34.
3. Pagano, N.J. and Wang, S.D. "Further Study of Composite Laminates under Cylindrical Bending." *J. Composite Materials*, Vol. 5, 1971, pp. 521-528.
4. Pagano, N.J. and Hatfield, S.J. "Elastic Behavior of Multilayered Bidirectional Composites." *AIAA Journal*, Vol. 10, No. 7, July 1972, pp. 931-933.
5. Pryor, C.W., Jr., and Barker, R.M. "A Finite Element Analysis Including Transverse Shear Effects for Applications to Laminated Plates." *AIAA Journal*, Vol. 9, No. 5, 1971, pp. 912-917.
6. Barker, R.M., Lin, F.T., and Dana, J.R. "Three-Dimensional Finite-Element Analysis of Laminated Composites." *National Symposium on Computerized Structural Analysis and Design*, George Washington University, March 1972.
7. Pian, T.H.H. "Derivation of Element Stiffness Matrices by Assumed Stress Distributions." *AIAA Journal*, Vol. 2, No. 7, 1964, pp. 1333-1336.
8. Pian, T.H.H. and Tong, Pin. "Rationalization in Deriving Element Stiffness Matrix by Assumed Stress Approach." *Proc. Second Conf. on Matrix Methods in Structural Mechanics*. AFFDL-TR-68-150, WP-AFB, 1968, pp. 441-469.
9. Cantin, R. and Clough, R. "A Curved Cylindrical Shell Discrete Element." *AIAA Journal*, Vol. 6, No. 6, June 1968, pp. 1052-1062.
10. Bogner, F.K., Fox, R.L. and Schmit, L.T. "A Cylindrical Shell Discrete Element." *AIAA Journal*, Vol. 5, No. 4, April 1967, pp. 745-750.
11. Wu, R.W., "Discrete Element Analysis of Beams, Plates and Cylindrical Shells, Including Transverse Shear Deformation." S.M. Thesis, Department of Aeronautics and Astronautics, M.I.T., June 1969.

12. Tanaka, M. "Development and Evaluation of a Triangular Thin Shell Element Based Upon the Hybrid Assumed Stress Model." Ph.D. Thesis, Department of Aeronautics and Astronautics, M.I.T., June 1970.
13. Key, S.W. and Beisinger, Z.E. "The Analysis of Thin Shells by the Finite Element Methods." Paper presented at IUTAM Symposium on High-Speed Computing of Elastic Structures, Liege, Belgium, August 23-28, 1970.
14. Atluri, S. "Static Analysis of Shells of Revolution Using Doubly-Curved Quadrilateral Elements Derived from Alternate Variational Models." M.I.T. ASRL TR 146-7, (also SAMSO TR 69-394), June 1969.
15. Clough, R.W. and Johnson, C.P. "A Finite Element Approximation for the Analysis of Thin Shells." J. Solids and Structures, Vol. 4, 1968, pp. 43-60.
16. Wolf, J.P. "Systematic Enforcement of Stress Boundary Conditions in the Assumed Stress Hybrid Model Based on the Deformation Method." Paper presented at the First International Conference on Structural Mechanics in Reactor Technology, Berlin, 1971.
17. Pian, T.H.H. and Mau, S.T. "Some Recent Studies in Assumed Stress Hybrid Model." Proceedings Second U.S.-Japan Seminar on Matrix Methods in Structural Analysis and Design, Berkeley, California, Aug. 14-19, 1972.
18. Timoshenko, S. and Woinowsky-Krieger, S. Theory of Plates and Shells. McGraw Hill Book Co., Inc., 1959.
19. de Veubeke, B.F., and Sander, G. "An Equilibrium Model for Plate Bending." International Journal of Solids and Structures, Vol. 4, 1968, pp. 447-468.
20. de Veubeke, B.F. "A Conforming Finite Element for Plate Bending." International Journal of Solids and Structures, Vol. 4, 1968, pp. 95-108.
21. Morley, L.S.D. "Bending of a Simply Supported Rhombic Plate under Uniform Normal Loading." Quarterly Journal of Mechanics and Applied Mathematics, Vol. 15, 1962, pp. 413-426.
22. Plantema, F.J. Sandwich Construction. John Wiley and Sons, 1966.
23. Whitney, J.M. "The Effect of Boundary Conditions on the Response of Laminated Composites." J. Composite Materials, Vol. 4, April 1970, pp. 192-203.

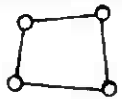
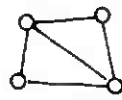
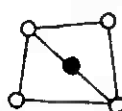



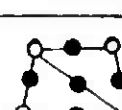
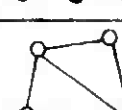
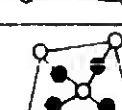
24. Whitney, J.M. and Pagano, N.J. "Shear Deformation in Heterogeneous Anisotropic Plates." *J. Applied Mechanics*, Vol. 37, No. 4, Dec. 1970, pp. 1031-1036.
25. Megard, G. "Planar and Curved Shell Elements." Finite Element Methods in Stress Analysis, edited by Holand, I. and Bell, K., TAPIR, 1969.
26. Valsov, V.Z. *General Theory of Shells and Its Applications in Engineering.* NASA Technical Translation TTF-99, April 1964.
27. Flugge, W. Stress in Shells. Springer-Verlag, Berlin, 1960.
28. Mack, E.W., Berg, B.A. and Witmer, E.A., "An Improved Discrete-Element Analysis and Program for the Linear-Elastic Static Analysis of Meridionally-Curved, Variable-Thickness, Branched Thin Shells of Revolution Subjected to General External Mechanical and Thermal Loads, Part 2: The SABOR 4 Program." MIT ASRL TR 146-4, Part 2, (also SAMSO TR 68-310, Part 2), March 1968. (AD840 614L).
29. Spilker, R.L. "A Finite Element Model for Laminated Plates Including Transverse Shear Deformation." MIT ASRL TR 169-1, (also AMMRC CTR 72-12), July 1972 .
30. Dungar, R., Severn, R.T., and Taylor, P.R. "Vibration of Plate and Shell Structures Using Triangular Finite Elements." *Journal of Strain Analysis*, Vol. 2, No. 7, 1963, pp. 73-83.
31. Dungar, R., and Severn, R.T. "Triangular Finite Elements of Variable Thickness and Their Application to Plate and Shell Problems." *Journal Strain Analysis*, Vol. 4, No. 1, 1969, pp. 10-21.
32. Henshell, R.D., Neale, B.K., and Warburton, G.B. "A New Hybrid Cylindrical Shell Element." *Journal of Sound and Vibration*, Vol. 16, No. 4, 1971, pp. 519-531.
33. Neale, B.K., Henshell, R.D., and Edwards, G., "Hybrid Plate Bending Elements." *Journal of Sound and Vibration*, Vol. 23, No. 1, 1972, pp.101-112.
34. Tabarrok, B., "Complementary Energy Methods in Elastodynamics." Technical Publication Series, Department of Mechanical Engineering, University of Toronto, Canada, UTME-TP 7101, January 1971.

35. Tabarrok, B. "A Variational Principle for the Dynamic Analysis of Continua by Hybrid Finite Element Method." *International Journal of Solids and Structures*, Vol. 7, No. 3, 1971, pp. 251-268.
36. Toupin, R.A. "A Variational Principle for the Mesh-Type Analysis of a Mechanical System." *Journal of Applied Mechanics*, Tran. ASME, Vol. 74, 1952, pp. 151-152.
37. Sakaguchi, R.L. "Energy Methods in Plate Vibration Analysis." Ph.D. Thesis, Department of Mechanical Engineering, University of Toronto, 1970.
38. Tong, P., Mau, S.T., and Pian, T.H.H. "Derivation of Geometric Stiffness and Mass Matrix for Hybrid Finite Element Models. (to be published).
39. Pian, T.H.H. "Finite Element Methods by Variational Principles with Relaxed Continuity Requirements." Paper presented at the International Conference on Variational Methods in Engineering, Southampton, England, September 25-29, 1972.
40. Karnopp, B.H. Reissner's Variational Principle of Elastodynamics." *ACTA Mechanics*, Vol. 6, 1968, pp. 158-164.
41. Tong, P., Pian, T.H.H., and Bucciarelli, L.L. "Mode Shapes and Frequencies by Finite Element Method Using Consistent and Lumped Masses." *Computers and Structures*, Vol. 1, 1971, pp. 623-638.
42. Wilkinson, J.H. The Algebraic Eigenvalue Problem. Oxford University Press, London, 1965.
43. Peters, G. and Wilkinson, J.H. "Eigenvalues of  $Ax = \lambda Bx$  with Band Symmetric A and B." *Computer Journal*, Vol. 12, 1969, pp. 398-404.
44. Gupta, K.K. "Solutions of Eigenvalue Problems by Sturm Sequence Method." *International Journal for Numerical Methods in Engineering*, Vol. 4, 1972, pp. 379-404.
45. Timoshenko, S. and Young, D.H. Vibration Problems in Engineering. Van Nostrand Reinhold Co., New York, 1961.

46. Jones, A.T. "Exact Natural Frequencies for Cross-Ply Laminates." *Journal of Composite Materials*, Vol. 4, 1970, pp. 476-491.
47. Srinivas, S., Rao, C.V.J., and Rao, A.K. "An Exact Analysis for Vibration of Simply-Supported Homogeneous and Laminated Thick Rectangular Plates." *Journal of Sound and Vibration*, Vol. 12, 1970, pp. 187-199.
48. Nelson, R.B., Dong, S.B., and Kalra, R.D. "Vibrations and Waves in Laminated Orthotropic Circular Cylinders." *Journal of Sound and Vibration*, Vol. 18, 1971, pp. 429-444.
49. Dong, S.B. and Tso, F.K.W. "On a Laminated Orthotropic Shell Theory Including Transverse Shear Deformation." *Journal of Applied Mechanics*, Paper No. 72-APM-7, 1972.
50. Dong, S.B. "Free Vibration of Laminated Orthotropic Cylindrical Shells." *Journal of the Acoustical Society of America*, Vol. 44, 1968, pp. 1628-1635.
51. Gallagher, R.H., Padlog, J., and Bijlaard, P.P. "Stress Analysis of Heated Complex Shapes." *Journal of American Rocket Society*, Vol. 32, No. 5, May 1962, pp. 700-707.
52. Webber, J.P.H. "Thermo-Elastic Analysis of Rectangular Plates in Plane Stress by the Finite-Element Displacement Method." *Journal of Strain Analysis*, Vol. 2, No. 1, 1967, pp. 43-51.
53. Heldenfels, R.R., and Roberts, W.M. "Experimental and Theoretical Determination of Thermal Stresses in a Flat Plate." NACA TN-2769, August 1952.
54. Boley, B.A., and Weiner, J.H. Theory of Thermal Stresses. John Wiley & Sons, New York, 1960.
55. Clough, R.W., Bath, K.I. "Finite Element Analysis of Dynamic Response." Advances in Computational Methods in Structural Mechanics and Design, edited by Oden, J.T., Clough, R.W., and Yamamoto, Y., UAH Press, The University of Alabama in Huntsville, Alabama, 1972, pp. 153-179.
56. Allman, D.J. "Finite Element Analysis of Plate Buckling Using a Mixed Variational Principle." Paper presented at the Air Force Third Conference on Matrix Methods in Structural Mechanics, Wright-Patterson Air Force Base, Ohio, October 19-21, 1971.

57. Lundgren, H.R. "Buckling of Multilayer Plates by Finite Elements." Ph.D. Thesis, Oklahoma State Univ. 1967.
58. Pirotin, S.D. "Incremental Large Deflection Analysis of Elastic Structures." Ph.D. Thesis, Department of Aeronautics and Astronautics, M.I.T. 1971.
59. Luk, C.H. "Application of the Assumed-Stress Hybrid Finite-Element Method on Fracture Mechanics and Elastic-Plastic Analysis." Ph.D. Thesis, Department of Aeronautics and Astronautics, M.I.T., September, 1972.

TABLE 1  
IDENTIFICATION OF THE VARIOUS TYPES OF HYBRID-STRESS  
FLAT-PLATE FINITE ELEMENTS EVALUATED

TYPE		STRESS	DISPLACEMENT	DOF	COMMENTS
ELEM1		L, L	L	20	Good Element
ELEMA		L, L	L	20	Too Stiff
ELEMB		L, L	L, Q	20*	Too Stiff
ELEMC		L, L	Q	32*	Singular
ELEMD		L, L <sup>(-)</sup>	L, Q	20*	Fair but Stress Field too Simple
ELEME		L, Q	L	20	Too Stiff
ELEMF		L, Q	Q	32*	Too Flexible
ELEMG		L, Q	Q <sup>-</sup>	20	Good but Use is Limited to Flat Plates
ELEMZ		L, Q	L, Q	20	Good but Complex

\* After static condensation

○ = Element corner node

● = Element side mid-point node

L, L<sup>-</sup> = Respectively, complete and incomplete linear functions of x and y

Q, Q<sup>-</sup> = Respectively, complete and incomplete quadratic functions of x and y

TABLE 2

## DATA FOR SINGLE-LAYER ISOTROPIC PLATES\*

## (a) Simply-Supported Thin Plate

Loading: Concentrate Central Loading

Aspect Ratio = 1:1

Thickness-to-side Ratio = 1:100

Boundary Condition: Simply-Supported, no tangential rotation

Finite Element Breakdown: Uniform mesh in a quarter

## (b) Clamped Square Thin Plate

Loading: Concentrate Central Loading

Aspect Ratio = 1:1

Thickness-to-side Ratio = 1:100

Boundary Condition: Clamped

Finite Element Breakdown: Uniform mesh in a quarter

## (c) Clamped Rectangular Plate

Loading: Uniform Load

Aspect Ratio = 1:2

Thickness-to-short-side Ratio = 1:100

Boundary Condition: Clamped

Finite Element Breakdown: Uniform mesh in a quarter with  
element aspect ratio 1:1 and 1:2

## (d) Skewed Simply-Supported Thin Plate

Loading: Uniform Load,  $p$ (psi)

Aspect Ratio = 1:1

Thickness-to-side Ratio = 1:100

Length of each side =  $a$ 

Boundary Condition = Simply-Supported, tangential rotation allowed

Finite Element Breakdown: Uniform mesh for the whole plate



## (e) Simply-Supported Square Thick Plate

Loading: Uniform

Aspect Ratio = 1:1

Thickness-to-side Ratio = 1:4

Boundary Condition: Simply-Supported, no tangential rotation

Finite-Element Breakdown: Uniform mesh in a quarter

\*  $E = 10^7$  psi,  $\nu = 0.3$  for all cases;  $D = \frac{Eh^3}{12(1 - \nu^2)}$ ,  $h$  = plate thickness

TABLE 3  
DATA FOR TWO-LAYER PLATES

(a) Clamped Cross-Ply Rectangular Thin Plate

Loading: Uniform

Aspect Ratio = 1:2

Thickness-to-side Ratio = 1:100



Boundary Condition: Clamped

Finite Element Breakdown: Uniform mesh in a quarter, square elements

Material:  $E_1/E_2 = 40$ ,  $G_{12}/E_2 = 0.5$ ,  $\nu_{12} = 0.25$

Orientation:  $0^\circ/90^\circ$

(b) Clamped Cross-Ply Square Thin Plate

Same as in (a), except Aspect Ratio = 1:1

(c) Clamped Angle-Ply Square Thin Plate

Same as in (b), except fiber orientation =  $\pm 45^\circ$

(d) Simply-Supported Angle-Ply Square Thick Plate

Loading:  $q_0 \sin(\pi x/a) \sin(\pi y/a)$

Aspect Ratio = 1:1

Thickness-to-side Ratio = 1:6

Boundary Condition: Simply-Supported, free in tangential direction,  
no normal displacement

Finite Element Breakdown: Uniform mesh for the whole plate

Material:  $E_1/E_2 = 40$ ,  $G_{12}/E_2 = 0.6$ ,  $G_{23}/E_2 = 0.5$ ,  $\nu_{12} = 0.25$

Orientation:  $\theta$  varies

TABLE 4

## DATA FOR THREE-LAYER PLATES

## (a) Cross-Ply Long Strip:

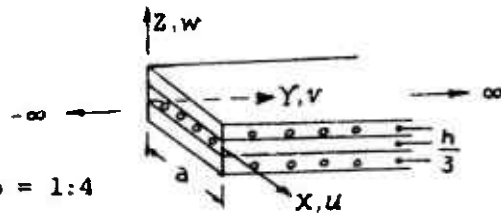
Loading:  $q_0 \sin(\pi x/a)$ 

Aspect Ratio = 1:∞

Thickness-to-short-side Ratio = 1:4

Boundary Condition: Simply-Supported, no tangential rotation

Finite Element Breakdown: Uniform mesh in half a strip in x-direction

Material:  $E_1 = 25 \times 10^6$  psi,  $E_2 = 10^6$  psi,  $G_{12} = 0.5 \times 10^6$  psi $G_{23} = 0.2 \times 10^6$  psi,  $\nu_{12} = \nu_{23} = 0.25$ Orientation:  $0^\circ/90^\circ/0^\circ$ Nondimensionalized quantities:  $\bar{u} = E_T u(0, z)/(hq_0)$  $\bar{\sigma}_x = \sigma_x(l/2, z)/q_0$ ,  $\sigma_{xz} = \sigma_{xz}(0, z)/q_0$  $\bar{w} = 100 \cdot E_T h^3 w(l/2, 0)/(q_0 \cdot l^4)$ 

## (b) Cross-Ply Plates

Loading:  $q_0 \sin(\pi x/a) \sin(\pi y/b)$ 

Boundary Condition: Same as in (a)

Finite Element Breakdown: Uniform mesh in a quarter

Material: same as in (a)

Orientation: Same as in (a)

(1) Aspect Ratio = 3:  $b = 3a$ Thickness-to-short-side Ratio  $h/a = 1/10$ (2) Aspect Ratio:  $a/b = 1$ Thickness-to-side Ratio  $h/a = 1/4$ 

Nondimensionalized Quantities

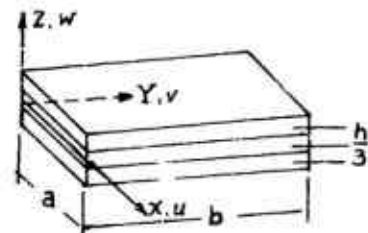
 $\bar{u} = u(a/2, 0, z) E_T/(q_0 a^3/h^2)$  $\bar{\sigma}_x = \sigma_x(0, 0, z)/(q_0 a^2/h^2)$  $\bar{\sigma}_{xy} = \sigma_{xy}(a/2, a/2, z)/(q_0 a^2/h^2)$  $\bar{\sigma}_{xz} = \sigma_{xz}(a/2, 0, z)/(q_0 a/h)$ 

TABLE 5

RESULTS OF THE 3-LAYER MODERATELY-THICK CROSS-PLY PLATE UNDER TRANSVERSE LOADING<sup>+</sup>

$$\text{NORMALIZATION: } (\bar{\sigma}_x, \bar{\sigma}_y, \bar{\sigma}_{xy}) = \frac{1}{q_0 S^2} (\sigma_x, \sigma_y, \sigma_{xy}); (\bar{\sigma}_{xz}, \bar{\sigma}_{yz}) = \frac{1}{q_0 S} (\sigma_{xz}, \sigma_{yz}); \bar{w} = \frac{100 E w}{q_0 h S^4}, S = \frac{a}{h}$$

MESH	DOF	$\bar{\sigma}_x$ (a/2, 3a/2, +h, 2)	$\bar{\sigma}_y$ (a/2, 3a/2, +h/6)	$\bar{\sigma}_{xz}$ (0, 3a/2, 0)	$\bar{\sigma}_{yz}$ (a/2, 0, 0)	$\bar{\sigma}_{xy}$ (0, 0, +h/2)	$\bar{w}$ (a/2, 3a/2, 0)
2x1	54	$\pm 0.328$ (14%)*	$\pm 0.0462$ (6%)	0.287 (-32%)	0.0104 (-32%)	$\pm 0.0136$ (11%)	1.0131 (10%)
4x2	135	$\pm 0.741$ (2%)	$\pm 0.0438$ (0.5%)	0.386 (-8%)	0.0139 (-9%)	$\pm 0.0126$ (2%)	0.9427 (2.5%)
8x4	405	$\pm 0.714$ (-1.5%)	$\pm 0.0426$ (-2%)	0.415 (-1%)	0.0151 (-1.5%)	$\pm 0.0122$ (-1%)	0.9255 (1%)
ELASTICITY (Ref. 2)		0.726 -0.725	0.0418 -0.0435	0.420	0.0152	- 0.0120 0.0123	0.919
CPT (Ref. 2)		$\pm 0.623$	$\pm 0.0252$	0.440	0.0108	$\pm 0.0083$	0.503

<sup>+</sup> Case b1 of Table 4 (h/a = 1/10)<sup>\*</sup> Error, compared with Elasticity Maximum Values

TABLE 6

DATA FOR THIN CYLINDRICAL SHELLS

(a. Pinched Cylindrical Shell

Loading: Pinch Load,  $P$  (lbs)

Radius:  $a = 10$  in.

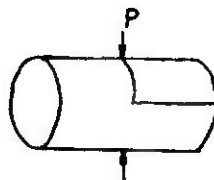
Length  $l = 31.42$  in.

Thickness:  $h = 0.1$  in.

Boundary Conditions: Simply-Supported, no tangential rotation

Finite Element Breakdown: Uniform mesh in one-eighth

Material: Isotropic,  $E = 1.0$  psi,  $\nu = 0.28$



(b) Ring-Loaded Cylindrical Shell

Loading: Axisymmetric Ring Load of  $Q = 1.0$  lb/in

Radius:  $a = 10$  in.

Length:  $l = 31.42$  in.

Thickness:  $h = 0.1$  in.

Boundary Conditions: Free edge

Finite Element Breakdown: Uniform mesh in one strip

Material: Isotropic,  $E = 1.0$  psi,  $\nu = 0.28$

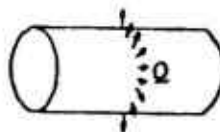


TABLE 7  
DATA FOR CONICAL SHELLS

(a) Isotropic Single-Layer Conical Shell

Loading: Axisymmetric Ring Loads near free end,  $Q$

Radius at smaller end = 10 in.

Radius at larger end = 15 in.

Length of meridian = 10 in

Semi-angle of cone =  $30^\circ$

Thickness = 0.025 in., 0.1 in., 0.5 in., 1.0 in.

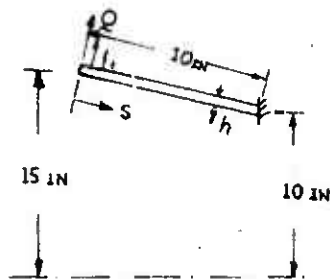
Boundary Condition: Clamped at smaller end, free at larger end

Material = Isotropic,  $E = 10^7$  psi,  $\nu = 0.3$

Finite Element Breakdown: 20 elements in the first 2 inches

from the free end, 15 elements in the next 3 inches, and

10 elements in the last 5 inches



Ring Loading $Q$ (lb/in)	at $s$ (in)
1.0	0
0.75	0.3
0.50	0.6
0.25	0.9

(b) Sandwich Conical Shell

Same as in (a), except

Thickness: 0.01 in. for top and bottom layer and 0.08 in. for the core

Material:  $E = 10^7$  psi,  $\nu = 0.3$ , isotropic for cover layers, and  
 $E = 10^4$  psi,  $\nu = 0.3$ ,  $G = 10^6$  psi for the core

(c) Two-Layer Conical Shell

Same as in (a), except

Thickness: 0.5 in. for cover material and 0.5 in. for base material

Material: Glass Phenolic cover,  $E = 10^6$  psi,  $\nu = 0.3$ , isotropic  
Aluminum base,  $E = 10^7$  psi,  $\nu = 0.3$  isotropic

TABLE 8  
PERCENTAGE ERROR OF THE LOWEST FREQUENCY PREDICTED FOR  
A SIMPLY-SUPPORTED SQUARE THIN PLATE USING ELEM1

$$\left( \frac{\omega - \omega_0}{\omega_0} - 1 \right) \times 100$$

MESH <sup>+</sup>	DOF	LUMPED MASS	HR MASS
2x2	27	- 5.2	5.1
4x4	75	- 1.3	1.2
6x6	147	- 0.6	0.6
8x8	243	-0.4	0.3

Thickness = 0.1 in., Side length = 20 in., E = 1 psi,  $\nu = 0.3$ ,  $\rho = 1(\text{lb-sec}^2)/\text{in}^4$

$\omega_0$  = Exact Lowest Frequency (Ref. 40) = 0.00149 rad/sec

<sup>+</sup> Uniform mesh in a quarter of the plate

TABLE 9  
PERCENTAGE ERROR OF THE LOWEST FREQUENCY PREDICTED FOR  
A CLAMPED RECTANGULAR THIN PLATE USING ELEM1

$$\left( \frac{\omega - \omega_0}{\omega_0} - 1 \right) \times 100$$

MESH <sup>+</sup>	DOF	LUMPED MASS	HR MASS
2x2	27	- 7.1	4.0
4x4	75	- 2.0	1.1
6x6	147	- 1.0	0.3
8x8	243	- 0.7	0.3

Thickness = 0.1 in., Short-side length = 20 in., Long-side length = 40 in.,

E = 1 psi,  $\nu = 0.3$ ;  $\rho = 1(\text{lb-sec}^2)/\text{in}^4$

$\omega_0$  = Exact Lowest Frequency (Ref. 40) = 0.00187 rad/sec

<sup>+</sup> Uniform mesh in a quarter of the plate.

TABLE 10  
FREQUENCY PREDICTIONS FOR THE FIRST SEVEN SYMMETRIC MODES OF VIBRATION  
OF A SIMPLY-SUPPORTED RECTANGULAR THIN PLATE USING ELEM1 AND THE  
HYBRID-RATIONAL MASS MATRIX

MODE*	EXACT**	6x12 MESH <sup>+</sup>		8x8 MESH <sup>++</sup>	
		$\bar{\omega}$	Error (%)	$\bar{\omega}$	ERROR(%)
1-1	1.25	1.2565	0.52	1.2540	0.32
3-1	3.25	3.2863	1.12	3.3340	2.58
5-1	7.25	7.5021	3.74	7.9220	9.27
1-3	9.25	9.7807	5.74	9.5198	2.92
3-3	11.25	11.7754	4.40	11.5685	2.83
7-1	13.25	14.2323	7.41	16.0343	21.01
5-3	15.25	15.9259	4.43	16.545	5.28

\* Mode Shape:  $\sin(m\pi/a) \sin(n\pi/b)$

\*\* Ref. 40 exact solution:  $\omega = \pi^2 \sqrt{D/\rho h} (m^2/a^2 + n^2/b^2)$ ;  $a = 2b$ ;  
normalized  $\bar{\omega} = (m^2/4 + n^2)$ ;  $D = Eh^3/[12(1 - \nu^2)]$ .

<sup>+</sup> Results of a 6x2 uniform mesh in a quarter of the plate (6 in the long dimension); total DOF = 273; total computing time on IBM 370/155 = 5.9 min.

<sup>++</sup> Results of an 8x8 uniform mesh in a quarter of the plate; total DOF = 243; total computing time on IBM 370/155 = 8.6 min.

TABLE 11

PERCENTAGE ERROR OF THE LOWEST FREQUENCY PREDICTED FOR A  
TWO-LAYER CROSS-PLY ( $0^\circ/90^\circ$ ) SQUARE THIN PLATE USING  
ELEMZ AND THE HR MASS MATRIX

$$\left( \frac{\omega - \omega_0}{\omega_0} - 1 \right) \times 100$$

MESH	DOF	HR MASS
2x2	45	3.0
4x4	125	- 0.5
6x6	245	- 0.13
8x8	405	- 0.16

$$E_1/E_2 = 40, G_{12}/E_2 = 0.5, \nu_{12} = 0.25, \rho = 1$$

$$\omega_0 = \text{Lowest frequency calculated in Ref. 22} = 0.00614 \text{ rad/sec}$$

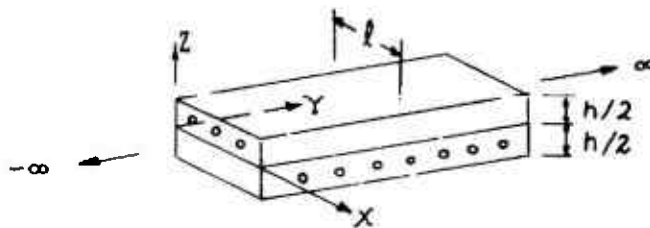
TABLE 12

DATA FOR THE VIBRATION ANALYSIS OF A SIMPLY-SUPPORTED TWO-LAYER  
CROSS-PLY ( $0^\circ/90^\circ$ ) INFINITE STRIP

(a) Material Properties

$$\text{Bottom-Layer} = E_1 = 1.0922, E_2 = 41.983, \nu_{12} = 0.00520, \nu_{23} = 0.2, G_{12} = G_{23} = 1$$

$$\text{Top-Layer} = E_1 = 43.516, E_2 = 1.0455, \nu_{12} = 0.20812, \nu_{23} = 0.2, G_{12} = G_{23} = 1$$



(b) Finite-Element Discretization

Eight ELEMZ elements in half strip ( $l/2$ ) and two sublayers for each layer;  
i.e., treating the two-layer plate as a four-layer plate.

TABLE 13  
COMPARISON OF PREDICTIONS FOR THE LOWEST FREQUENCIES OF 3-LAYER  
SIMPLY-SUPPORTED SQUARE PLATES

CASE	$d_1/d_2$	$G_1/G_2$	FREQUENCY ( $\lambda$ )			ERROR %	
			CPT	ELEMZ <sup>†</sup>	EXACT	CPT	ELEMZ
1	1	1	0.077054	0.07533	0.0745	3.4	1.1
2	1	2	0.093994	0.090973	0.089986	4.5	1.1
3	1	5	0.13239	0.12437	0.123072	7.6	1.1
4	1	15	0.215642	0.18529	0.183664	17.4	0.9
5	2	15	0.196852	0.16897	0.167574	17.5	0.8
6	3	15	0.18225	0.15633	0.155032	17.5	0.8

Isotropic,  $\nu_1 = \nu_2 = \nu_3 = 0.3$ ,  $G_1 = G_3$ ,  $d$  = Mass Density,  $d_1 = d_3$

$h_1/a = 0.01$ ,  $h_2/a = 0.08$ ,  $h_1 = h_3$

$\lambda = \omega(d_2 h_2^2 / G_2)^{1/2}$ ,  $\omega$  = angular frequency (rad/sec)

CPT = classical plate theory, Ref. 42

EXACT = Ref. 42

Finite-Element Discretization = uniform 4x4 mesh in a quarter of the plate

<sup>†</sup> ELEMZ with the HR Mass Matrix

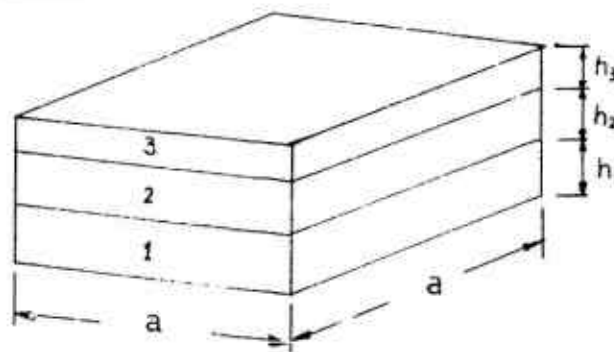


TABLE 14  
PROPERTIES OF A THREE-LAYER CYLINDRICAL SHELL.

LAYER	THICKNESS (in.)	$C_{11}^*$	$C_{22}$	$C_{33}$	$C_{12}$	$C_{13}$	$C_{23}$	$C_{44}$	$C_{55}$	$C_{66}$
Inside	0.2	33.03	3.032	33.32	0.3998	10.03	1.03	1.154	1.154	1.154
Middle	0.5	33.02	3.032	33.32	0.3998	10.03	1.03	1.154	0.1154	0.1154
Outside	0.3	33.02	3.032	33.32	0.3998	10.03	1.03	1.154	1.154	1.154

\* Elastic constants  $C_{ij}$  defined by  $\sigma_i = C_{ij} E_j$ ,  $i, j = 1, 2, \dots, 6$  (units in  $10^6$  psi)

TABLE 15  
COMPARISON OF PREDICTIONS FOR THE LOWEST FREQUENCIES OF 3-LAYER  
SIMPLY-SUPPORTED CYLINDRICAL SHELLS IN AXISYMMETRIC VIBRATION

$H/l$	$a$ (in)	FREQUENCY (RAD/SEC)					ERROR <sup>++</sup> (%)			
		CST	RST	ELEMR <sup>+</sup>	ELEMZ <sup>+</sup>	ET	CST	RST	ELEMR	ELEMZ
0.01	0.5	171.65	171.65	172.91	172.91	171.65	0.0	0.0	0.7	0.7
0.05	0.5	177.54	177.28	177.37	177.35	177.35	0.1	0.0	0.0	0.0
0.10	0.1	233.14	228.15	230.10	229.11	228.63	2.0	- 0.2	0.6	0.2
0.20	.05	647.82	560.22	593.67	574.00	568.52	13.7	- 1.6	4.4	0.9
0.40	.025	2502.9	1607.8	1874.2	1728.5	1704.4	46.8	- 5.7	9.9	1.4
0.60	.016	5620.8	2751.2	3411.4	3099.1	3052.3	84.1	- 9.9	11.7	1.5
0.80	.012	9989.3	3886.9	5003.0	4557.3	4495.2	122.2	-13.5	11.3	1.4
1.00	.01	15607.0	5005.5	6593.2	6062.4	5991.7	160.5	-16.5	10.0	1.2

$H/l$  = Thickness-to-length ratio, Mean Radius  $R = 10$  in.  $H = 1$  in.

$a$  = Width of flat-plate element

CST = Classical Shell Theory, Ref. 50.

RST = Refined Shell Theory, Ref. 49.

ET = Elasticity Theory, Ref. 48

<sup>+</sup>The HR mass matrix is employed

<sup>++</sup>ERROR = Compared with the Elasticity Solution of Ref. 48.

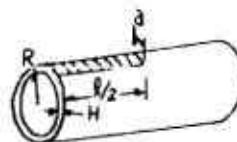


TABLE 16  
DATA FOR A FREE SINGLE-LAYER ISOTROPIC THIN RECTANGULAR  
PLATE SUBJECTED TO THERMAL LOADING

- (a) Material Properties:  
 $E = 10.4 \times 10^6$  psi,  $\nu = 0.3$ ,  $\alpha = 12.7 \times 10^{-6}$  in/in-°F
- (b) Dimensions:  
 Rectangular plate with long-side length =  $2a = 36$  in, short-side length =  $2b = 24$  in, and thickness = 0.25 in
- (c) Temperature Distribution  
 Linear variation in the short-span direction and constant in the long-span direction. Maximum temperature rise  $T_1$  is 150 °F (see Fig. 28b)
- (d) Finite Element Discretization:  
 Uniform 5x4 mesh in a quarter of the plate with ELEMZ "degeneralized" for this single-layer problem

TABLE 17  
DATA FOR A CLAMPED RECTANGULAR SINGLE-LAYER ISOTROPIC THIN PLATE  
SUBJECTED TO THERMAL LOADING

- (a) Material Properties:  
 $E = 1.0$  psi,  $\nu = 0.3$ ,  $\alpha = 1.0 \times 10^{-6}$  in/in-°F
- (b) Dimensions:  
 Rectangular plate with long-side length = 32 in, short-side length = 16 in and thickness = 0.16 in
- (c) Temperature Distribution:  
 Parabolic in the short-span direction and constant in the long-span direction (see Fig. 29a)
- (d) Finite-Element Discretization:  
 Uniform 8x8 mesh in a quarter of the plate with ELEMZ "degeneralized" for this single-layer problem

TABLE 18

DATA FOR A SIMPLY-SUPPORTED TWO-LAYER CROSS-PLY ( $0^\circ/90^\circ$ )  
INFINITELY-LONG THIN STRIP

(a) Material Properties:

$E_1/E_2 = 25$ ,  $G_{12}/E_2 = 0.5$ ,  $G_{23}/E_2 = 0.2$ ,  $\nu_{12} = \nu_{23} = 0.25$ ,  
 $E_2 = 1$  psi (Longitudinal  $\alpha$ )/Transverse  $\alpha$ ) =  $1/3$ ,  
Longitudinal  $\alpha = 1.0 \times 10^{-6}$  in/in- $^\circ\text{F}$

(b) Dimensions:

Short-span length = 16 in, Thickness = 0.16 in (0.08 in. for  
each layer)

(c) Temperature Distribution:

1  $^\circ\text{F}$  uniformly distributed over the entire strip

(d) Finite-Element Discretization:

Eight ELEMZ elements in a half span

(e) Boundary Condition: only transverse displacements along  
the supported edges ( $x = \pm 8$  in.) are constrained.

TABLE 19

DATA FOR A SIMPLY-SUPPORTED THREE-LAYER CROSS-PLY ( $0^\circ/90^\circ/0^\circ$ )  
CYLINDRICAL SHELL SUBJECTED TO THERMAL LOADING

(a) Material Properties:

$E_1/E_2 = 25$ ,  $G_{12}/E_2 = 0.5$ ;  $G_{23}/E_2 = 0.2$ ,  $\nu_{12} = \nu_{23} = 0.25$ ,  
 $E_2 = 1$  psi (Longitudinal  $\alpha$ )/(Transverse  $\alpha$ ) =  $1/3$ , Longi-  
tudinal  $\alpha = 1.0 \times 10^{-6}$  in/in- $^\circ\text{F}$

(b) Dimensions:

Mean Radius = 20 in., Thickness = 1 in. (0.2 in. for inside  
layer, 0.5 in. for middle layer and 0.3 in. for outside  
layer). Total length = 16 in.

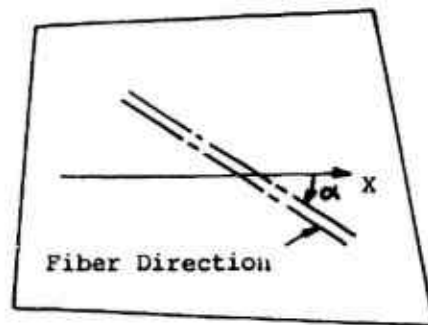
(c) Temperature Distribution:

1  $^\circ\text{F}$  uniformly distributed over the entire shell

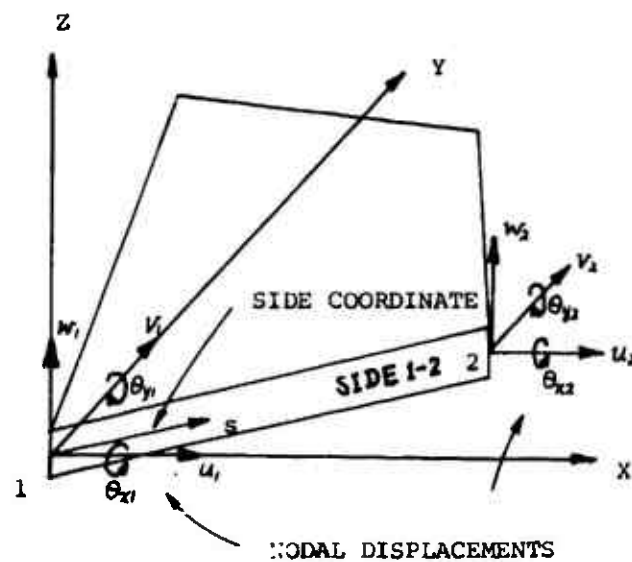
(d) Finite-Element Discretization:

Eight ELEMZ elements in half strip

(e) Boundary Conditions: only radial displacements along the  
supported edges are constrained.

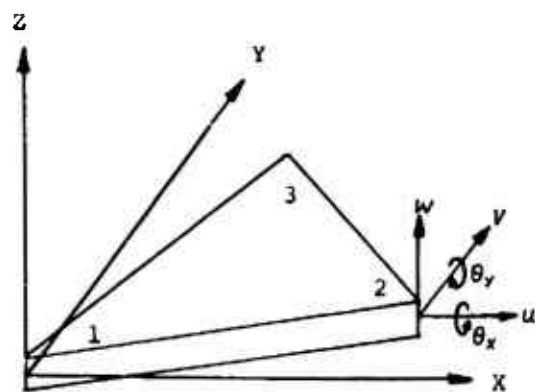


(a) Fiber Orientation

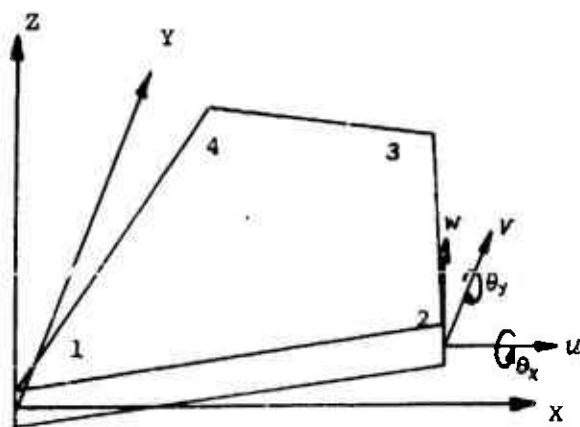


(b) Geometry, Coordinate, and Displacement Nomenclature

FIG. 2 NOMENCLATURE FOR COMPOSITE PLAT-PLATE FINITE ELEMENTS



(c) Triangular Element



(d) General Quadrilateral Element

FIG. 1 CONCLUDED

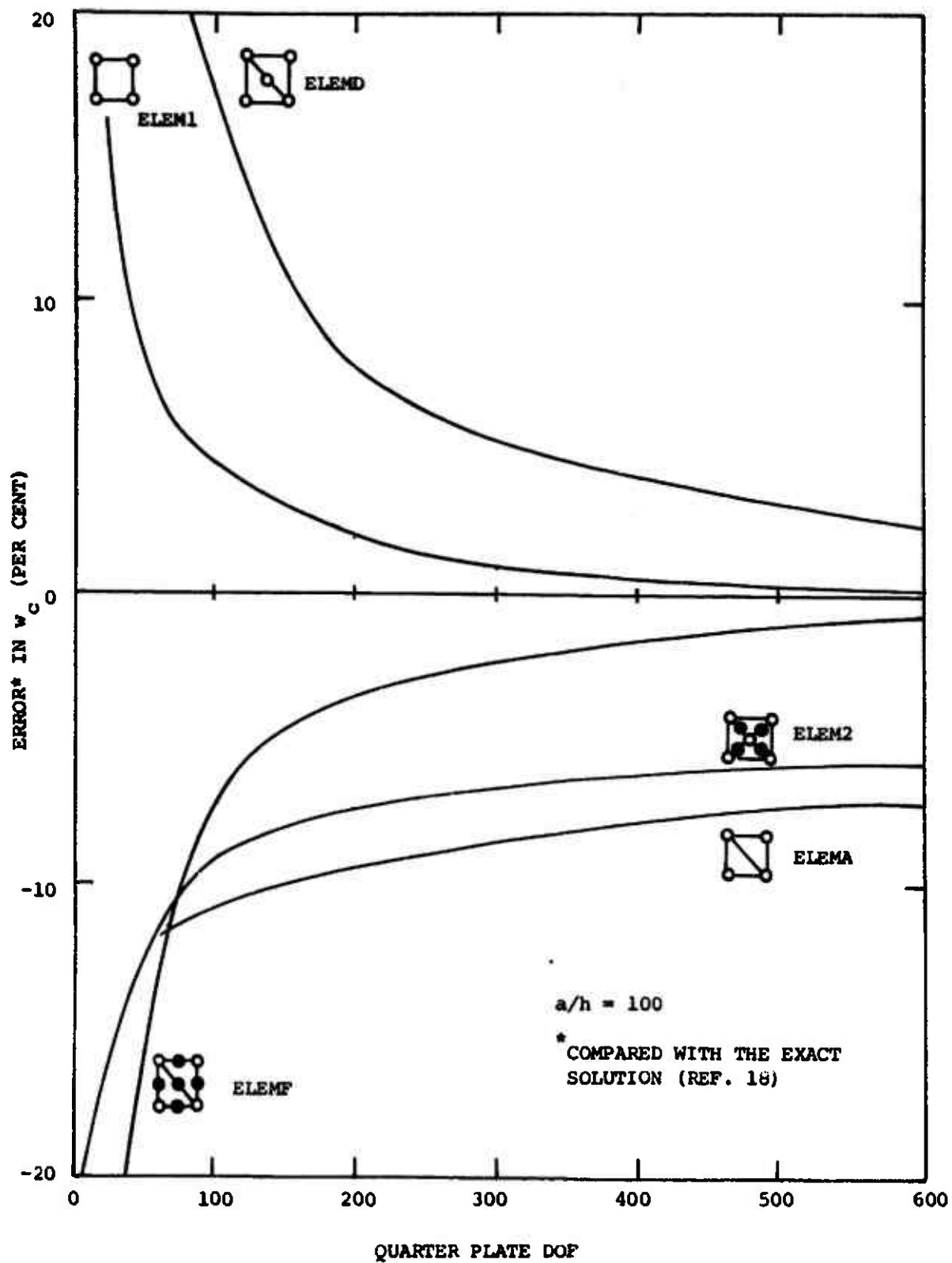


FIG. 2 CENTRAL DEFLECTION OF A SIMPLY-SUPPORTED, CENTRALLY-LOADED, SQUARE, ISOTROPIC, THIN, SINGLE-LAYER PLATE

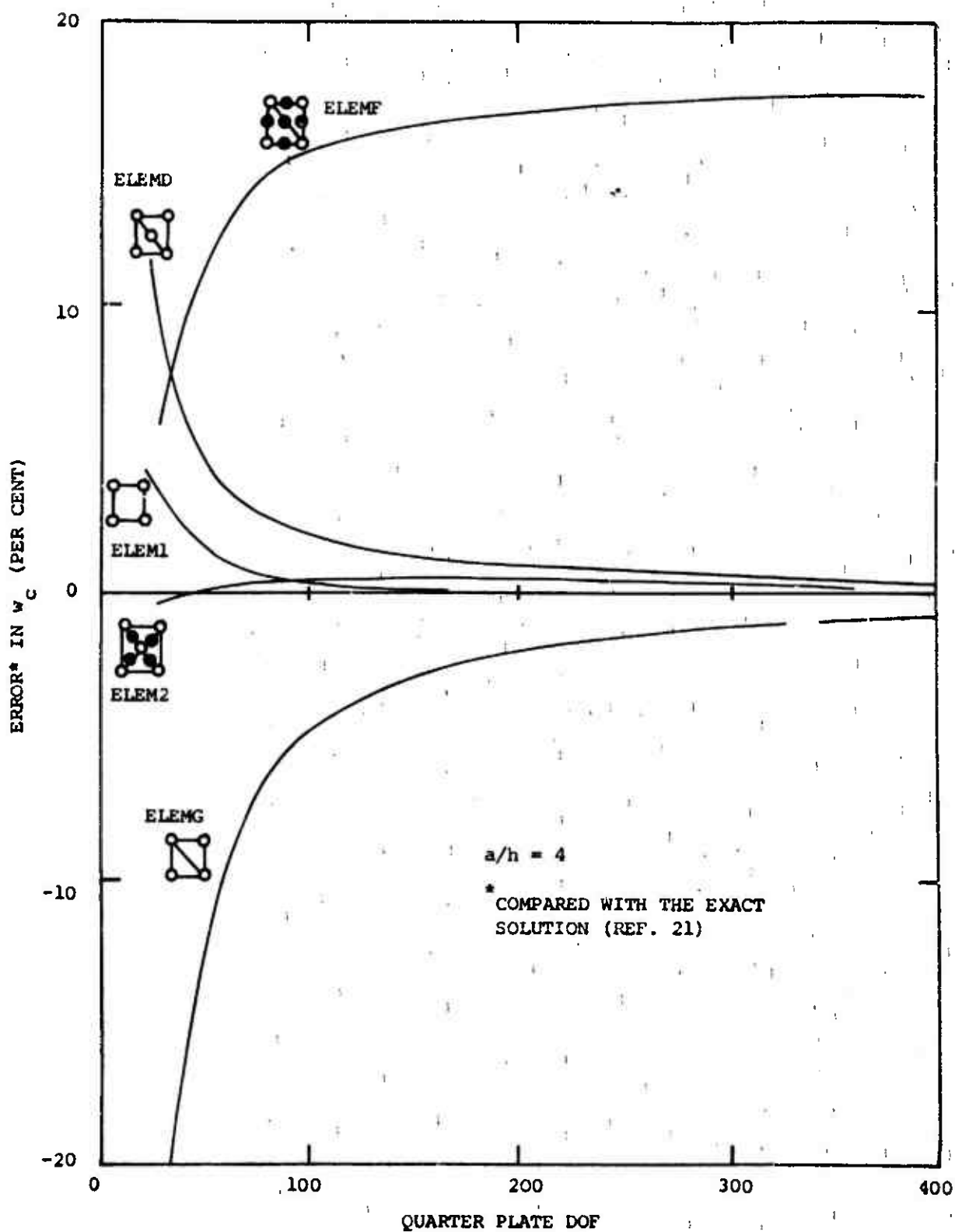


FIG. 3 CENTRAL DEFLECTION OF A SIMPLY-SUPPORTED, UNIFORMLY-LOADED, SQUARE, ISOTROPIC, THICK, SINGLE-LAYER PLATE

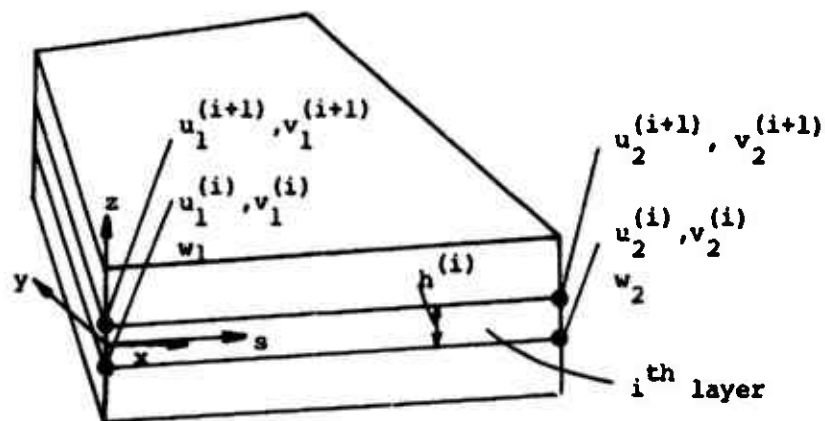


FIG. 4 A MULTILAYER ELEMENT

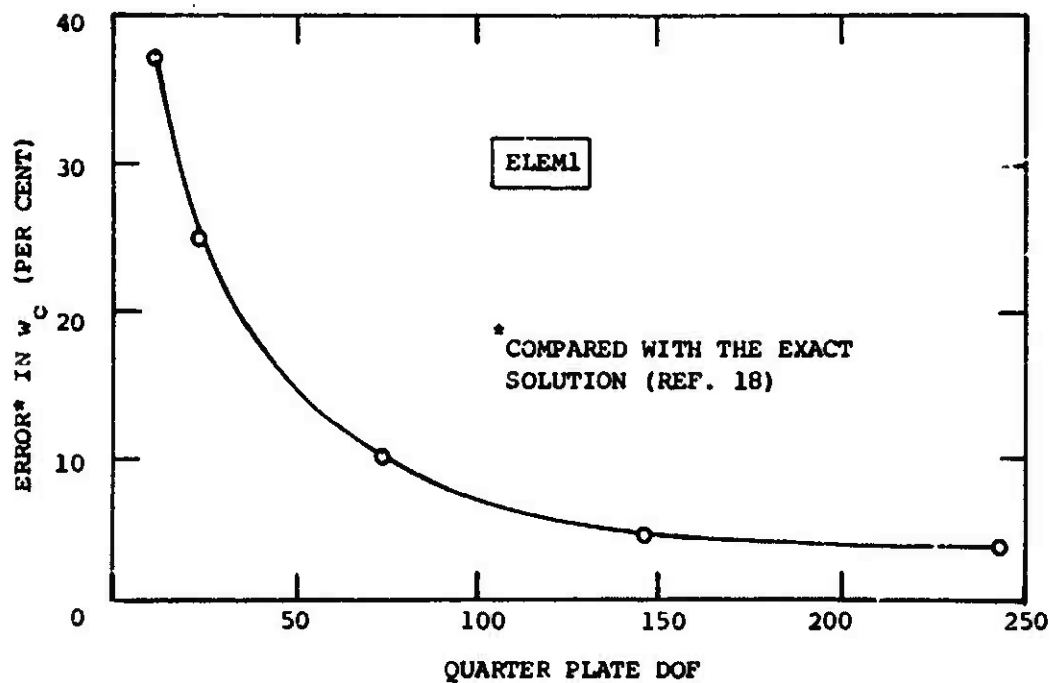


FIG. 5 CENTRAL DEFLECTION OF A CLAMPED, SQUARE, ISOTROPIC, THIN, SINGLE-LAYER PLATE UNDER CONCENTRATED CENTRAL LOAD

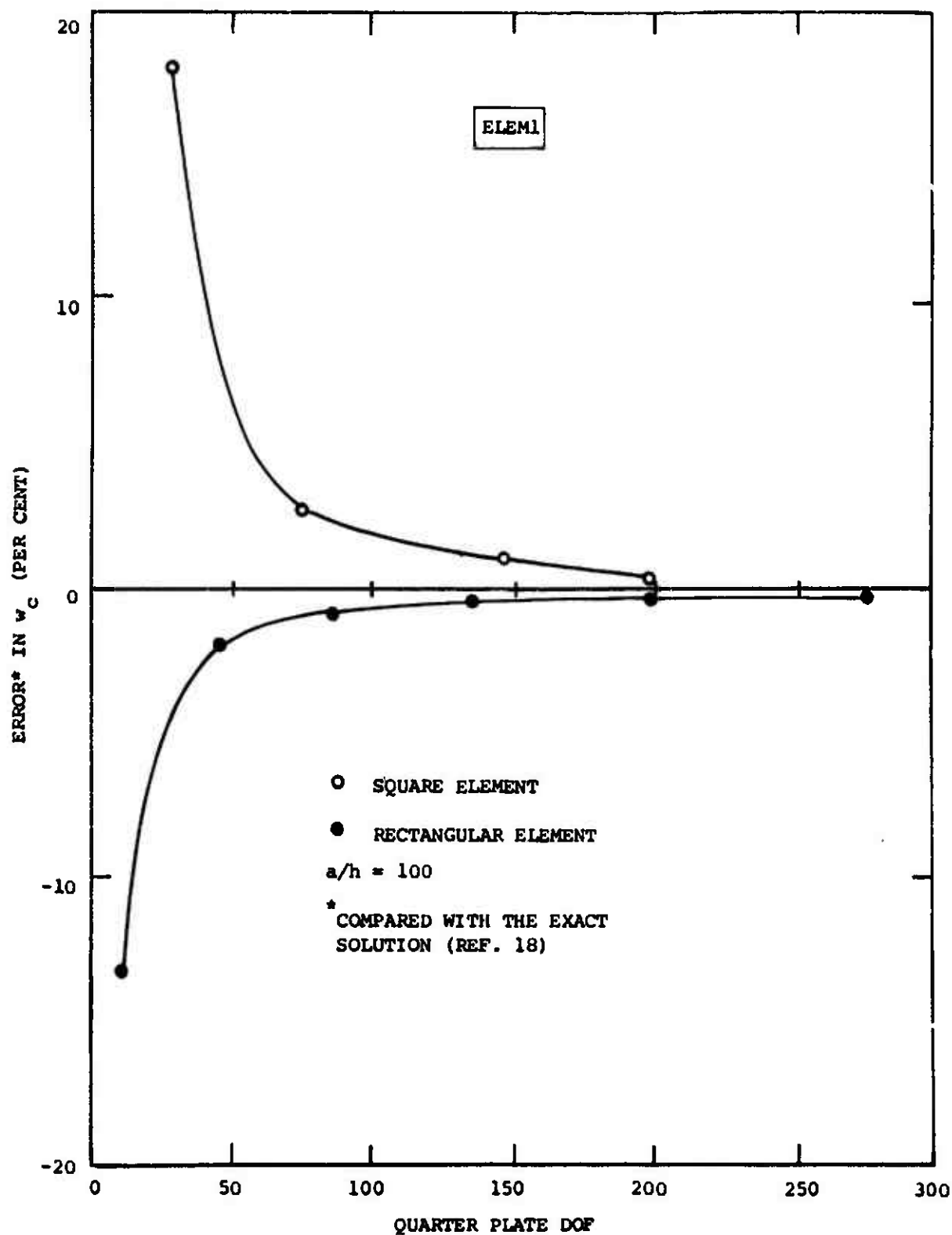


FIG. 6 CENTRAL DEFLECTION OF A CLAMPED, ISOTROPIC, RECTANGULAR, THIN, SINGLE-LAYER PLATE UNDER UNIFORM LOAD

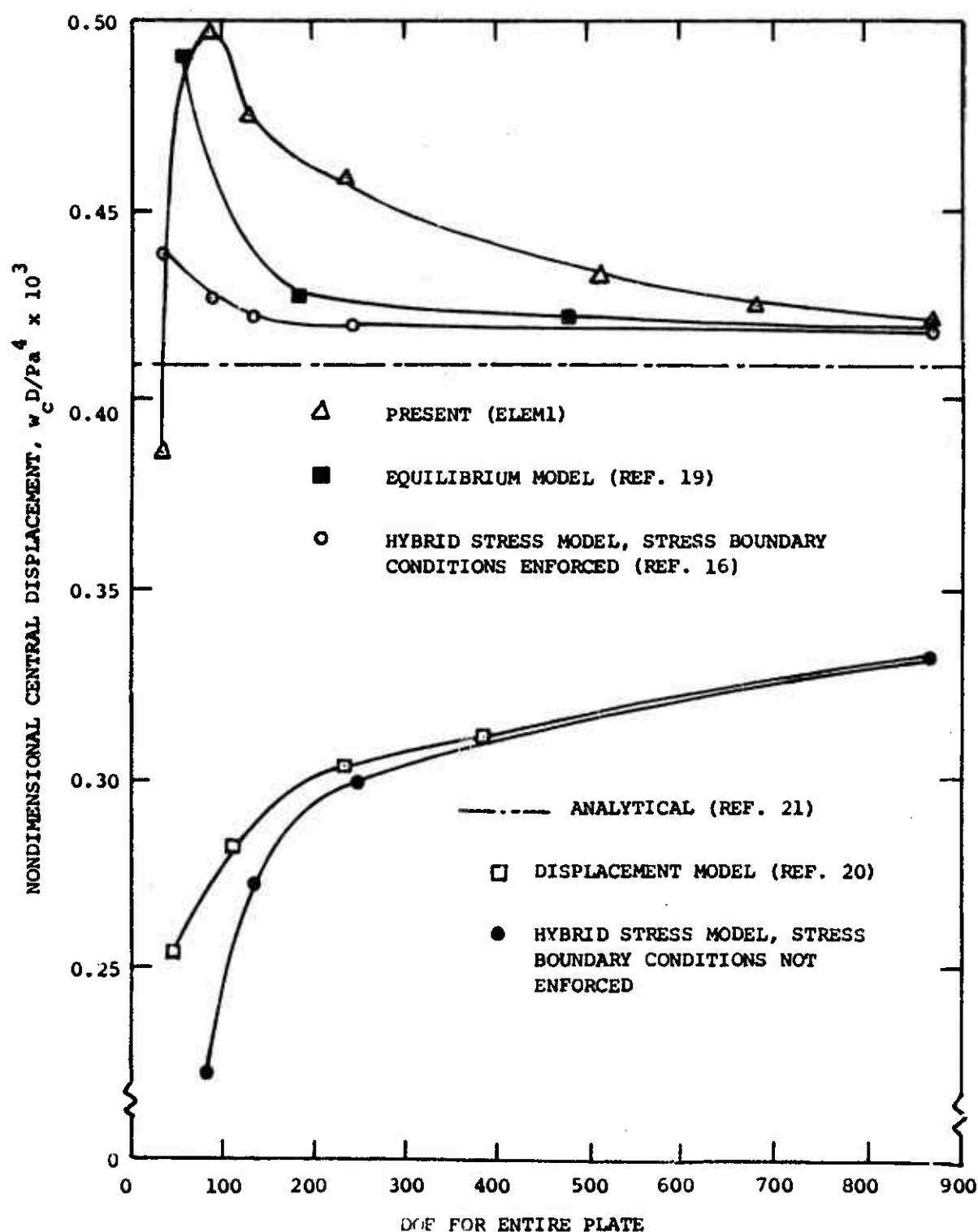


FIG. 7 CENTRAL DEFLECTION OF A SKEWED, SINGLE-LAYER, ISOTROPIC THIN PLATE UNDER UNIFORM LOAD

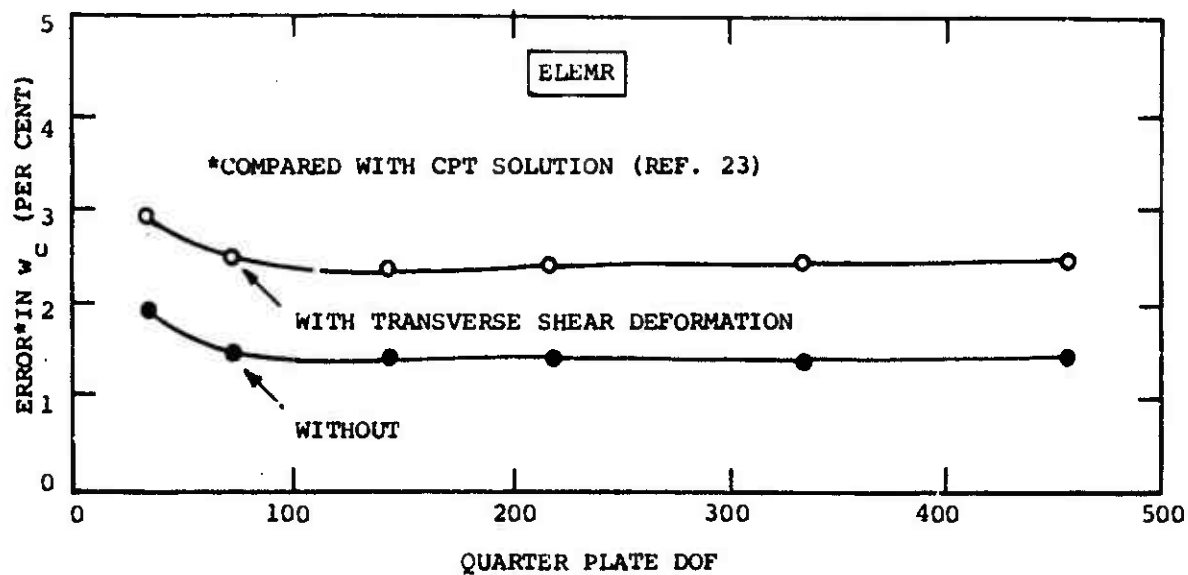


FIG. 8 CENTRAL DEFLECTION OF A CLAMPED, TWO-LAYER RECTANGULAR, CROSS-PLY PLATE UNDER UNIFORM LOAD

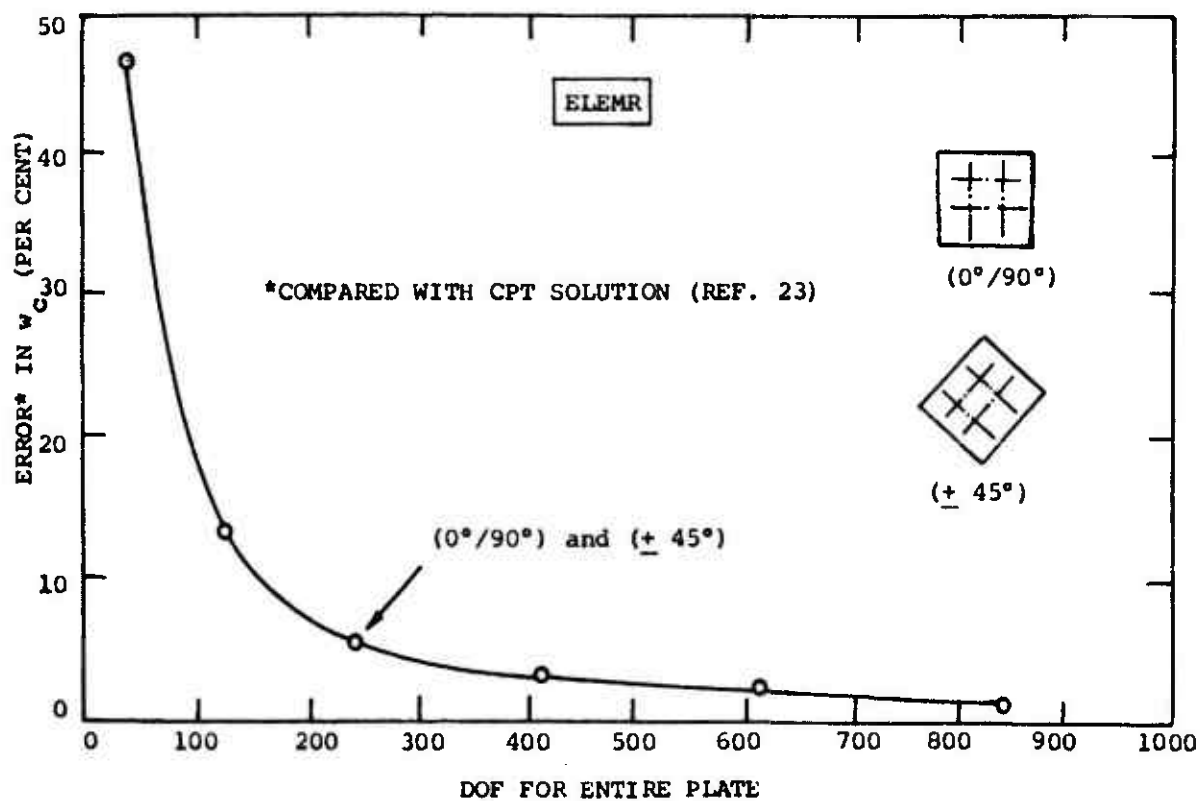


FIG. 9 CENTRAL DEFLECTION OF A CLAMPED, TWO-LAYER, SQUARE, CROSS-PLY PLATE UNDER UNIFORM LOAD

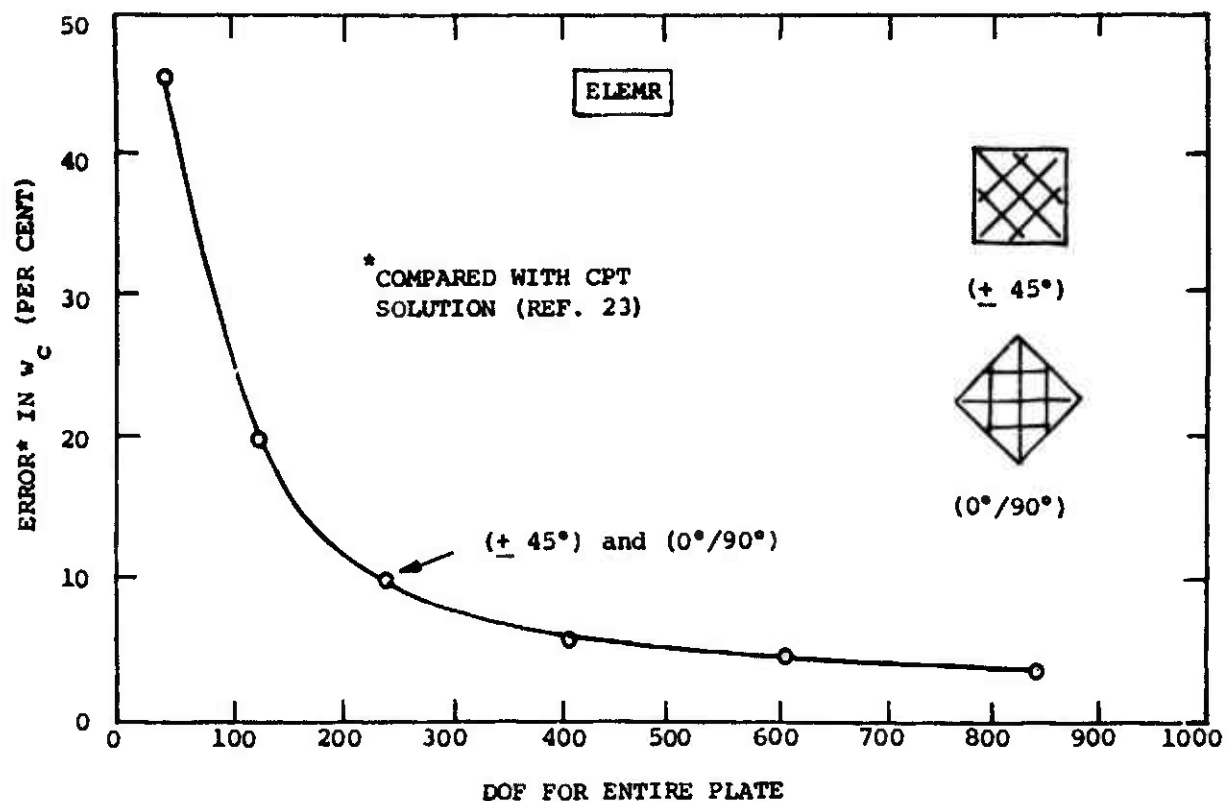


FIG. 10 CENTRAL DEFLECTION OF A CLAMPED, TWO-LAYER, SQUARE ANGLE-PLY PLATE UNDER UNIFORM LOAD

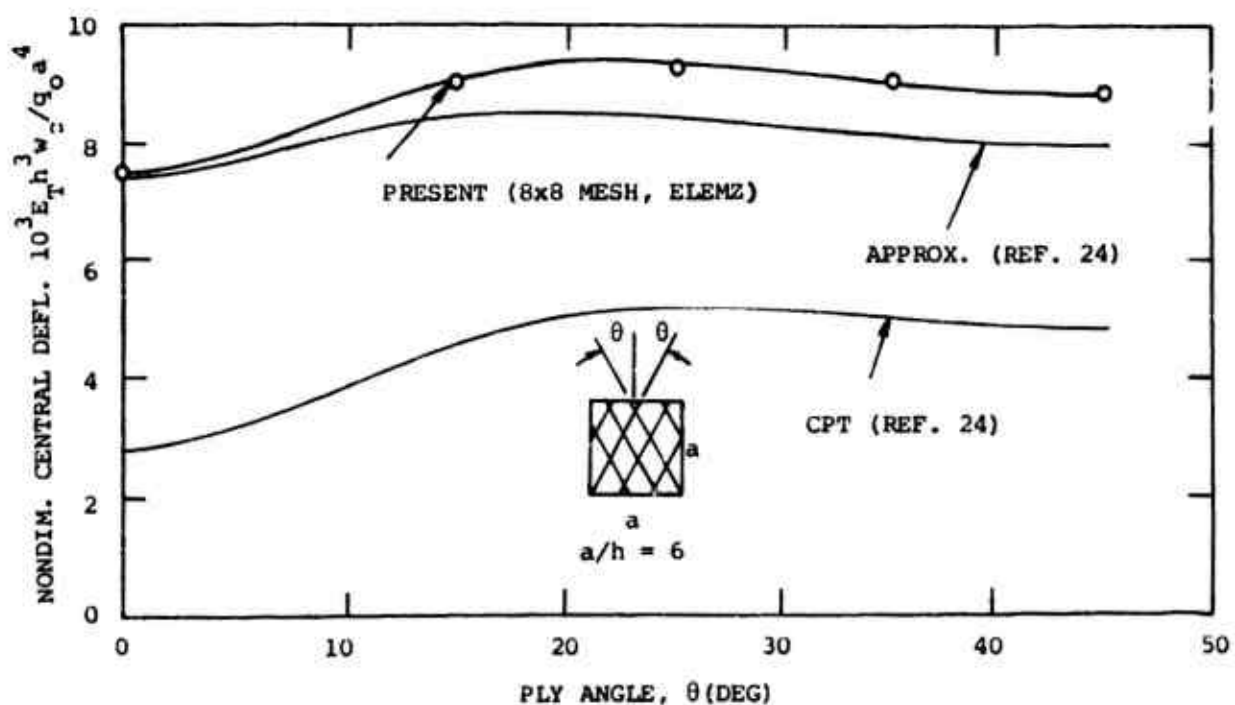
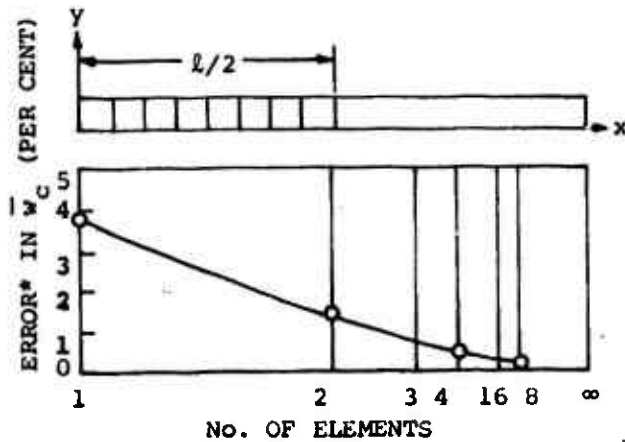


FIG. 11 CENTRAL DEFLECTION FOR SIMPLY-SUPPORTED TWO-LAYER  $(+ \theta)$  SQUARE, ANGLE-PLY PLATES

LEGEND FOR FIG.12

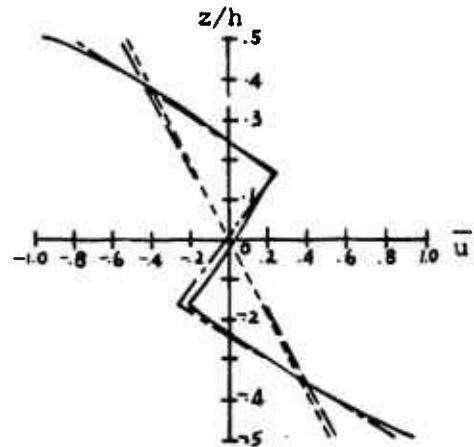
- ELASTICITY (REF. 1)
- - - PRESENT (ELEMZ)
- FINITE ELEMENT (REF.5)
- - - CPT (REF. 1)

(SEE TABLE 4a FOR DIMENSIONS AND  
NONDIM. ( ) QUANTITIES)

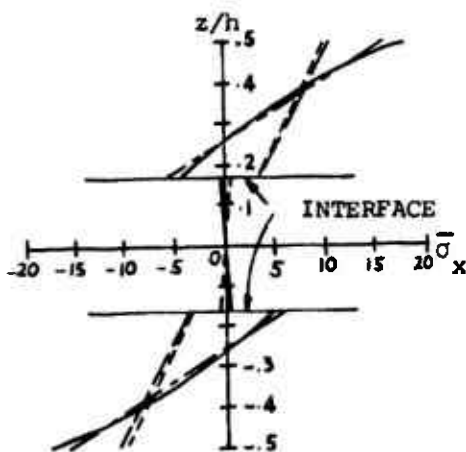


\*COMPARED WITH EXACT SOLUTIONS (REF. 1)

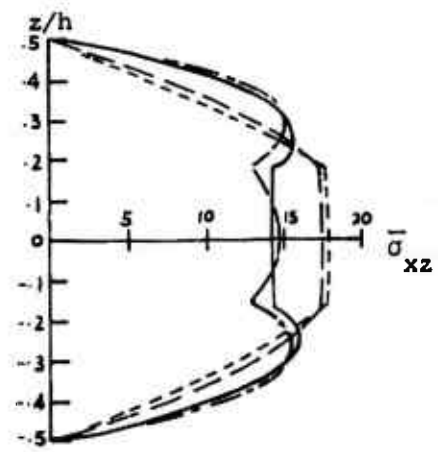
(a) Central Displacement,  $\bar{w}_c$



(b) In-plane Displacement,  $\bar{u}$



(c) Normal Stress,  $\bar{\sigma}_x$



(d) Shear Stress,  $\bar{\sigma}_{xz}$

FIG. 12 DISPLACEMENT AND STRESS SOLUTIONS FOR AN INFINITE THREE-LAYER CROSS-PLY PLATE WITH SIMPLY-SUPPORTED EDGES, SUBJECTED TO SINUSOIDAL LOADING

LEGEND FOR FIG.13

- ELASTICITY (REF. 2)  
 - - CPT (REF. 2)  
 --- PRESENT (ELEMZ)  
 ○ FINITE ELEMENT (REF. 6)  
 (See b2 of Table 4 for Dimensional and Non-Dimensional ( ) Quantities)

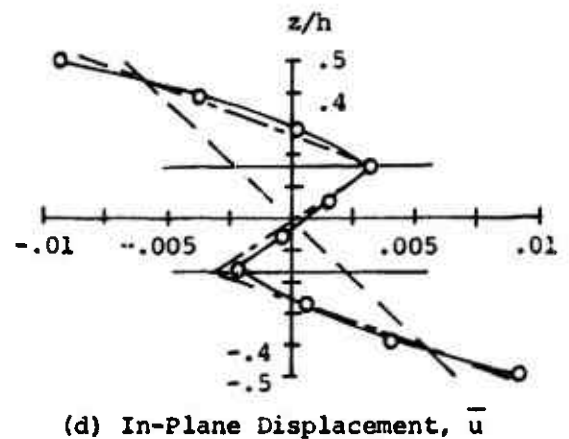
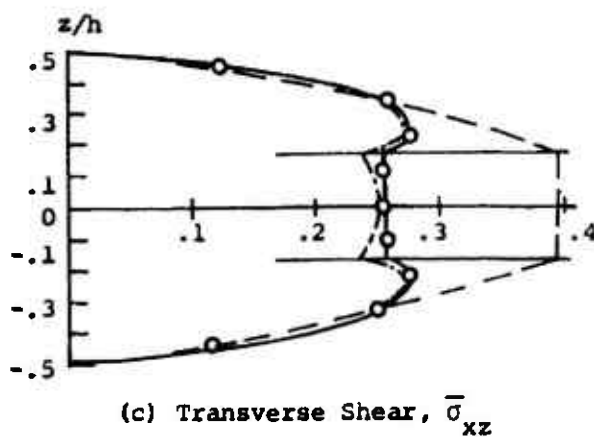
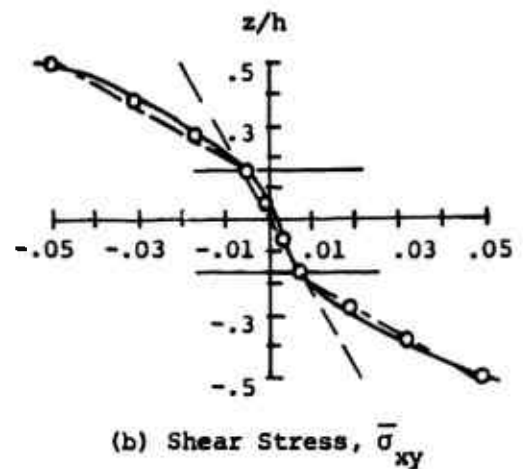
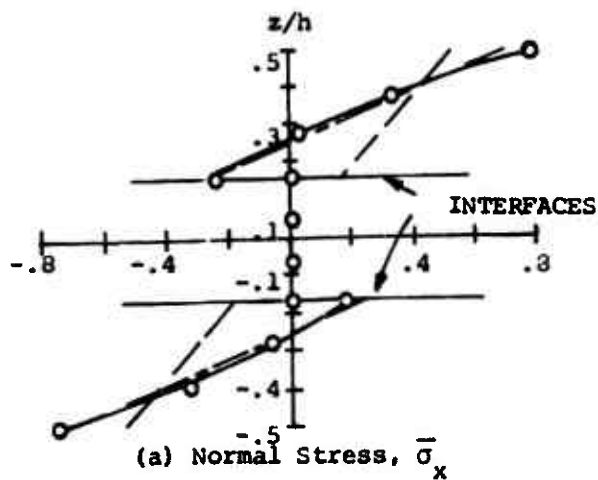


FIG. 13 DISPLACEMENT AND STRESS SOLUTIONS FOR A SIMPLY-SUPPORTED THREE-LAYER CROSS-PLY SQUARE PLATE SUBJECTED TO SINUSOIDAL LOADING

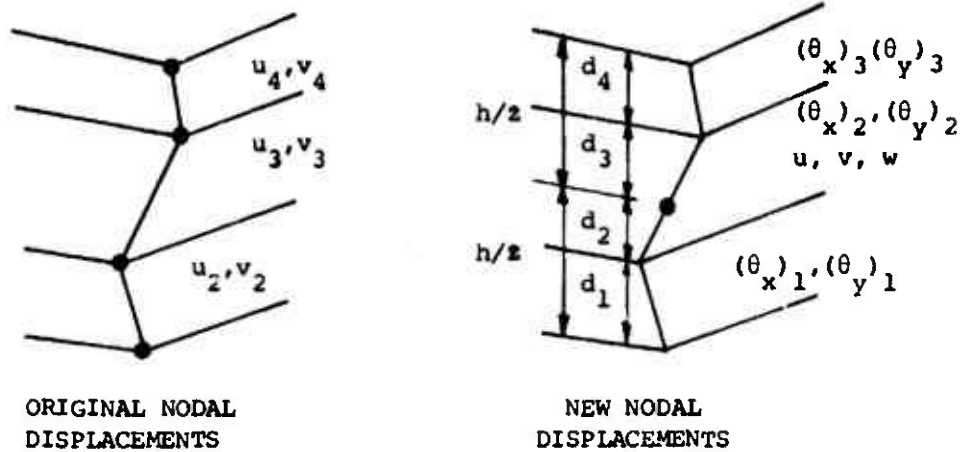


FIG. 14 COORDINATE TRANSFORMATION

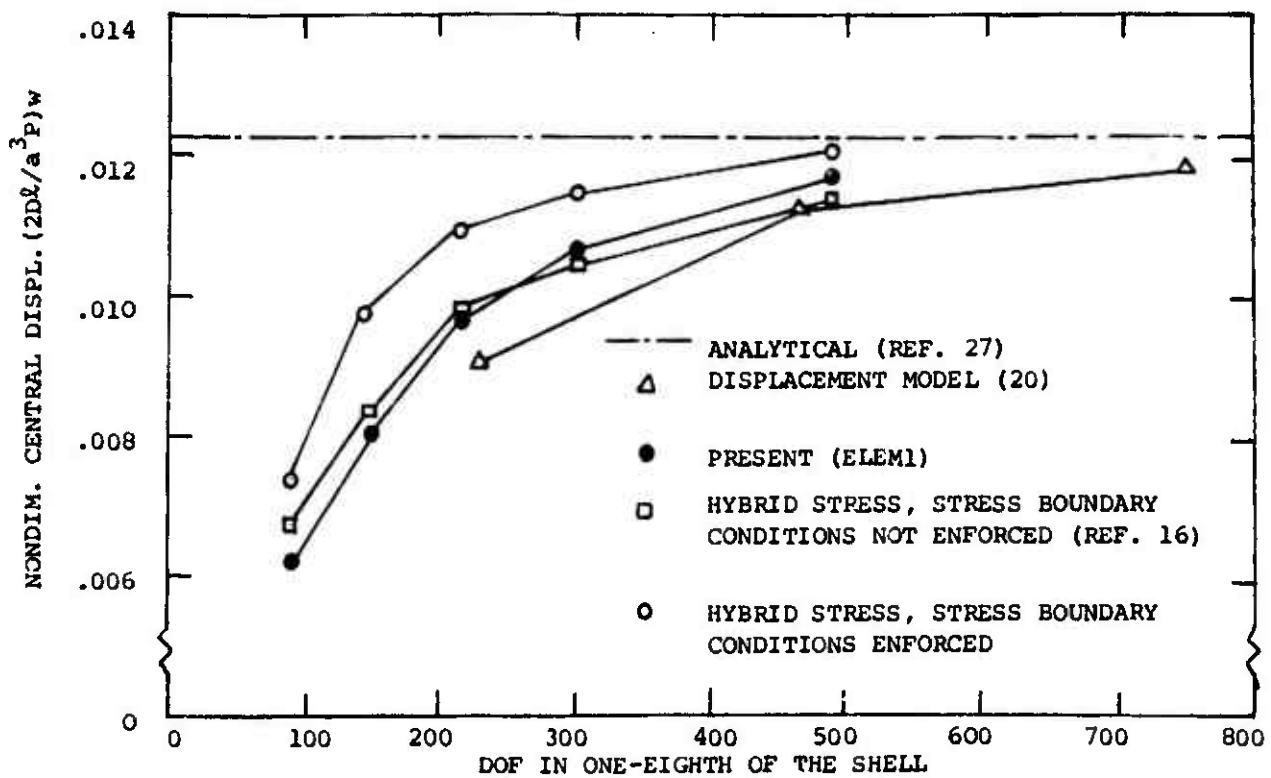


FIG. 15 CENTRAL DEFLECTION OF A SINGLE-LAYER, ISOTROPIC, PINCHED CYLINDRICAL THIN SHELL

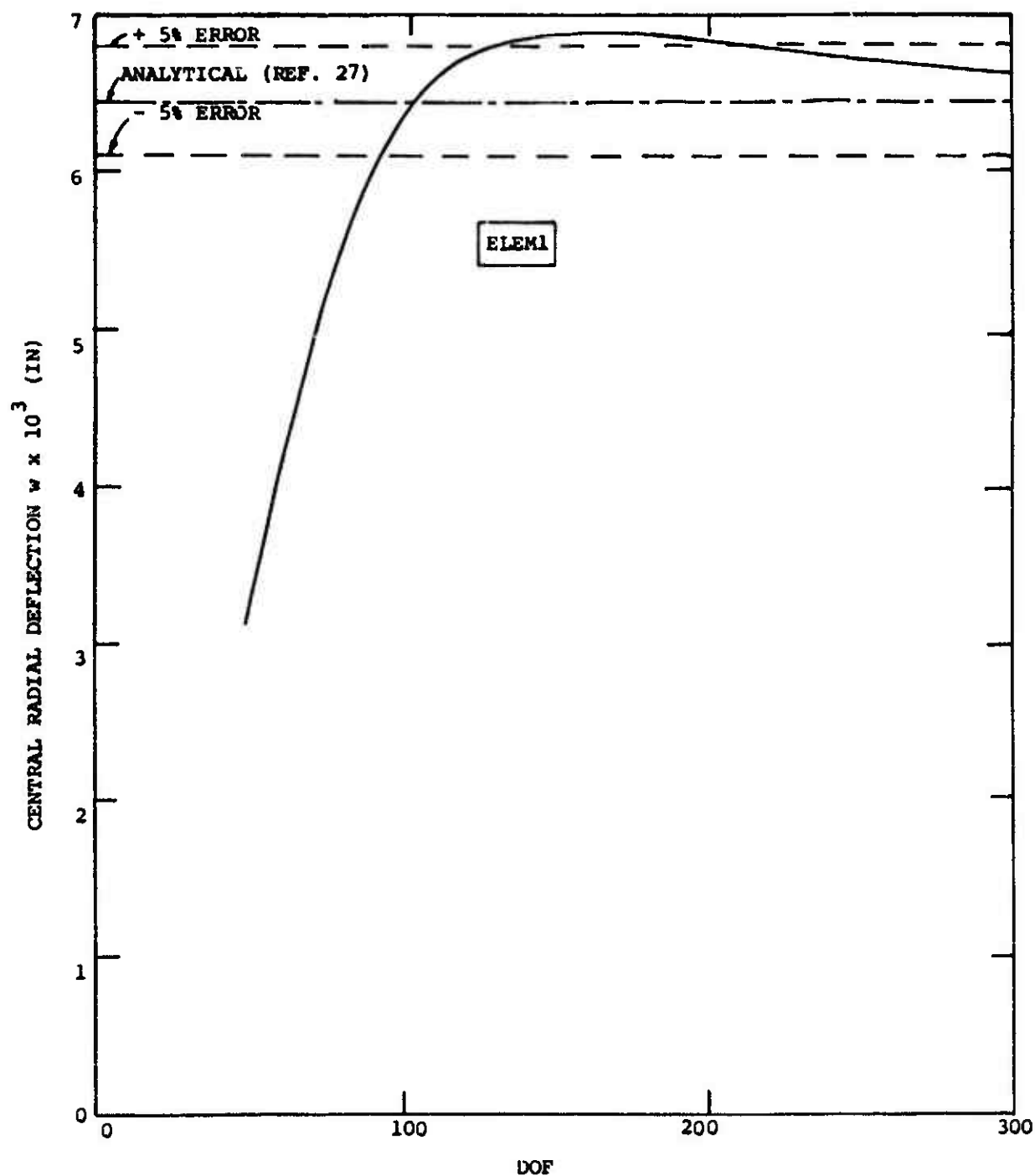


FIG. 16 PREDICTED CENTRAL RADIAL DEFLECTION OF A THIN, SINGLE-LAYER, ISOTROPIC CYLINDRICAL SHELL UNDER RING LOAD

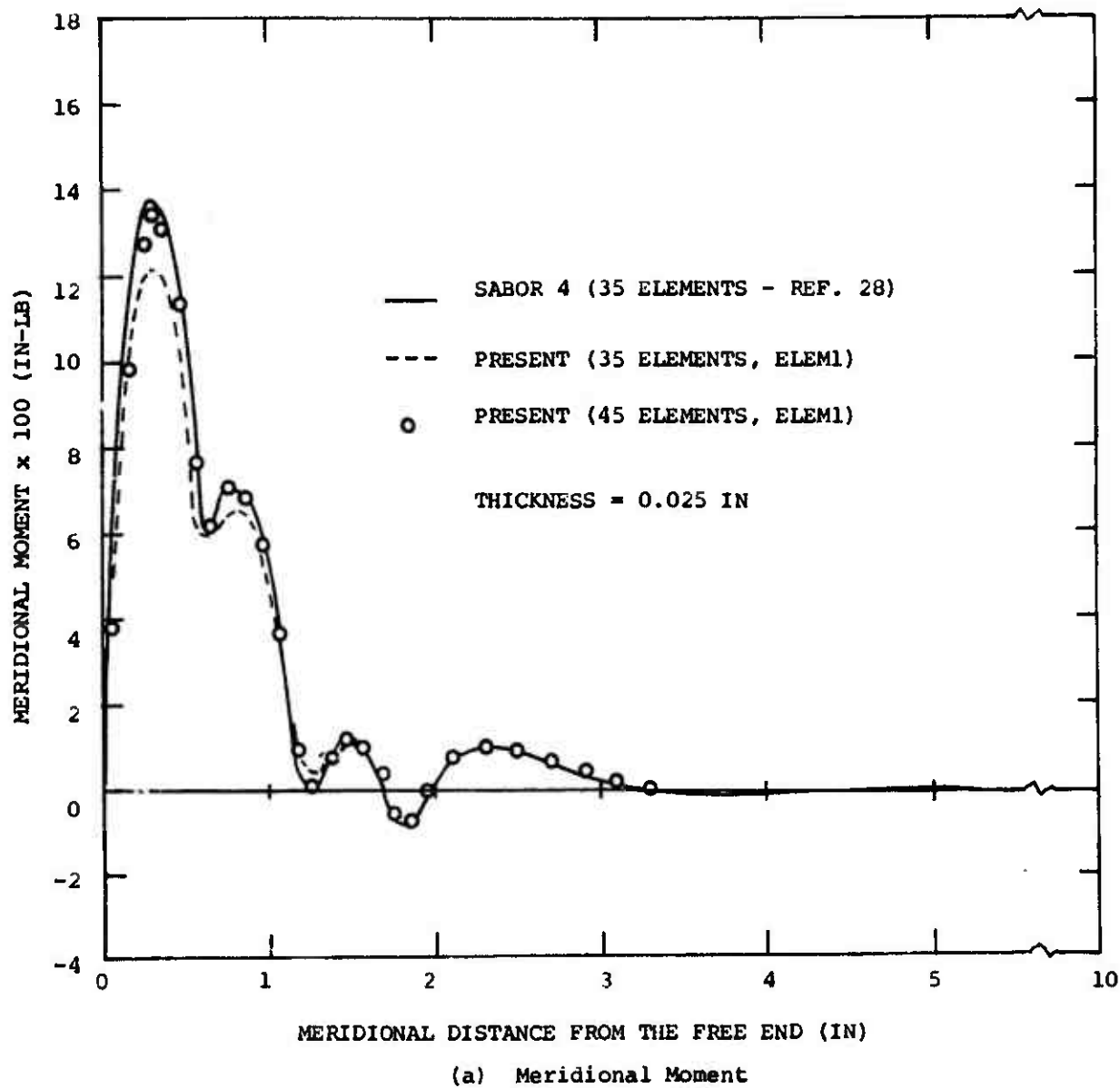
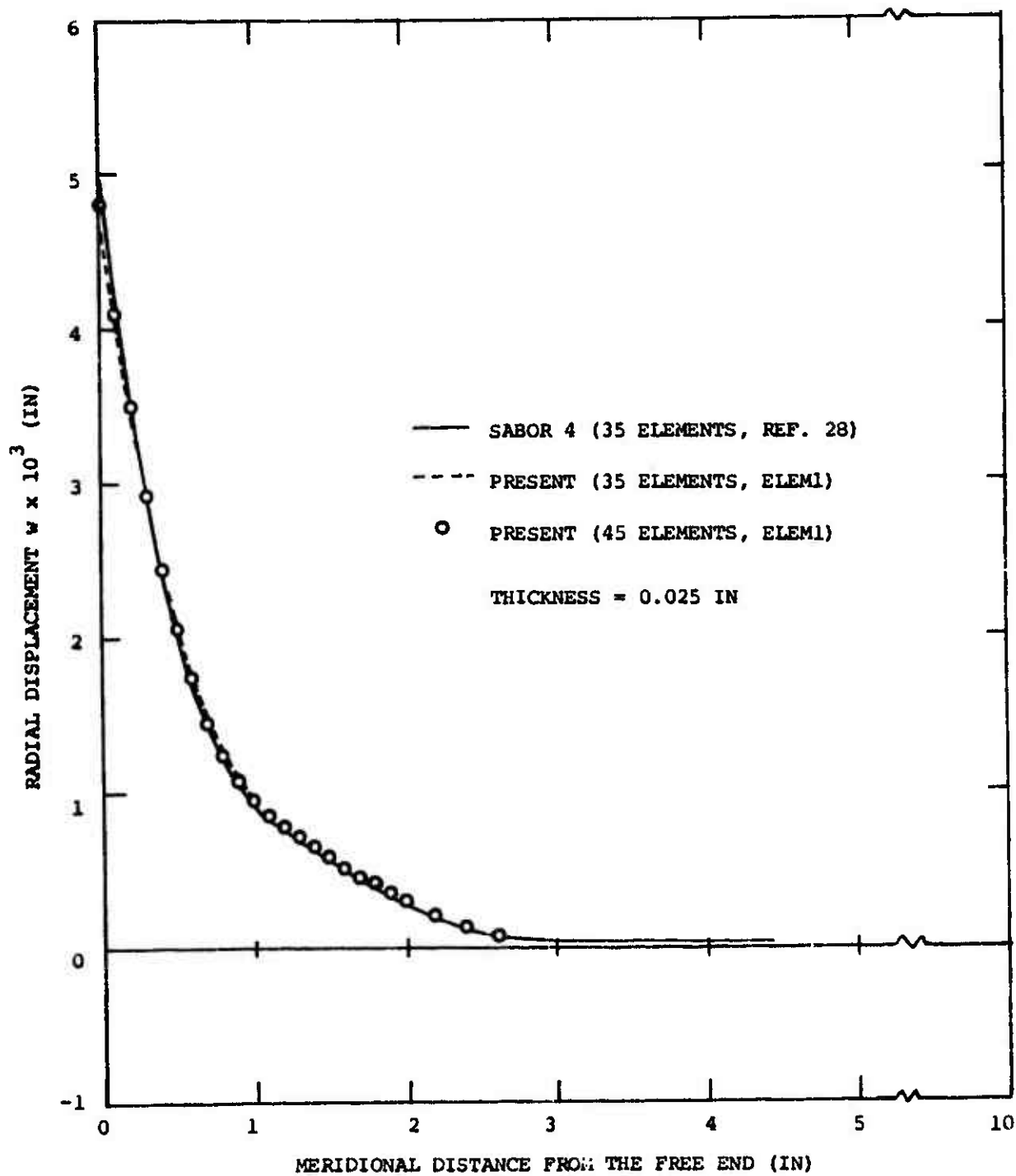
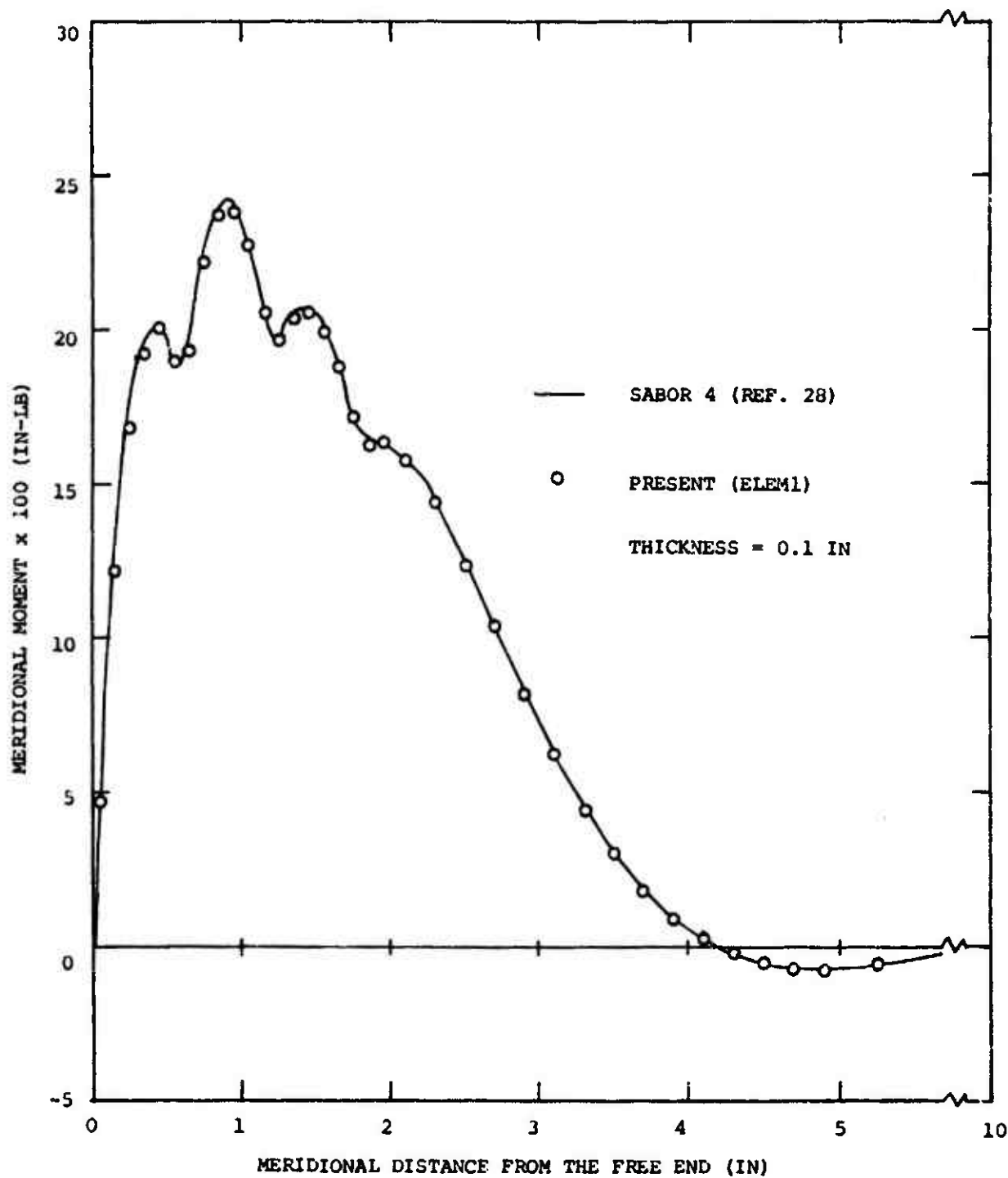


FIG. 17 MERIDIONAL MOMENT AND RADIAL DEFLECTIONS OF A THIN,  
 SINGLE-LAYER, ISOTROPIC, CONICAL SHELL UNDER RING  
 LOADS



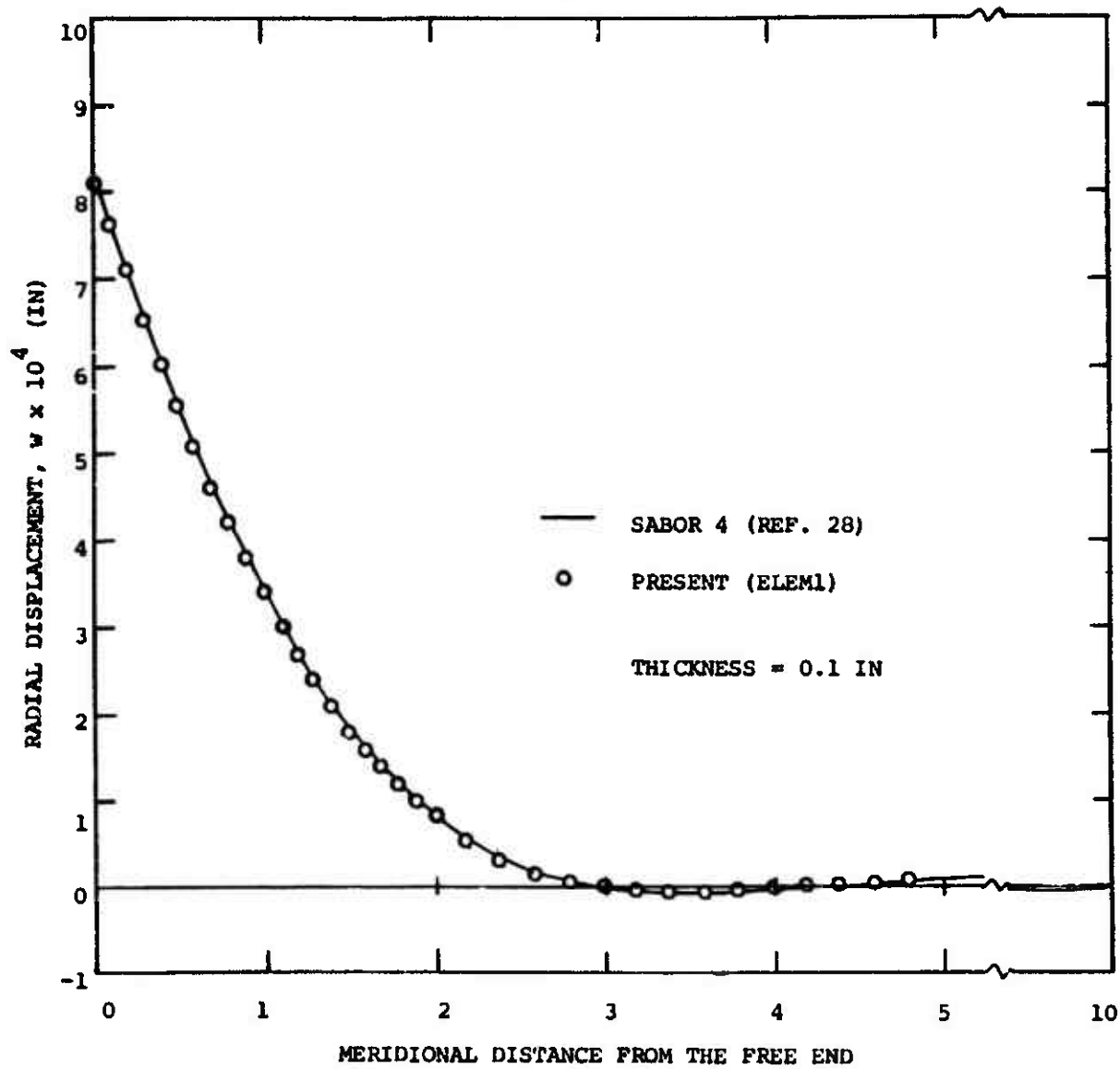
(b) Radial Displacement  $w$

FIG. 17 CONCLUDED



(a) Meridional Moment

FIG. 18 MERIDIONAL MOMENT AND RADIAL DISPLACEMENT OF A THIN, ISOTROPIC, SINGLE-LAYER, CONICAL SHELL UNDER RING LOADS



(b) Radial Displacement,  $w$

FIG. 18 CONCLUDED

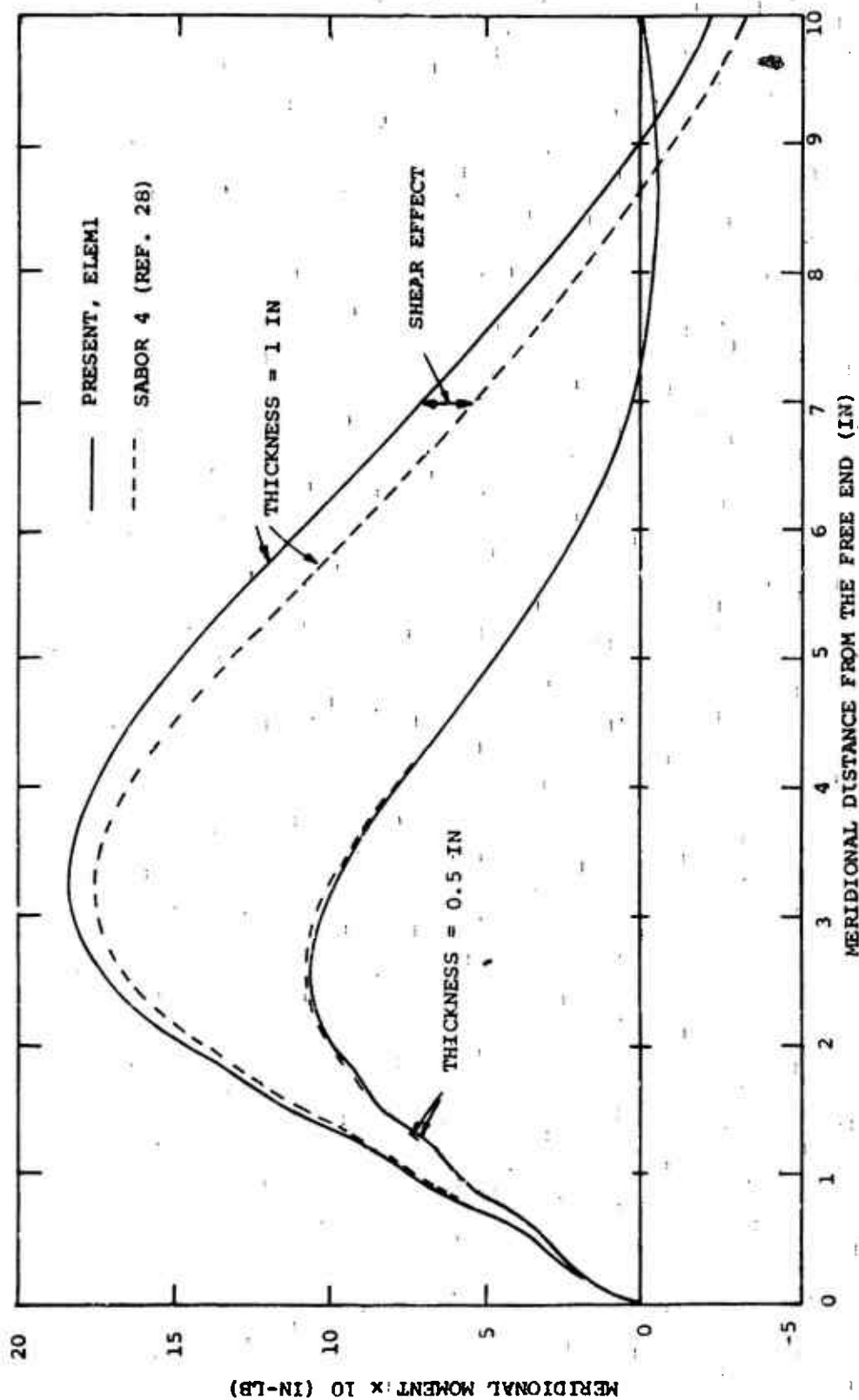


FIG. 19 MERIDIONAL MOMENT OF TWO MODERATELY THICK, SINGLE-LAYER, ISOTROPIC, CONICAL SHELLS UNDER RING LOADS

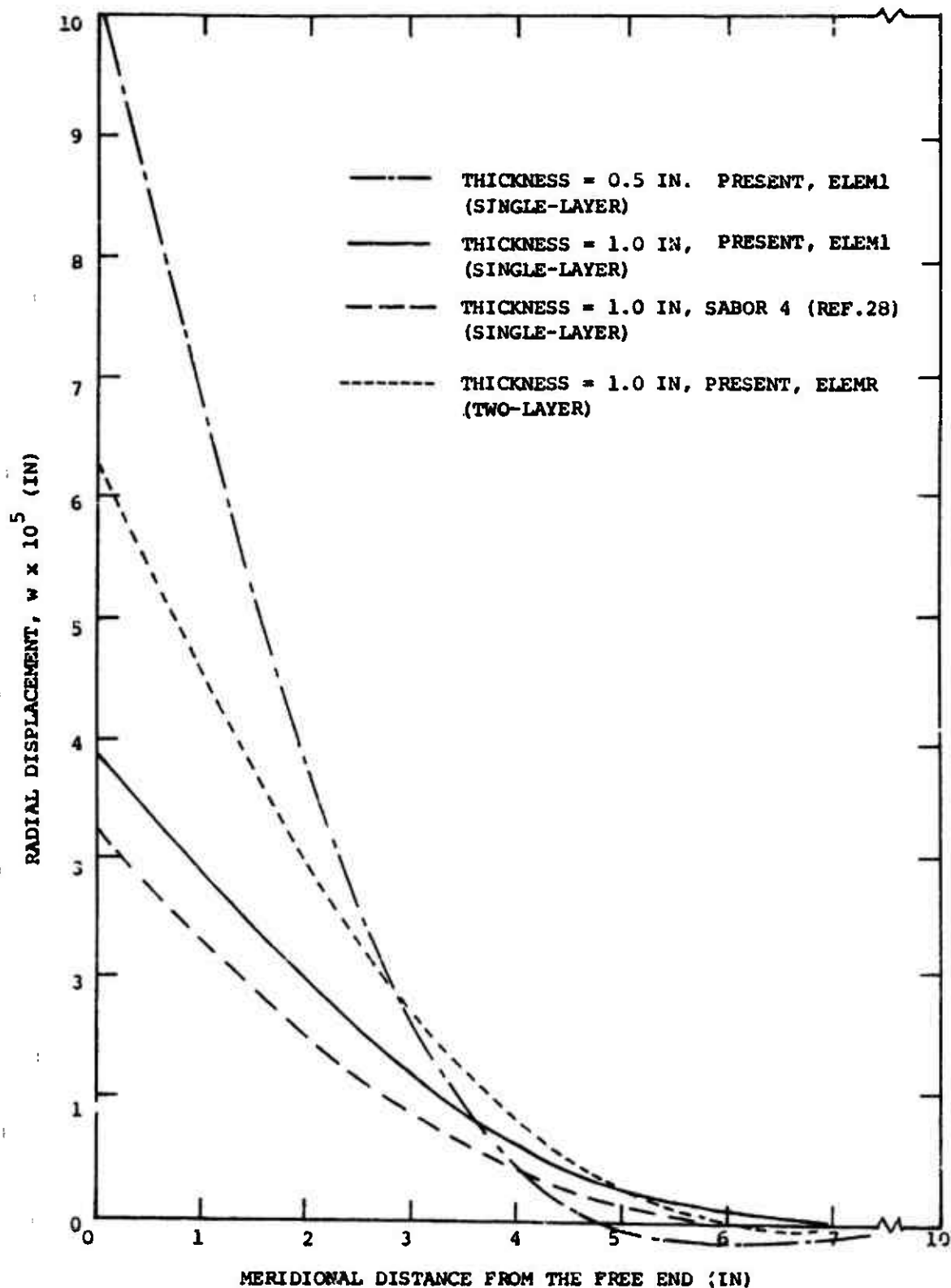


FIG. 20 RADIAL DISPLACEMENTS OF TWO SINGLE-LAYER AND ONE TWO-LAYER, CONICAL SHELLS UNDER RING LOADS

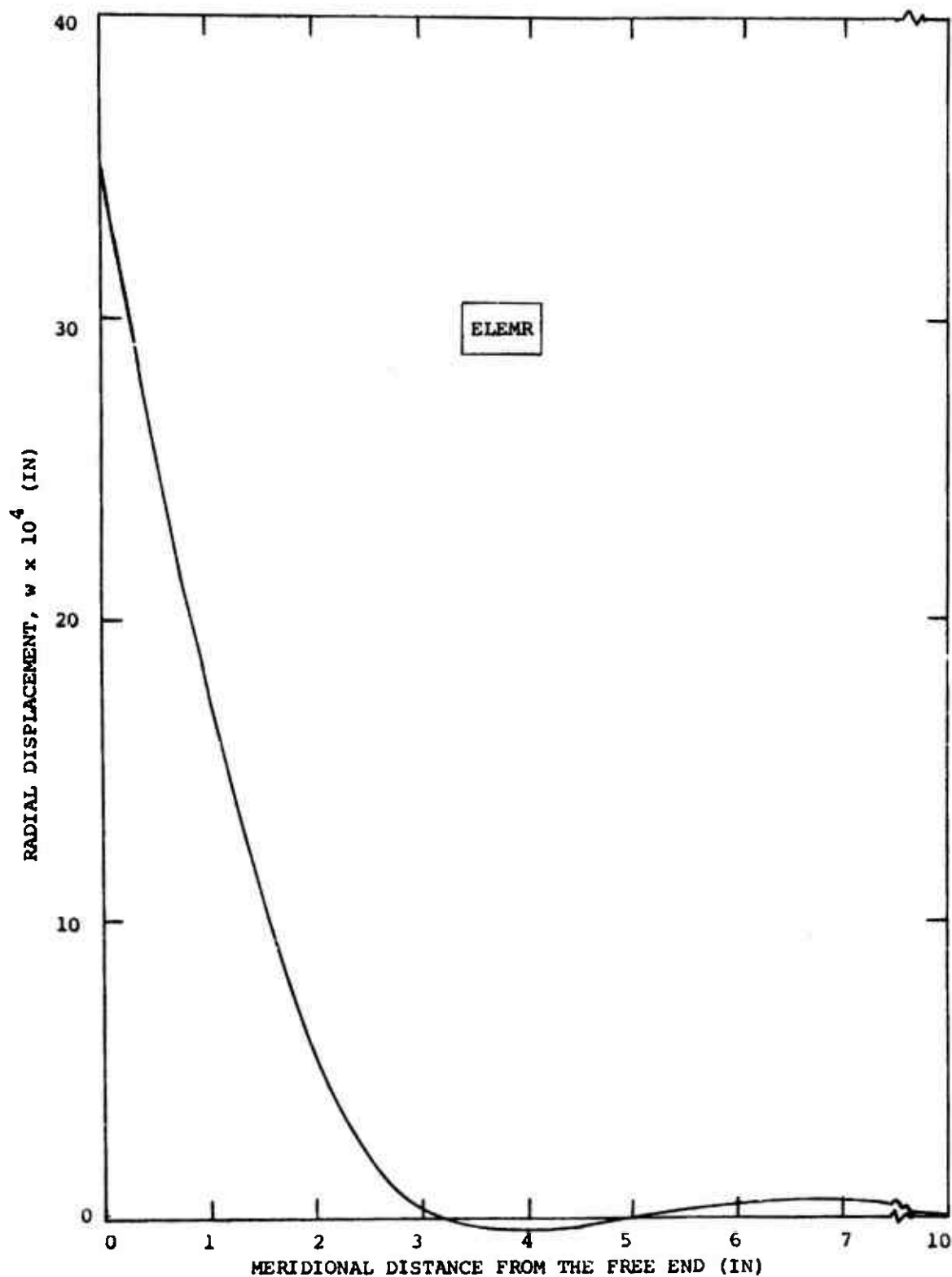
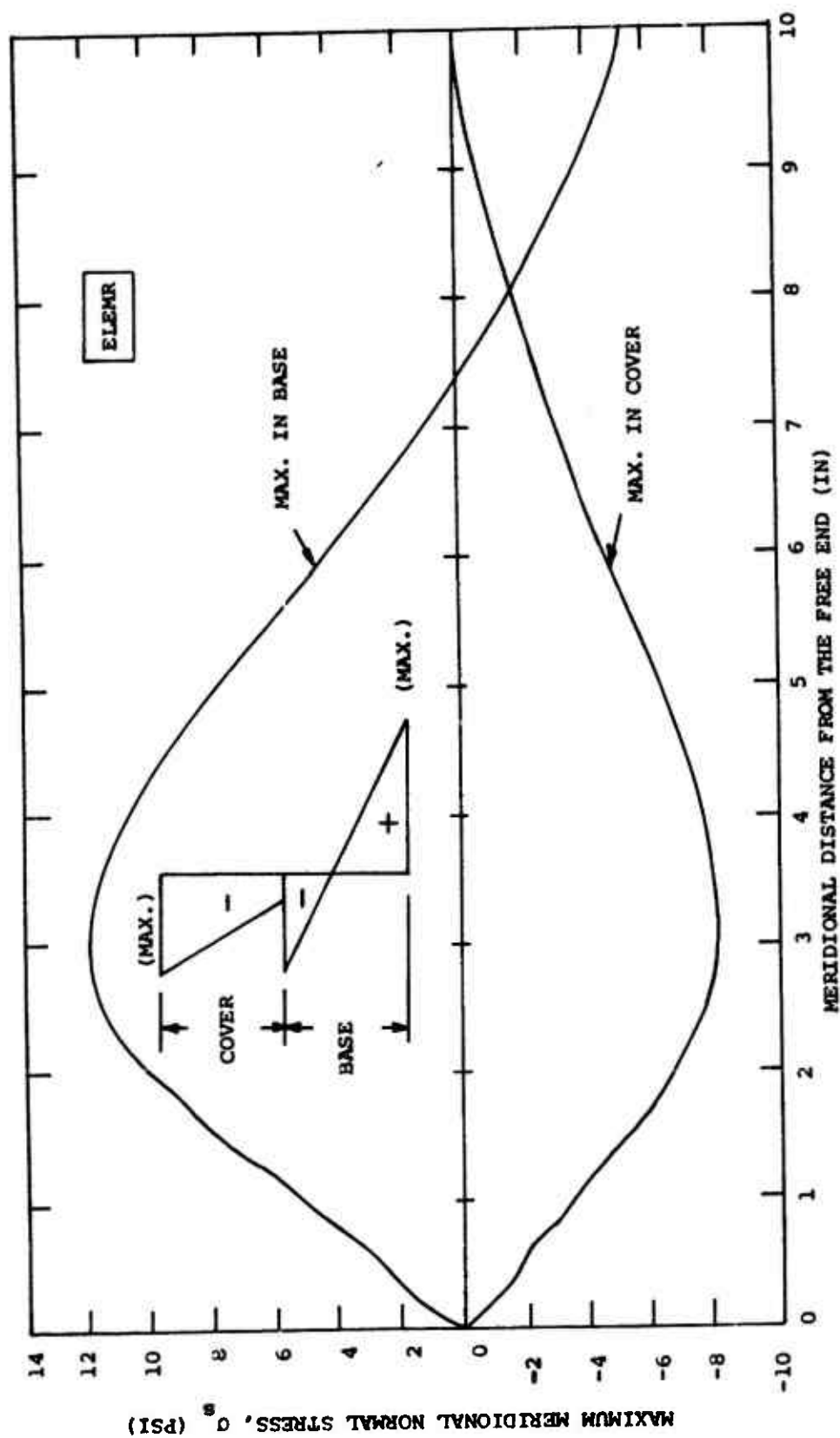
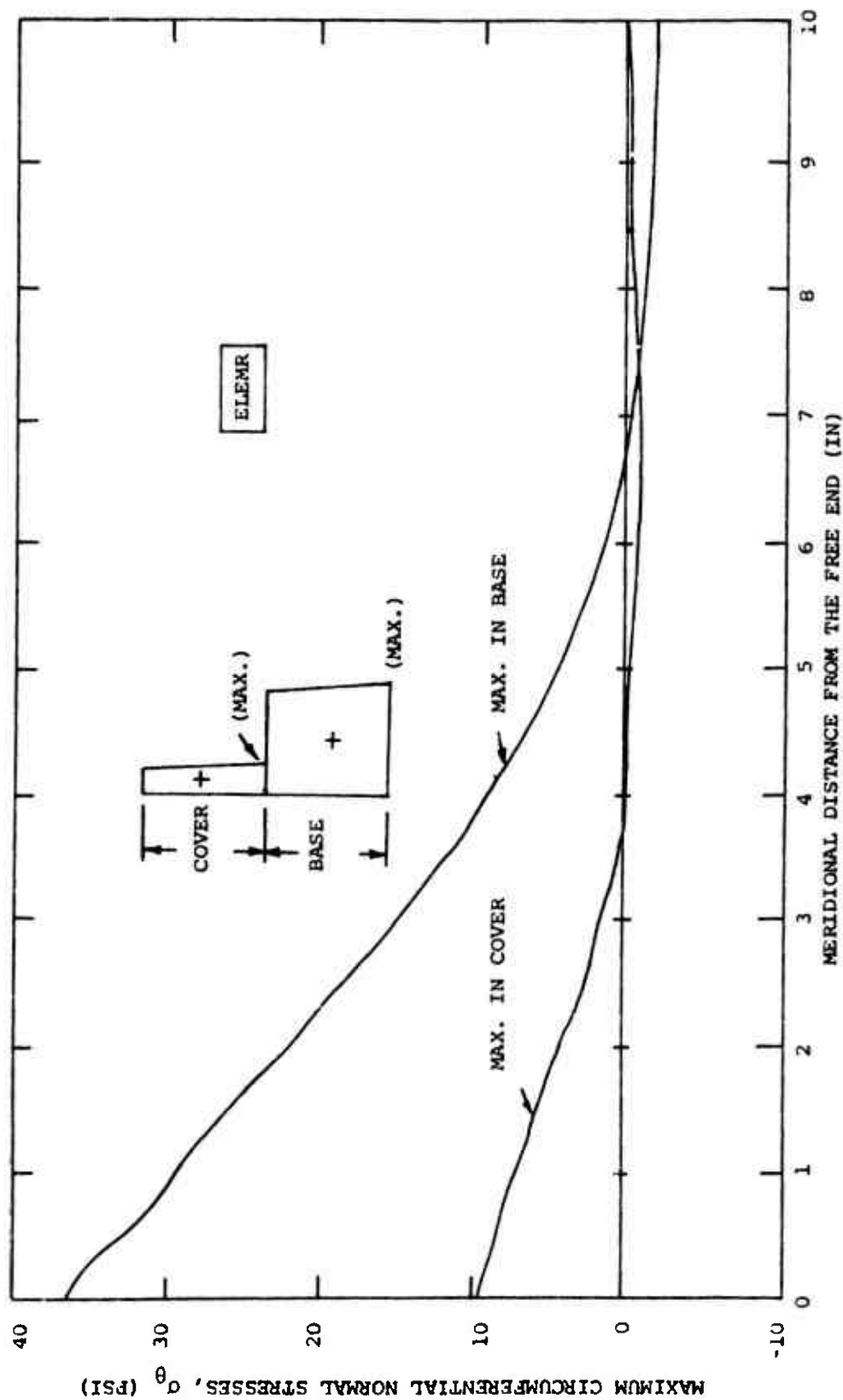


FIG. 21 RADIAL DISPLACEMENT OF A SANDWICH CONICAL SHELL UNDER RING LOADS



(a) Maximum Meridional Normal Stresses in the Cover and in the Base  
 FIG. 22 MAXIMUM MERIDIONAL AND CIRCUMFERENTIAL NORMAL STRESSES IN THE COVER AND  
 IN THE BASE OF A TWO-LAYER CONICAL SHELL UNDER RING LOADS



(b) Maximum Circumferential Normal Stresses in the Cover and in the Base

FIG. 22 CONCLUDED

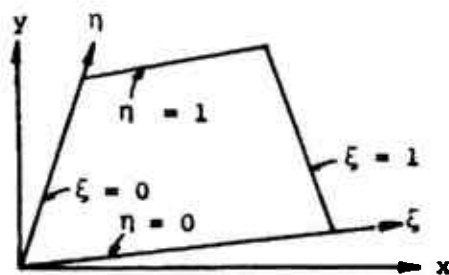


FIG. 23 COORDINATE TRANSFORMATION FOR A QUADRILATERAL ELEMENT

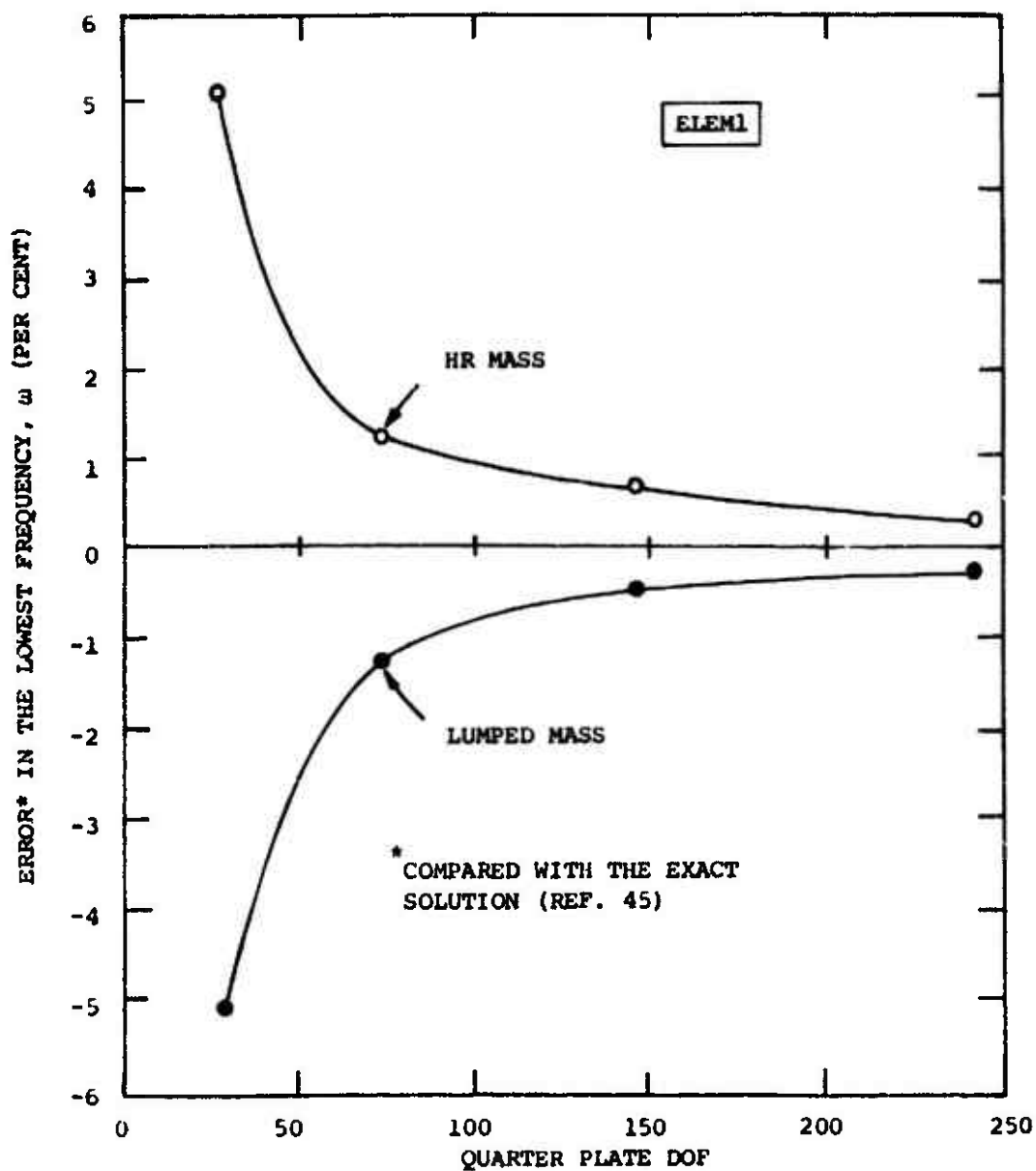


FIG. 24 THE LOWEST FREQUENCY OF A SIMPLY-SUPPORTED, SINGLE-LAYER, THIN, ISOTROPIC, SQUARE PLATE

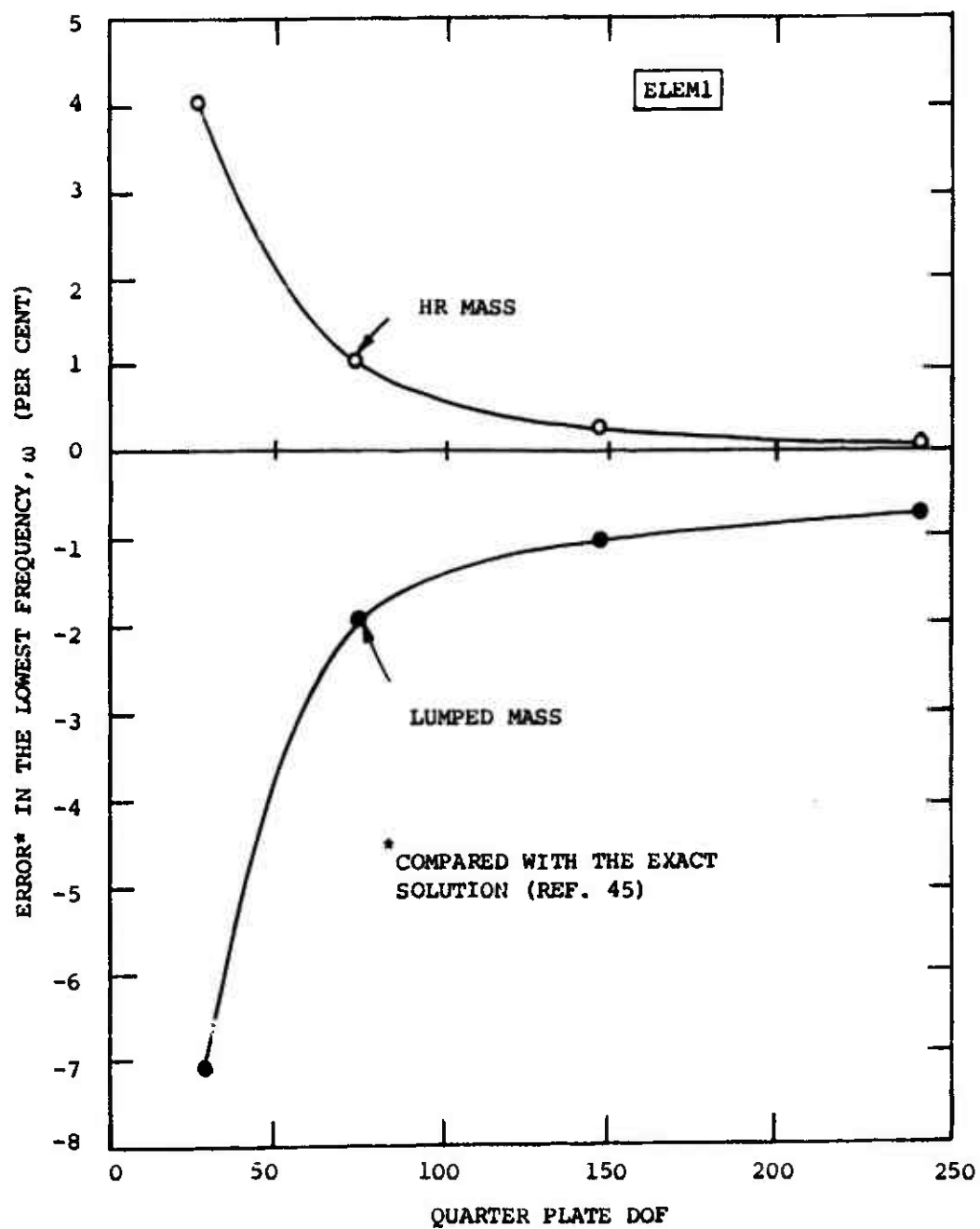


FIG. 25 THE LOWEST FREQUENCY OF A CLAMPED, SINGLE-LAYER, ISOTROPIC, THIN, RECTANGULAR PLATE

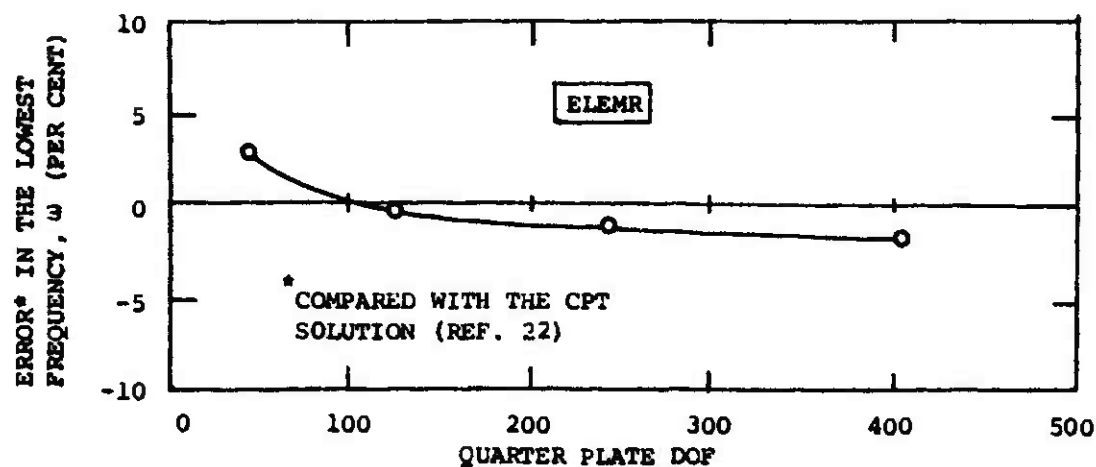


FIG. 26 THE LOWEST FREQUENCY OF A CLAMPED, TWO-LAYER, CROSS-PLY THIN, SQUARE PLATE

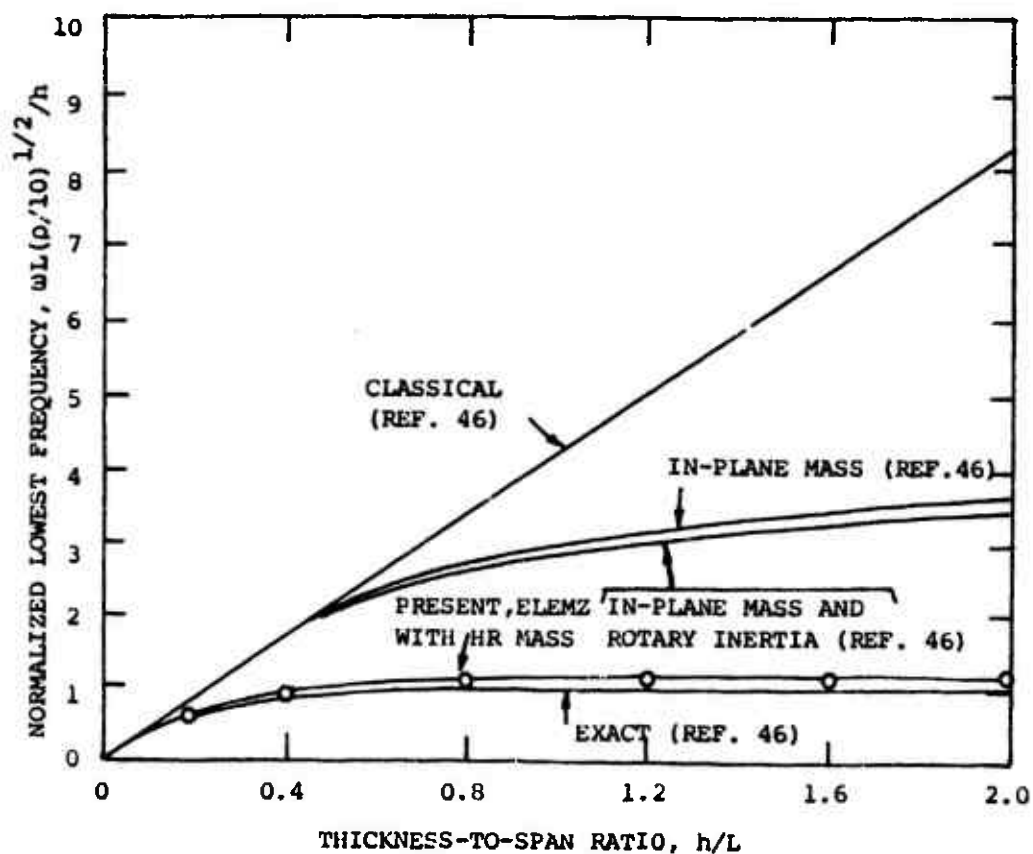
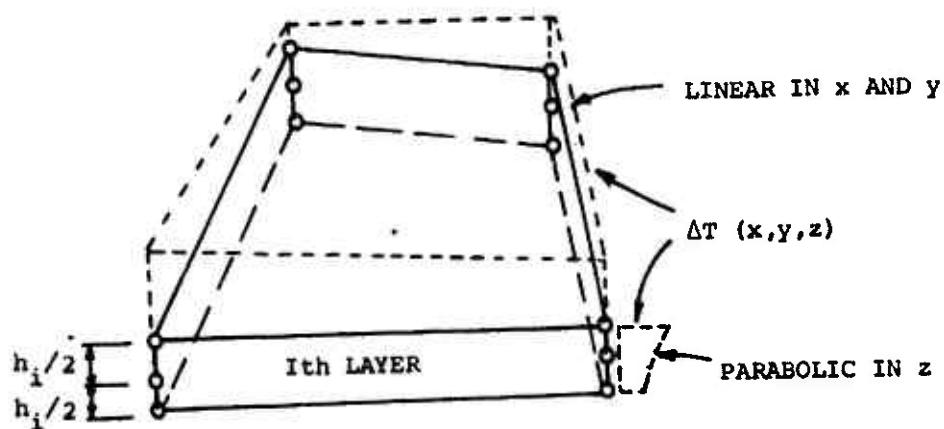
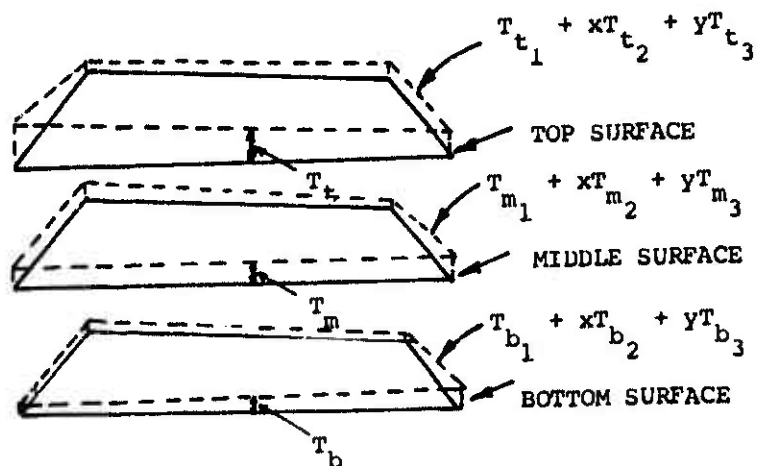


FIG. 27 THE LOWEST FREQUENCIES OF INFINITE TWO-LAYER, CROSS-PLY PLATES WITH SIMPLY-SUPPORTED EDGES



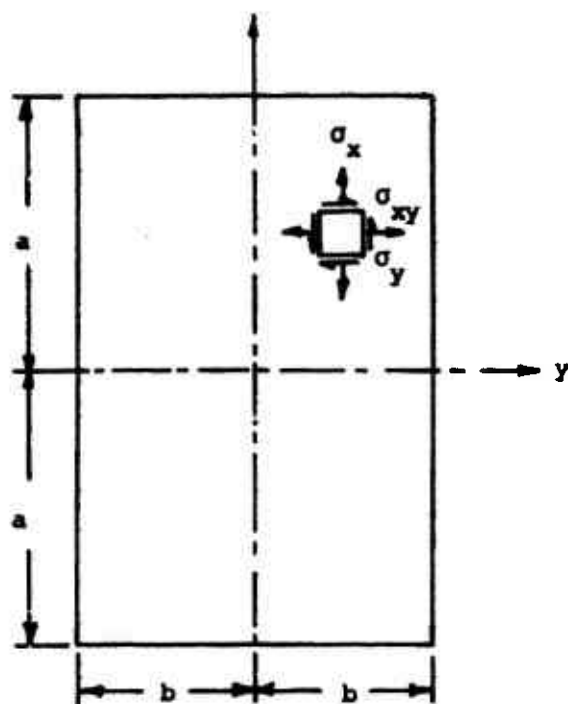
(a) Corner Points and Temperature Assumptions



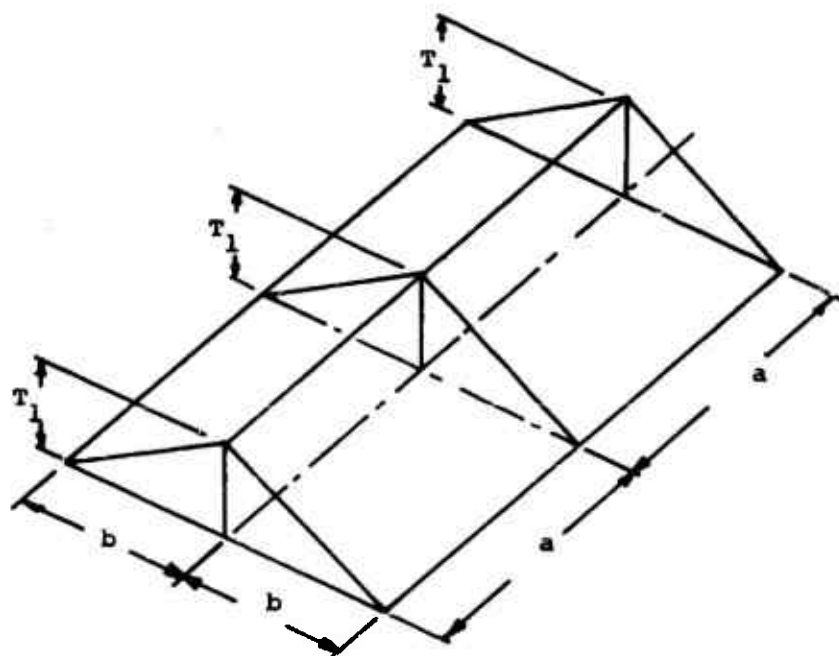
(b) Temperature Assumptions on Three Surfaces

FIG. 28 TEMPERATURE ASSUMPTIONS FOR ONE LAYER OF A MULTILAYER QUADRILATERAL ELEMENT

$a = 18 \text{ IN}$   
 $b = 12 \text{ IN}$



(a) Dimensions and Coordinate System



(b) Temperature Distribution

FIG. 29 DIMENSION, COORDINATE SYSTEM, AND TEMPERATURE DISTRIBUTION OF A FREE, SINGLE-LAYER, THIN, ISOTROPIC RECTANGULAR PLATE

— ORIGINAL SHAPE  
 - - - DEFORMED SHAPE  
 0.01 IN. SCALE FOR DISPLACEMENT

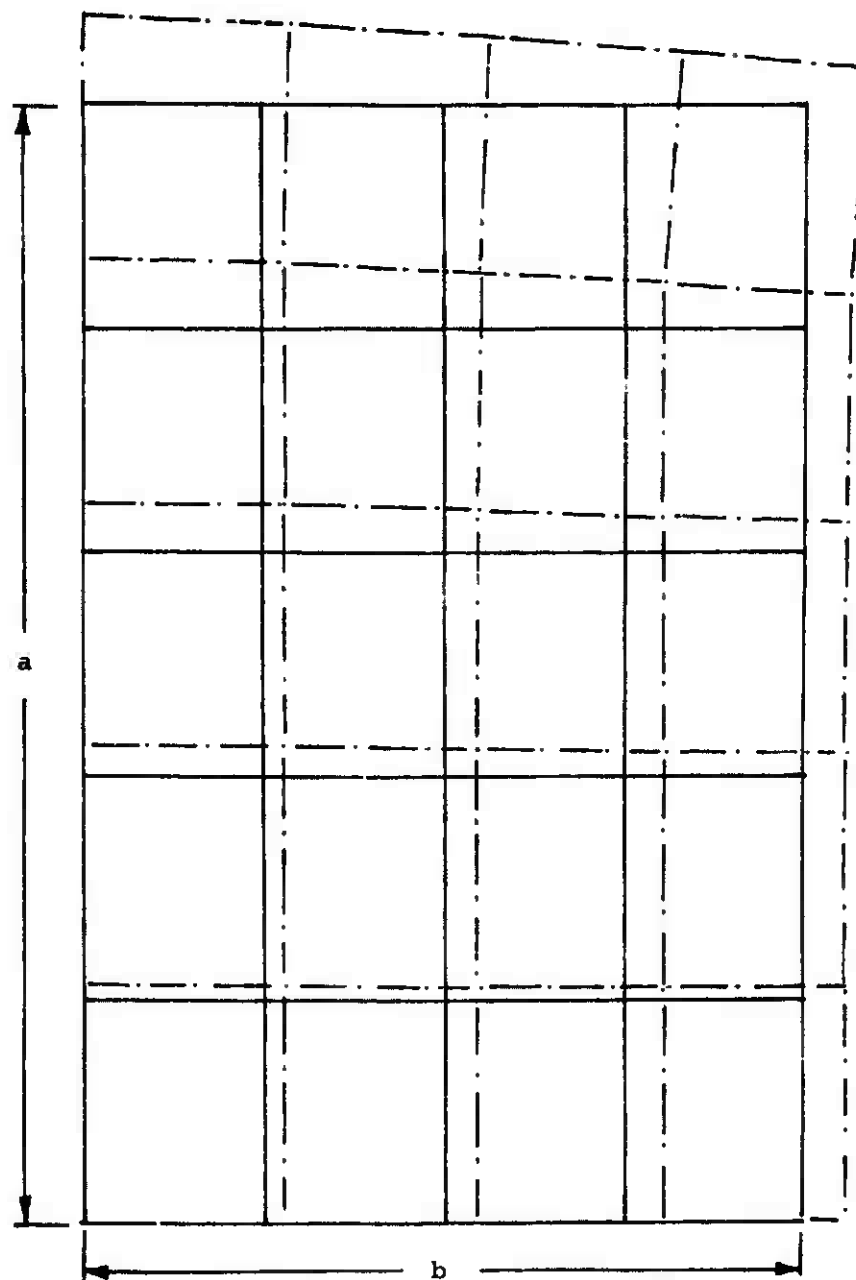
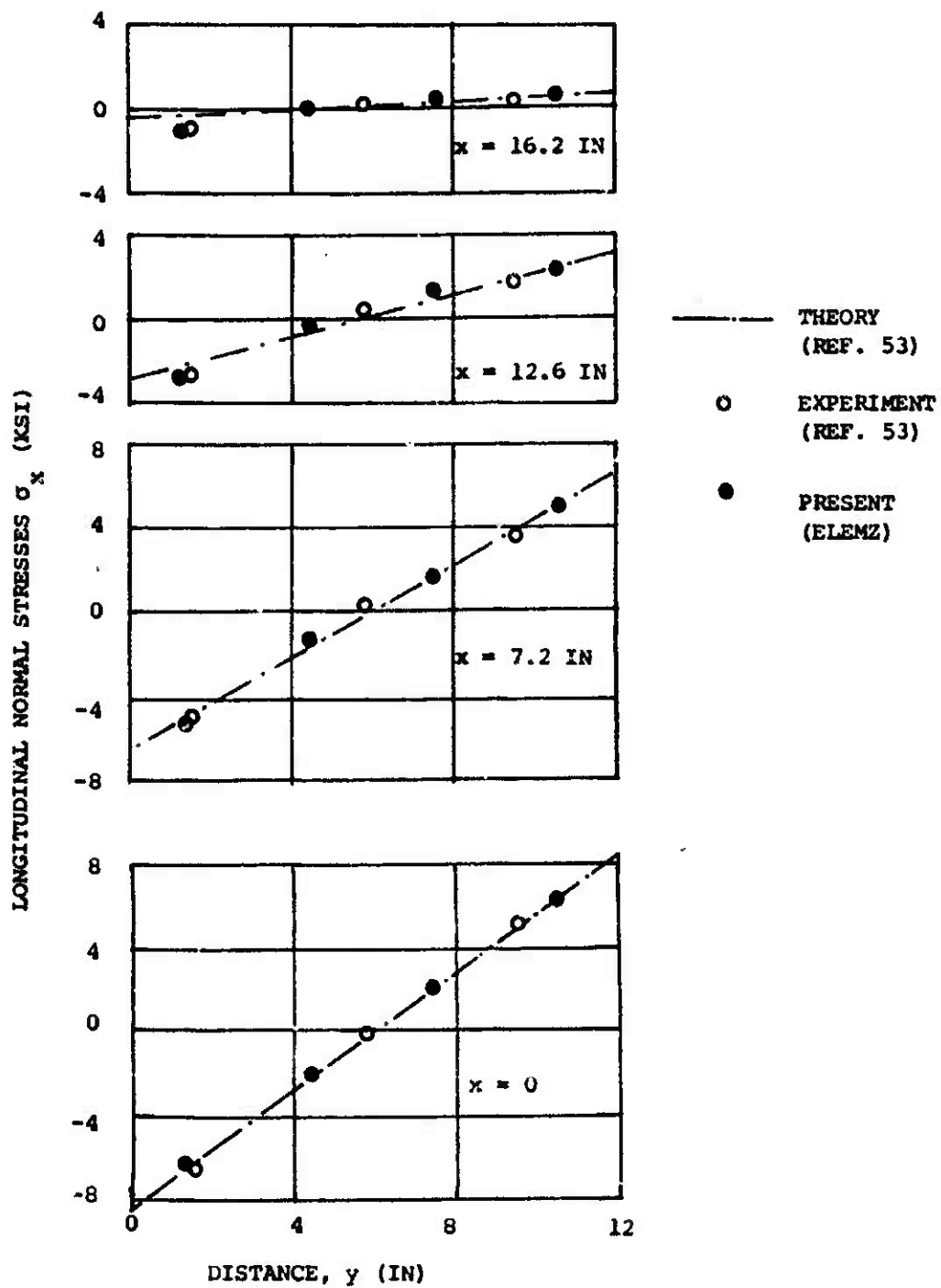
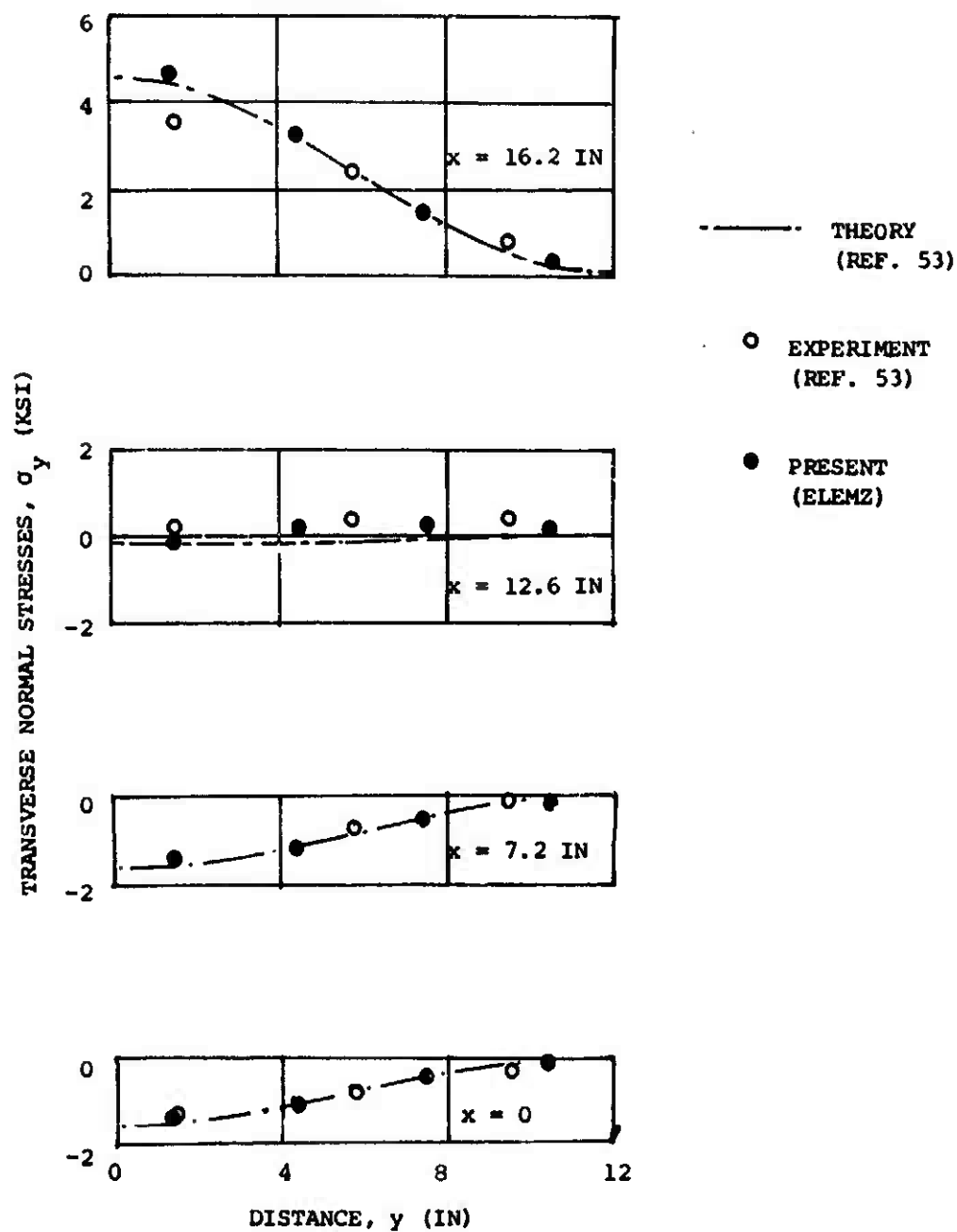


FIG. 30 DISPLACEMENTS OF A QUARTER OF THE PLATE OF FIG. 29



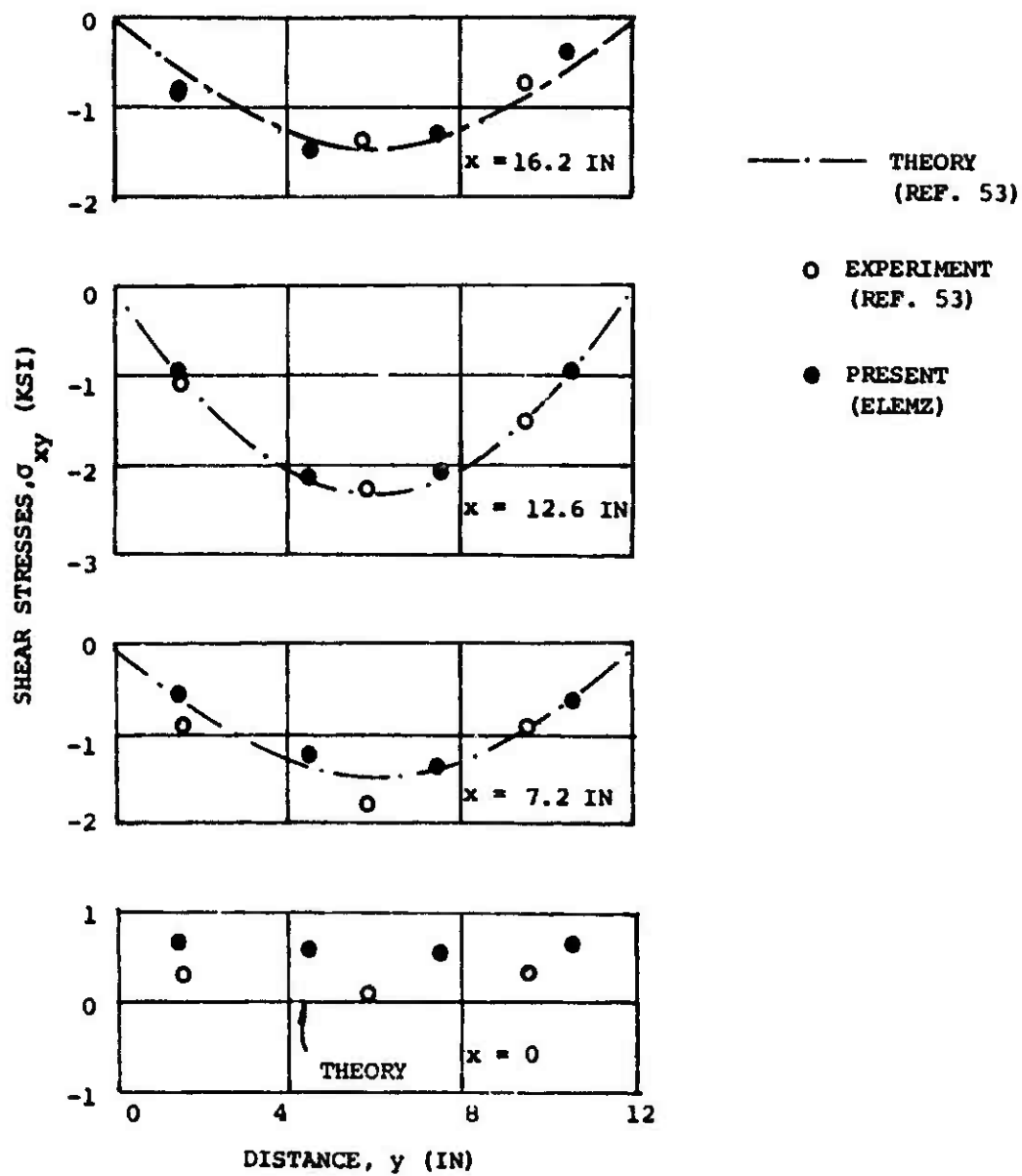
(a) Longitudinal Normal Stress,  $\sigma_x$

FIG. 31 IN-PLANE NORMAL AND SHEAR STRESSES OF THE PLATE OF FIG. 29



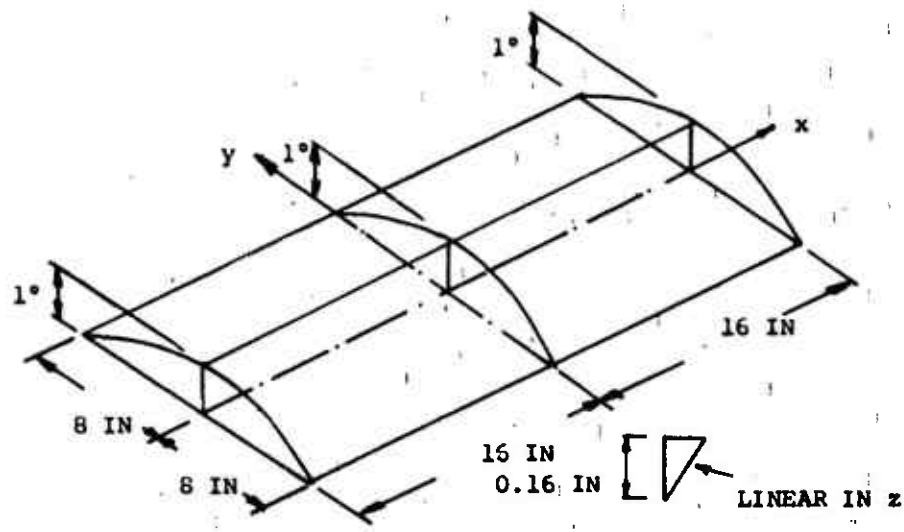
(b) Transverse Normal Stresses,  $\sigma_y$

FIG. 31 CONTINUED

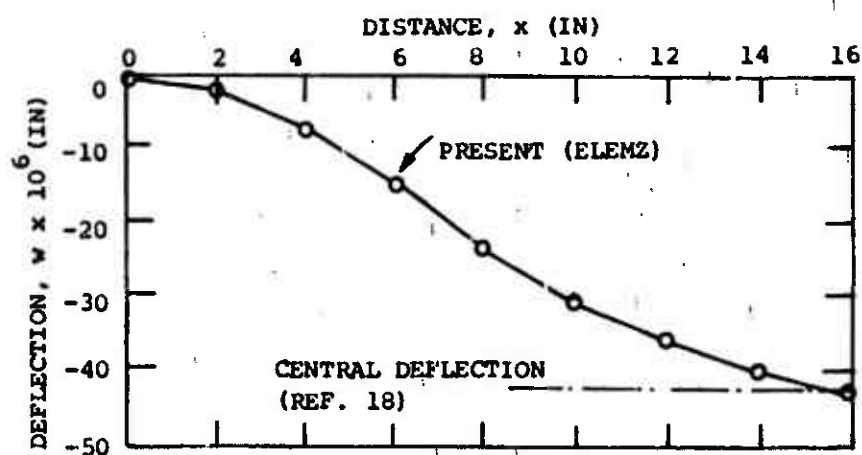


(c) Shear Stresses,  $\sigma_{xy}$

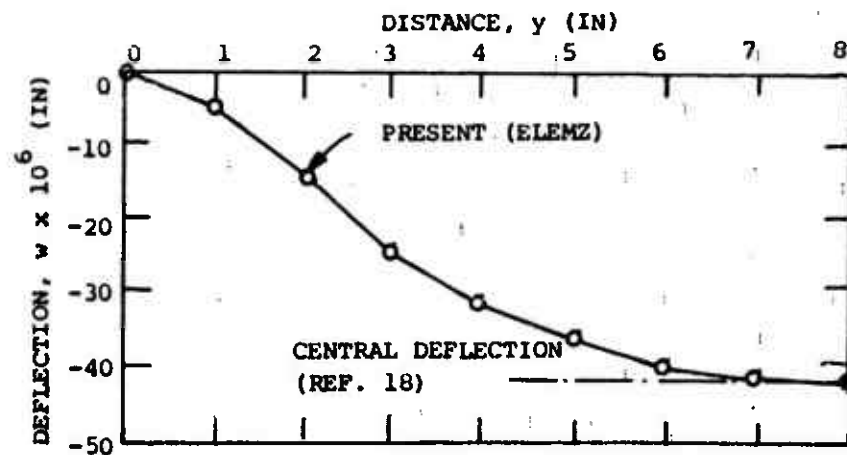
FIG. 31 CONCLUDED



(a) Dimensions and Temperature

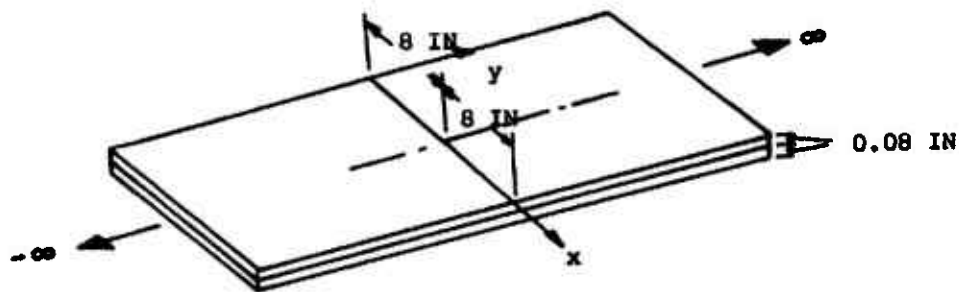


(b) Deflection of x-Centerline

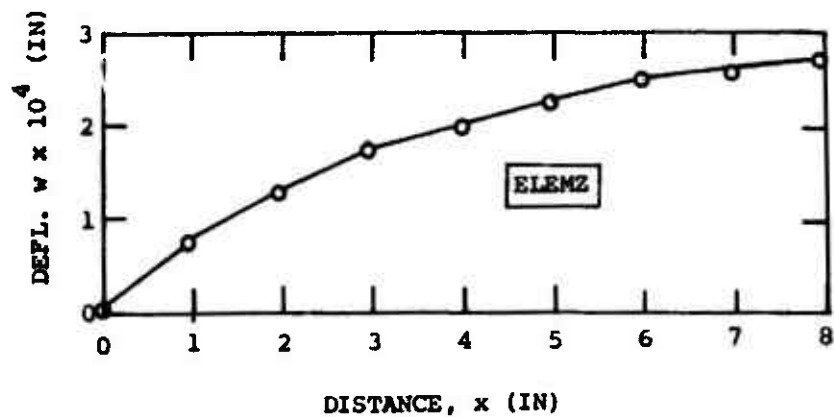


(c) Deflection of y-Centerline

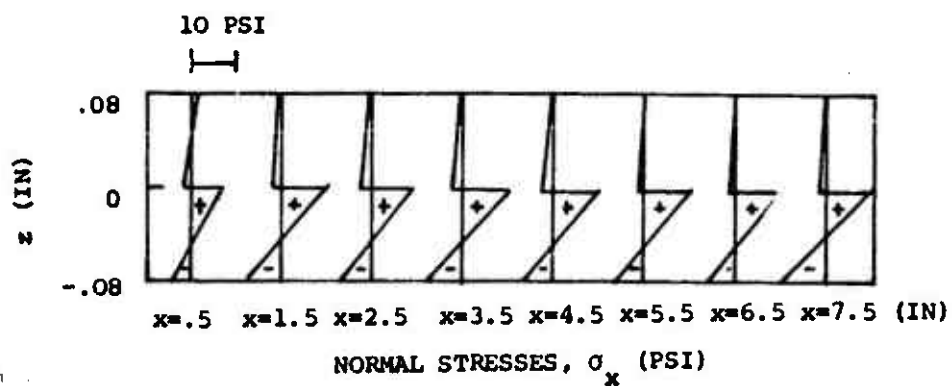
FIG. 32 DIMENSIONS, TEMPERATURE, AND CENTERLINE DEFLECTIONS OF A CLAMPED SINGLE-LAYER, THIN, ISOTROPIC RECTANGULAR PLATE



(a) Dimensions and Coordinate System

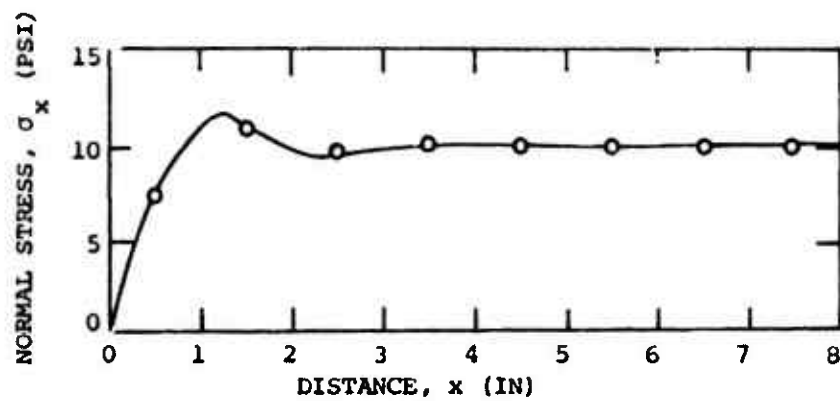


(b) Deflection, w

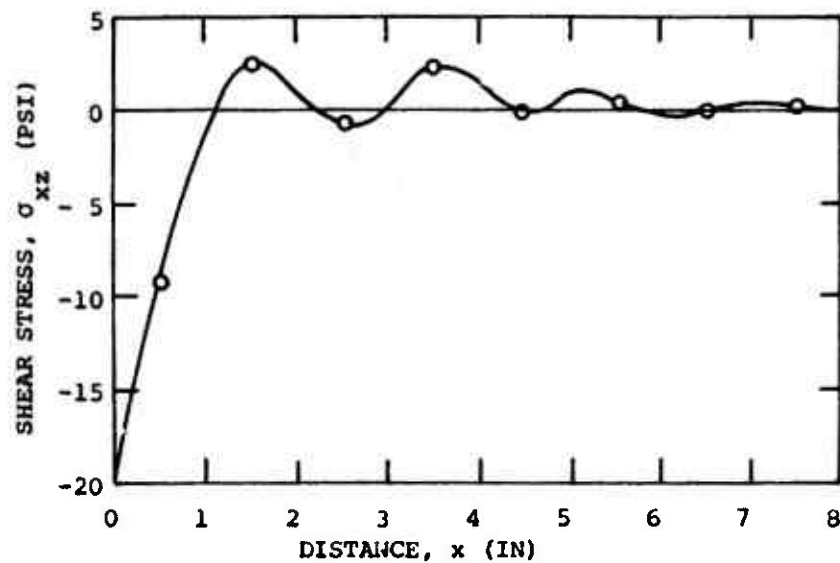


(c) Normal Stresses,  $\sigma_x$

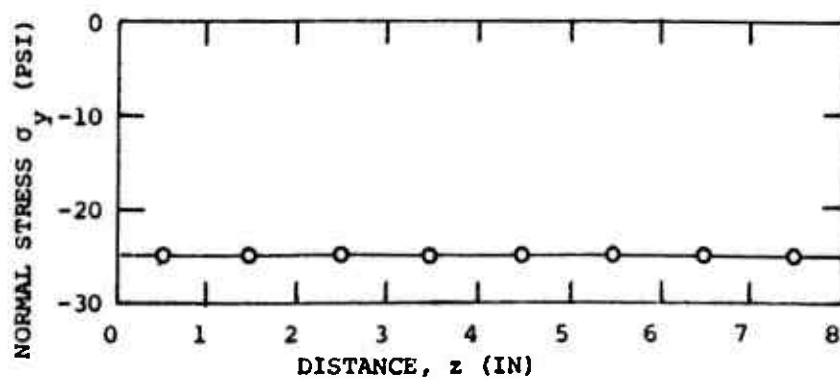
FIG. 33 DIMENSIONS, COORDINATE SYSTEM, DEFLECTIONS, AND STRESSES OF AN INFINITE TWO-LAYER CROSS-PLY THIN PLATE SIMPLY SUPPORTED ALONG EDGES AND SUBJECTED TO UNIFORM TEMPERATURE



(d) Normal Stresses,  $\sigma_x$  ( $z=0$ )

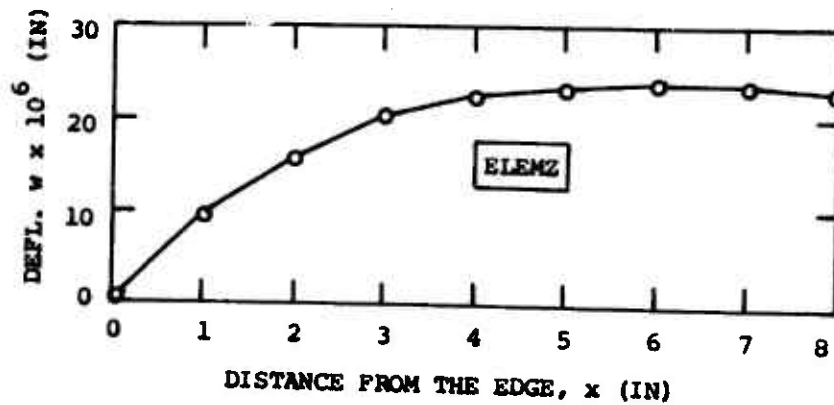


(e) Transverse Shear Stresses,  $\sigma_{xz}$  ( $z=0$ )

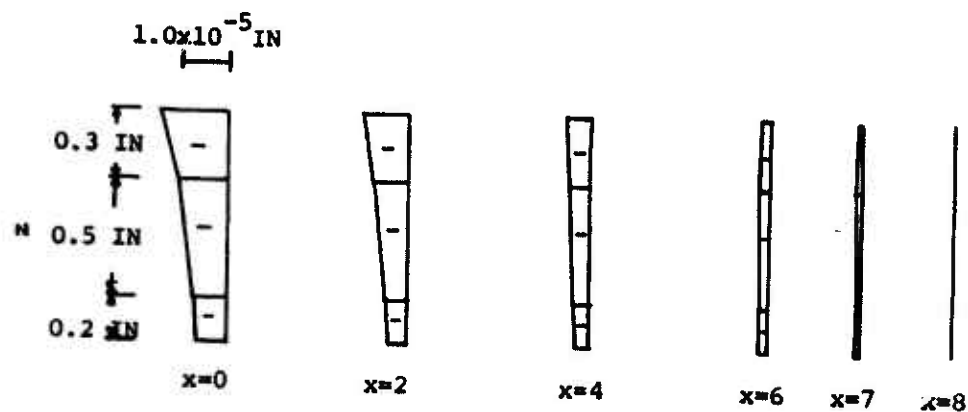


(f) Normal Stresses,  $\sigma_y$  ( $z=0$ )

FIG. 33 CONCLUDED



(a) Radial Deflections, w



(b) Axial Deflections, u (IN)

FIG. 34 RADIAL AND AXIAL DEFLECTION OF A SIMPLY-SUPPORTED THREE-LAYER CROSS-PLY CYLINDRICAL SHELL SUBJECTED TO UNIFORM TEMPERATURE

## APPENDIX

### COMPUTATIONAL SCHEMES FOR STATIC AND VIBRATION ANALYSIS

Since the purpose of this study is to develop and evaluate new useful finite elements, example problems chosen are often relatively simple in geometry so that results can be compared with those of other existing solutions and computation can be completed economically. Consequently, the computational schemes chosen for use in this study are suitable for medium-sized problems with total degrees-of-freedom no more than about 1000.

A thermal stress analysis, as shown in Section 4, can be reduced to a static analysis by transforming the initial thermal strains into an equivalent loading vector. Thus, for both static and thermal stress analyses, the system equations to be solved may be represented by

$$\underline{K} \underline{\delta}^* = \underline{F} \quad (\text{A.1})$$

where  $\underline{K}$  is the system stiffness matrix,  $\underline{\delta}^*$  is the unknown nodal displacement vector, and  $\underline{F}$  is the force vector. To solve Eq. A.1 the method of triangular factorization is used. The  $\underline{K}$  matrix is decomposed into three matrices:

$$\underline{K} \equiv \underline{L} \underline{D} \underline{L}^T \quad (\text{A.2})$$

where  $\underline{L}$  is a lower triangular matrix with zero elements in the upper triangle and unity on the diagonal, and  $\underline{D}$  is a diagonal matrix. Note that the decomposition is easily achieved by successive substitution starting from the first row-and-column element of  $\underline{K}$ . Combining Eq. A.1 and Eq. A.2, one obtains

$$\underline{L} \underline{D} \underline{L}^T \underline{\delta}^* = \underline{F} \quad (\text{A.3})$$

Defining a new unknown vector

$$\underline{Y} \equiv \underline{D} \underline{L}^T \underline{\delta}^* \quad (\text{A.4})$$

one obtains

$$\underline{L} \underline{Y} = \underline{F} \quad (\text{A.5})$$

Now Eq. A.5 can be solved readily for  $\underline{y}$  since  $\underline{L}$  is a lower triangular matrix; the solution of  $\underline{y}$  can be obtained by successive substitution starting from the first unknown. Once  $\underline{y}$  is obtained,  $\underline{q}^*$  can be obtained similarly from Eq. A.4 by noting that  $\underline{D} \underline{L}^T$  is an upper triangular matrix. Thus, two steps are involved in the solution of Eq. A.1: (a) decomposition, which also involves only successive substitution, and (b) successive substitution to obtain  $\underline{y}$  and then  $\underline{q}^*$ .

For vibration analysis, a system mass matrix is added and the system equations are, from Eq. 3.15,

$$(\underline{K} - \omega^2 \underline{M}) \underline{q}^* = 0 \quad (\text{A.6})$$

where  $\omega$  is the natural frequency to be determined.

Many eigenvalue schemes can be used to solve Eq. A.6, but it is convenient in programming to make use of the triangular factorization scheme of the static analysis. Thus, the eigenvalue solution using the Sturm-sequence method [42,43,44] is selected for this study. The Sturm sequence property, when applied to Eq. A.6, states that for any given value of  $\omega$ , the number of successive sign changes in the determinants of the leading minors of matrix  $[\underline{K} - \omega^2 \underline{M}]$  equals the number of eigenvalues that are less than  $\omega$ . Obviously, this property can be utilized to locate or "bracket" any eigenvalue by simply assuming a series of  $\omega$ 's and counting the number of sign changes in the determinants.

An important observation from the decomposition

$$(\underline{K} - \omega^2 \underline{M}) = \underline{L} \underline{D} \underline{L}^T \quad (\text{A.7})$$

is that the number of sign changes of the determinant of the leading minors equals the number of negative values in the diagonal of  $\underline{D}$ . Therefore, it is a simple task to determine the number of eigenvalues less than a given  $\omega$  once the decomposition of Eq. A.7 is complete.

Using the above procedure, any eigenvalue can be isolated, and lower and upper bounds can be established. But for accurate determination, it is necessary to use an interpolation scheme to reduce further the bracket interval of an

eigenvalue to desirable accuracy. In this study, a parabolic curve of  $\omega$  vs. the determinant of  $(\underline{K} - \omega^2 \underline{M})$  is fitted between the bounds of an eigenvalue, and the interpolated value of  $\omega$  is the estimated eigenvalue. This interpolation process is continued until changes in  $\omega$  is within a certain prescribed amount of tolerance (for example, 1/100 of the calculated  $\omega$ ).

Once an eigenvalue is obtained, the corresponding eigenvector is obtained by solving Eq. A.6 with one of the degrees-of-freedom constrained.